UNIVERSITÀ
DEGLI STUDI
DI PADOVA

UNIVERSITÀ DEGLI STUDI DI PADOVA

DIPARTIMENTO DI INGEGNERIA DELL'INFORMAZIONE

DIPARTIMENTO DI INGEGNERIA INDUSTRIALE

CORSO DI LAUREA MAGISTRALE IN BIOINGEGNERIA

Tailoring interactions between degradable polymers and proteins, exploiting nanodiamond particles and Quartz Crystal Microbalance

Relatore:
Ch.mo Prof. Andrea Bagno

Laureanda:
Vera Carniello

ANNO ACCADEMICO 2012-2013

16 Luglio 2013

Abstract

La Microbilancia al Cristallo di Quarzo (QCM) è una tecnica altamente sensibile ed efficiente per analizzare le variazioni di massa all'interfaccia tra un materiale solido e un liquido. Per l'attività sperimentale di questa tesi, la QCM è stata utilizzata per studiare le interazioni che intercorrono tra determinati polimeri degradabili, nanodiamanti e proteine.

La prima fase della ricerca aveva come obiettivo l'ottimizzazione di alcuni parametri per consentire di effettuare misure di polimeri degradabili con la QCM. In particolare, tra i parametri più rilevanti sono stati individuati temperatura, spessore dello strato polimerico e trattamento della superficie dei sensori. Questi sono stati modificati per poter analizzare polimeri come acido polilattico (PLA), un copolimero dell'acido L-lattico con ϵ-caprolattone (poly(LLA-co-CL)) e un copolimero dell'acido D-lattico con trimetilene carbonato (poly(TMC-D-LA)).

La QCM ha consentito di ottenere informazioni quantitative relative all'adsorbimento di proteine su polimeri degradabili. É stato approfondito particolarmente il comportamento di PLA e poly(LLA-co-CL) in relazione all'adsorbimento proteico. Inoltre, è stato dimostrato che questo dipende dal materiale considerato e dalla concentrazione di proteine in soluzione. Infine, è stato osservato che, se le superfici polimeriche sono funzionalizzate con nanodiamanti, l'adsorbimento proteico aumenta sensibilmente.

La presente tesi è stata svolta presso la School of Chemical Science and Engineering del Royal Institute of Technology (KTH) di Stoccolma, da gennaio 2013 a giugno 2013, sotto la supervisione della Prof.ssa Assoc. Anna Finne Wistrand.

Parole chiave: Microbilancia al Cristallo di Quarzo, polimeri degradabili, acido polilattico, proteine, nanodiamanti.

Abstract

Quartz Crystal Microbalance (QCM) is a sensitive and effective technique to analyze mass changes at the interface between a solid material and a liquid environment. In this Master thesis, QCM was employed for evaluating the interactions between selected degradable polymers, nanodiamond particles and proteins.

First of all, several parameters had to be adapted to allow QCM measurements involving degradable polymers. In particular, temperature, thickness of polymer layer and treatment of the sensor surface were found to be relevant. These parameters were tailored to allow QCM measurements involving polylactide (PLA), a copolymer of L-lactide with ϵ-caprolactone (poly(LLA-co-CL)) and a copolymer of D-lactide with trimethylene carbonate (poly(TMC-D-LA)).

QCM allowed to obtain quantitative measurements of protein adsorption on degradable polymers. The behavior of PLA and poly(LLA-co-CL), with respect to protein adsorption, was demonstrated to be different for the two polymers considered and to be dependent on protein concentration in solution. Eventually, it was also possible to conclude that if nanodiamond particles were employed for polymer functionalization, a great enhancement in protein adsorption was recorded by QCM.

The present Master Thesis was developed at the School of Chemical Science and Engineering of the Royal Institute of Technology (KTH) in Stockholm, from January 2013 to June 2013, with the supervision of Assoc. Prof. Anna Finne Wistrand.

Keywords: Quartz Crystal Microbalance, degradable polymers, polylactide, proteins, nanodiamond particles.

ACKNOWLEDGEMENTS

First of all, I would like to thank my main supervisor Assoc. Prof. Anna Finne Wistrand and my co-supervisor Yang Sun, for giving me the opportunity to work at my Master thesis in their research group. Their constant guidance, support and enthusiasm were essential for my continuous learning and improvement.

I would also like to thank my co-supervisor Assoc. Prof. Massimiliano Colarieti-Tosti, for the interest shown for my Master thesis and for giving me the possibility to work at this project.

My supervisor in Universitá degli Studi di Padova, Prof. Andrea Bagno, is especially thanked for the helpfulness, the advices and suggestions I received throughout my thesis work.

Eventually, the other Master students and the whole Ann-Christine Albertsson's group are gratefully thanked for accepting me in their friendly and challenging working environment and for the useful and positive discussions.

CONTENTS

1 INTRODUCTION

Quartz Crystal Microbalance (QCM) is a powerful method for analyzing the adsorption, detachment or changes of mass at the interface between a solid material and a liquid or gaseous environment.

Even though the relationship between the mass of a resonator and the resonance frequency was first investigated by Sauerbrey in 1959 [1] and the first theoretical studies towards the development of the Quartz Crystal Microbalance were performed around 1980-1985 [2], the employment of this technique for experimental purposes was not widely spread until the years 2000-2001. Since then, the number of publications concerning this topic increased considerably [3].

Because of its several advantages, such as accuracy and high sensititivity in determining real-time mass changes, the Quartz Crystal Microbalance has been applied for evaluating the behavior of proteins, cells and other particles or macromolecules with respect to different materials like polymers and metals.

1.1 PURPOSE OF THE STUDY

Since the Quartz Crystal Microbalance is a recently developed technique, several improvements still have to be developed, for example by finding optimal experimental conditions and sets of parameters, on the basis of the materials or macromolecules under investigation. This is the context in which the idea of this project was developed and the main aims of this Master thesis were:

1. To evaluate if the Quartz Crystal Microbalance (QCM) is a suitable technique to analyze the behavior of proteins and nanodiamond particles on degradable polymers:
    - To find the optimal parameters for the frequency shift detection by the QCM;
    - To evaluate whether there is a relationship between the concentration of proteins in solution and the maximum frequency shift recorded by the Quartz Crystal Microbalance;
2. To compare the behavior of different polymers, in terms of protein and nDP mass adsorption;

3. To observe whether the presence of nanodiamond particles (nDP) leads to an improvement in protein adsorption and if the QCM apparatus is able to detect it.

As for the choice of the polymers to investigate, the initial selection included at least one polymer, or copolymer, for each of the following categories:

- *Synthetic hydrophobic polymers.* Among these, polylactide (PLA) and poly(L-lactide-co-ϵ-caprolactone) (in the following text it is indicated as poly(LLA-co-CL)) were chosen. This is because there are many studies already published about these polymers and the properties of poly(LLA-co-CL)) can be modified and known in advance. Moreover, these polymers have already been proven to be suitable for the design of scaffolds for bone tissue engineering [4];
- *Synthetic hydrophilic polymers.* In this case, a triblock copolymer of poly(L-lactide) and poly(ethylene glycol), that will be indicated as PLA-PEG-PLA in the following text, was tested;
- *Bacterial polymers.* The poly((R)-3-hydroxybutyrate) (P(3HB)) and its copolymer with 5-hydroxyvalerate (abbreviated as P(3HB)-co-5HV) were considered, to make a comparison with synthetic polymers.

Later, it was decided to test an additional selection of polymers, including a copolymer of trimethylene carbonate and D-lactide, that will be abbreviated as TMC-co-D-LA, polyglycolide (PGA) and polystyrene (PS).

As for the choice of the proteins, fibronectin was preferred in this case, because it is one of the main adhesive components in plasma and extracellular matrix and it accelerates cell adhesion [5]. Besides, it has been demonstrated that the polymers PLLA and poly(LLA-co-CL) can be effectively functionalized with fibronectin, to improve cell adhesion [6].

Furthermore, the growth factor Bone Morphogenetic Protein-2 (BMP-2) was employed in this thesis, to compare its behavior to fibronectin, in relation to the QCM technique and to the selected polymers.

1.2 STRUCTURE OF THE THESIS

In the following chapters of this thesis, a general description of the Quartz Crystal Microbalance technique is provided, including its basic principles, applications, advantages and drawbacks (Chapter 2). Also,

an introduction about the degradable polymers is given in Chapter 3 and an overview of the proteins and nanodiamond particles employed in this work for the polymer surfaces functionalization are found in Chapter 4. The two following chapters describe the experimental conditions, including materials used for the project (Chapter 5) and the experimental methods applied (Chapter 6). Eventually, the results obtained are presented and discussed in Chapter 7.

The present Master Thesis was developed at the School of Chemical Science and Engineering of the Royal Institute of Technology (KTH) in Stockholm, from January 2013 to June 2013, with the supervision of Assoc. Prof. Anna Finne Wistrand.

2 QUARTZ CRYSTAL MICROBALANCE (QCM)

2.1 THE QCM TECHNIQUE

Quartz Crystal Microbalance (QCM) is a technique employed to study adsorption processes and mass changes at the interface between a gas or liquid environment and a solid material [7]. The main idea is to measure the frequency shift of quartz sensing electrodes in order to calculate the adsorption of mass on the sensors [2, 8].

The Quartz Crystal Microbalance technique is based on the usage of a thin quartz crystal between two metal electrodes. The crystal is usually AT-cut, meaning that, if it lays on the XY-plane, it makes an angle of about 35° with the Z-axis (optic axis) (Figure 1). This type of crystal cut is employed because it guarantees low temperature coefficient at room temperature. That is to say, small changes in temperature only result in small changes in frequency.

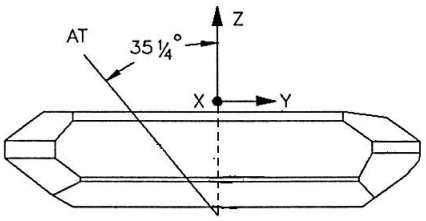

Figure 1: Scheme of an AT-cut quartz crystal. Image from http://www.4timing.com/techcrystal.htm

By applying an alternating electric field across the crystal, the resonance frequency of the quartz crystal is induced and the crystal presents a vibrational mode of thickness shear deformation (Figure 2). This is due to the piezoelectric properties of the crystal and to the crystal orientation.

If a mass is attached to the crystal, the oscillation frequency f decreases (negative frequency shift). So, measuring the change in resonance frequency, it is possible to calculate the mass of a thin and rigid layer attached to the crystal, exploiting the Sauerbrey equation [9]:

$$\Delta f = -\frac{2f_0^2 \Delta m}{A\sqrt{\rho_q \mu_q}} = -C_f \Delta m \tag{2.1}$$

where
f_0 is the fundamental resonance frequency of the crystal (Hz),

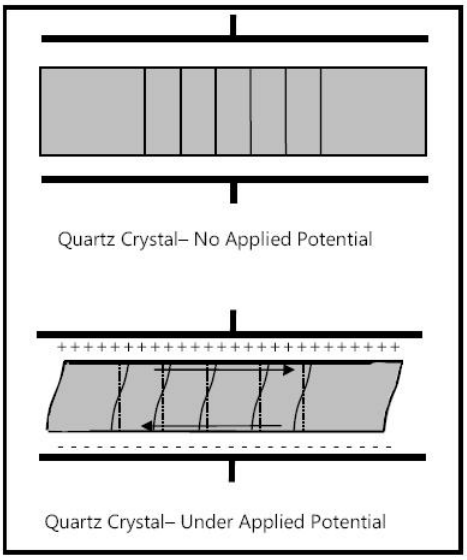

Figure 2: Scheme of thickness shear deformation of an AT-cut quartz crystal. Image from http://www.gamry.com/assets/Application-Notes/Basics-of-an-eQCM.pdf

A is the area of the electrode (cm^2),
ρ_q is the density of the quartz (g/cm^3),
μ_q the shear modulus of the quartz ($g/(cm\ s^2)$),
C_f is the integral mass sensitivity (m^2Hz/g),
Δf is the frequency shift, i.e. change in oscillation frequency of the crystal (Hz),
Δm is the change in oscillator mass per area (g/m^2).
This relationship points out that the frequency shift (Δf) is linearly dependent on the adsorbed mass. It is also possible to monitor the frequency shift for a harmonic overtone of the fundamental frequency and extract the mass change per area as [7]:

$$\Delta m = -C\frac{\Delta f}{n} \tag{2.2}$$

where $C = \frac{1}{C_f}$ is the sensitivity constant ($g/(m^2Hz)$) n is the overtone number.

Some of the advantages of the QCM method are that it requires a short equilibration time (about 3-30 minutes) and assures high accuracy. Oliveira et al. [10] demonstrated that QCM is an efficient and accurate method for studying the solubility of gases in polymers, in particular if compared to other methods like gravimetric or pressure decay. However, the authors highlight the fact that it is necessary to assume that the adsorbed material spreads uniformly through the crystal and vibrates synchronously with it. Another positive aspect of QCM technique is that it can be applied to several different liquids, being not necessary to isolate and purify the analyte. Besides, it allows

to analyze conformational and functional changes of proteins in real time [3].

On the other hand, for a soft or thick layer of material bound to the crystal, the frequency shift due to dissipation will be higher and the Sauerbrey equation cannot be applied [11]. In these cases, the Quartz Crystal Microbalance with dissipation monitoring (QCM-D) is a more suitable technique. Furthermore, the Sauerbrey relation holds for layers that are much thinner of the extinction depth of the shear acoustic wave (about 250 nm). Otherwise, the Sauerbrey relation is not valid [12].

2.2 QUARTZ CRYSTAL MICROBALANCE WITH DISSIPATION MONITORING (QCM-D)

In QCM, if the adsorbed material is cells, that is a non-rigid material, the viscoelasticity of the cells enhances the decrease of the crystal resonance frequency. The main idea of the Quartz Crystal Microbalance with dissipation monitoring (QCM-D) is to measure the damping of crystal oscillations as a variation in crystal dissipation energy D, that gives information on the viscoelasticity of the adsorbed material. The dissipation energy is given by

$$D = \frac{E_{lost}}{2\pi E_{stored}} \tag{2.3}$$

where E_{lost} is the energy dissipated in one cycle of oscillation, E_{stored} is the total energy stored in the oscillator [13].

From the relationship between dissipation energy and frequency shift, it is possible to obtain information about the viscoelastic properties of the absorbed layer, by applying the Voigt-based model [3] (see section **??**). Other parameters useful to evaluate the viscolelasticity are the resistance, inductance, transient decay time constant and maximal oscillation amplitude [14].

An advantage of QCM-D is that it allows to monitor structural changes of the adsorbed material during reactions or interactions with other biological or synthetic materials. As a matter of fact, it is possible to obtain a plot of the variation in rigidity as a function of time or of mass changes [15]. Otherwise, it can be useful to plot the frequency shift as a function of the temperature, as Alf and co-workers [16] exploited for evaluating the lower critical solution temperature for polymer films.

QCM-D also permits to analyze changes in viscoelasticity and stiffness of the adsorbed material. So, the material dynamics (e.g. cellular dynamics) and the viscoelastic properties can be modeled with the

Voigt-based model. For instance, changes in viscoelasticity and dissipation energy often reflect homeostatic phenomena, such as blood coagulation. [3].

Furthermore, this technique permits to understand the nature of the interactions between a protein and the surface. For example, it allows to distinguish between monolayer adsorption, multilayer adsorption and penetration into a film. At the same time, QCM-D also gives information about the kinetics of these processes [16].

Because harmonic acoustic frequencies penetrate at different depths in viscous layers, with QCM-D it is possible to measure frequency shift and dissipation simultaneously at different overtones. Some authors suggest to consider the third overtone rather the fundamental frequency, in order to exploit its higher stability and sensitivity [12].

Another advantage of QCM-D is that the obtained data, that is to say frequency and dissipation shifts, are highly reproducible [17].

Besides, if compared to other optical methods to investigate adsorbed proteins, such as surface plasmon resonance (SPR), optical waveguide lightmode spectroscopy (OWLS) or ellipsometry, QCM-D allows to detect higher mass adsorptions [18]. In fact, the frequency shift takes into account both the protein mass adsorbed and the water bonded to the proteins [3].

QCM-D guarantees better performances in evaluating cell adhesion as well, in comparison with other methods such as counting technique and MTS assay. In particular, it does not require counting the cells, it reduces the errors when calculating the number of adhered cells and it is sensitive even to a small number of adhered cells [19, 20].

2.3 APPLICATIONS OF QUARTZ CRYSTAL MICROBALANCE

In general, QCM can be employed to evaluate and monitor formation of polymer films, lipid bilayers or bacterial biofilms, protein and vesicle adsorption on a material, as well as cell adhesion and spreading on a surface [14].

As an example, the aim of the experiment presented by Wegener et al. [9] was to study the attachment and spreading and of mammalian cells to a surface with the QCM technique. In this case, the surface considered was copper, which was deposited in the crystal by electrodeposition. Several parameters were evaluated, such as frequency shift in dependence both of the time and of the cell number, cellular density, hydrodynamic radius, and rate of sedimentation of the cells. As a result, the authors found out that the frequency shift is dependent on the type of cells. However, they pointed out that QCM is more sensitive to the cells attached directly to the crystal surface, without taking into account cells that pile up on each other. That is to say, the

QCM detects primarily the confluent layer of cells directly adhered to the crystal, not multi-cellular layers. This is due to the fact that the shear wave only propagates with a limited amplitude beyond the first layer of cells [21].

Another study was aimed to analyze protein adsorption on polyesters, in particular polylactide (PLA), polyglycolide (PGA) and polyethylene terephthalate (PET), and the effect of surface alterations. By using the QCM and other techniques, the authors demonstrated that protein adsorption into the polymer is enhanced by polyester degradation. That is to say, the spontaneous hydrolysis by the ester group allows protein adsorption into the polymer. Furthermore, for polyesters that degrade under physiological conditions (at pH 7.4, PLA degrades slowly, PGA more rapidly), surface modifications are not necessary, because the polymer hydrolysis generates binding sites where the proteins can attach. Instead, nondegradable polyesters (e.g. PET) need a surface treatment to enhance protein adhesion by increasing the number of binding sites [11].

Chung and co-workers [8] exploited the QCM technique to investigate the adhesion of Mesenchymal Stem Cells (MSCs) on matrices obtained by combinations of different polymers. They concluded that carbon nanotubes were a good substrate for fast and effective MSCs adhesion, while chitosan showed a slower and less extended cell attachment. Interestingly, they underlined that a first absorption of carbon nanotubes on QCM electrodes can also increase a following absorption of chitosan on the electrodes and that this also leads to an enhancement of the sensitivity of QCM.

The effect of chitosan and hyaluronic acid adsorption on PCL and PEG/PCL was investigated with QCM as well [19]. QCM was proved to be an effective technique to analyze the early adhesion (i.e. up to 3 hours) of cells, in particular fibroblasts, to these polymers.

As for Quartz Crystal Microbalance with dissipation monitoring (QCM-D), it has been used to confirm the finding that preadsorption of extracellular matrix (ECM) proteins in a synthetic matrix can enhance cell adhesion and spreading. For instance, a study evaluated the effect of preadsorbed fibronectin and fibrinogen for accelerating cell adhesion [5]. QCM-D was also used to analyze fibrinogen adsorption in polymers and the binding of the platelet receptor GPIIb-IIIa to the fibrinogen [17].

The study presented by Modin et al. [14] was aimed to evaluate the validity of QCM-D technique to monitor cell adhesion in real time. Besides, they used this method to test different materials and find the better response with respect to pre-osteoblasts attachment and spreading.

Tagaya et al. [7] exploited QCM-D to analyze osteoblast-like cells attachment on hydroxyapatite and oxidized polystyrene. They modeled

these interactions with a Voigt-based viscoelastic model and demonstrated that both cell cytoskeleton and ECM modifies after adhesion, according to the surface material. This leaded also to different types of cell-surface interactions. Furthermore, the authors pointed out that cell adhesion on the surfaces depends on cell seeding density. As a matter of fact, if seeding density increases, then also mass and dissipation shift ΔD increase.

Interestingly, Fredriksson and co-workers [22] found out that cell spreading after adhesion leads to a decrease of the dissipation energy.

Other authors exploited QCM-D, in addition to fluorescence microscopy, to evaluate cell cytoskeleton modifications, through monitoring changes of cell shape and of actin filaments [20].

QCM-D and the Voigt-based model were also used to investigate preadsorption of fibronectin and collagen, in relation to osteoblast-like cells adhesion to a surface. This confirmed the effect of enhancement of cell adhesion in presence of preadsorbed ECM proteins fibronectin and collagen [23].

Eventually, a particular application of QCM, which was applied for calculating the sorption enthalpy and degradation of PLA, is the Quartz Crystal Microbalance heat conduction calorimeter (QCM/HCC). This consists of a quartz crystal microbalance coated with a polymer layer in thermal contact with a heat-flow sensor on a heat sink. This technique allows to monitor the change in mass per unit area and heat at the same time. The heat flow is due to the uptake or release of solvent vapor by the polymer [24].

2.4 INPUT PARAMETERS FOR QUARTZ CRYSTAL MICROBALANCE

In the Quartz Crystal Microbalance apparatus, several parameters can be set and changed in order to optimize the detection of protein adsorption, cell adhesion or the property under investigation.

Temperature

In the Quartz Crystal Microbalance equipment, the temperature of the crystal chamber can be tuned, within certain limits. For example, in the QCM apparatus employed during this thesis (model E4, from *Q-Sense*), it is possible to set the temperature to a value in the range 18-45 °C. Some researchers chose a value of temperature of 37 $\pm$ 0.05 °C to monitor cell adhesion on different materials [7, 9, 14, 25]. Instead, others set a temperature of 22 °C and 32 °C, waiting thirty minutes to equilibrate after each temperature setting, for studying bovine serum albumin (BSA) adsorption and diffusion into hydrogel films [16]. Yamada et al. [26] chose a temperature of 25 °C to analyze

the interactions between poly((R)-3-hydroxybutyrate) (P(3HB)) and DNA. The value 25 °C was employed by other authors to study other materials as well, such as P(3HB), PLA and PET [27, 28].

Flow rate

The rate at which the solution with the analyte is injected into the crystal chamber can also be tuned. For example, the QCM system used during this project allows to choose a value for the flow rate in the range 50-200 μL/min. In the literature there are some examples of values. Alf and co-workers [16] used a flow rate of 100 μL/min for monitoring the absorption of several polymers onto the crystal. The same value was also employed when investigating other materials, e.g. thermoresponsive nanocomposites or polyelectrolytes [29, 30]. Chung et al. [8] chose a value of 60 μL/min to flow a solution with mesenchymal stem cells over a polymer or a crystal with adhered fibronectin. The flow rate value of 30 μL/min was used in other studies to investigate chitosan adsorption onto a QCM crystal and fibroblasts adhesion on the polymer layer [19].

Frequency range and number of overtones

In Q-sense E4 (Q-Sense, Goteborg, Sweden) QCM, the resonance frequency of the sensors is 4.95 ± 0.05 MHz. Besides, it permits to measure changes in frequency in the range 1-70 MHz and up to the 13th overtone. For instance, some authors registered the 3rd overtone [7, 23], while others recorded four overtones at the same time (overtone number n=1,3,5,7) [14, 15]. Other authors also tried to monitor the harmonics for n=1,3,5,7, but they had to eliminate the first overtone, because inconsistent with the other results [16]. Li et al. [31] registered the odd harmonics up to the 13th overtone.

As for the time required to monitor frequency changes, Oliveira and co-workers [10] measured the values until the frequency was stabilized in a range of ± 2 Hz, while other authors registered the frequency for one hour [25]. Modin et al. [14] recorded the signal for 30-60 minutes. In some works, Δf and ΔD were measured every 15 seconds [9], while in others they were registered every minute [15].

3 DEGRADABLE POLYMERS

3.1 SYNTHETIC POLYMERS

Two main classes of synthetic polymers will be considered in this work:

1. Hydrophobic polymers:
    - Polylactide (PLA);
    - Poly(ϵ-caprolactone) (PCL);
    - Poly(trimethylene carbonate) (PTMC).
2. Hydrophilic polymers: Poly(ethylene glycol) (PEG).

In general, degradable polymers are widely applied in biomedical engineering, especially for temporary devices. The main advantage of synthetic degradable polymers is that it is possible to modify their mechanical properties and the degradation rate. Besides, their chemical composition is known and well-defined.

On the other hand, a drawback for the application of these polymers in tissue engineering is their lack of specific signals for cell recognizing and adhesion. So, some authors are working to improve the materials properties and to make them suitable for different applications. For example, degradable polymers can be modified by conventional grafting, photografting, mutual irradiation and vapor-phase-grafting [32, 33, 34].

3.1.1 *Polylactide (PLA)*

Polylactide (PLA) is a hydrophobic aliphatic polyester; it is a biodegradable polymer derived from petroleum or renewable resources.

Since the glass transition temperature of typically synthesized PLA is around 53-65 °C, that is higher than body temperature, this material is stiff and easy to break if implanted into the body.

The degradation of PLA in vitro is due to the hydrolysis of its ester bonds. The degradation kinetic is precisely predictable and the degradation rate depends on the degree of crystallinity, which can range from 0% to 40%. Moreover, the degradation rate can be increased by grafting. For instance, the degradation rate was found to increase if the lactide content decreases in the case of L-lactide-chitosan copolymers [35, 36].

PLA is a chiral molecule that can be found in the form of two stereoisomers, L- and D-lactic acid. From L-lactide, a semi-crystalline polymer (poly(L-lactide), PLLA) is obtained. Poly(D-lactide) (PDLA) is a semi-crystalline polymer obtained from D-lactide and it is often applied in the construction of drug delivery system. Besides, poly(L-lactide-co-D-lactide) (PDLLA) is an amorhpus copolymer obtained from L-lactide and D-lactide.

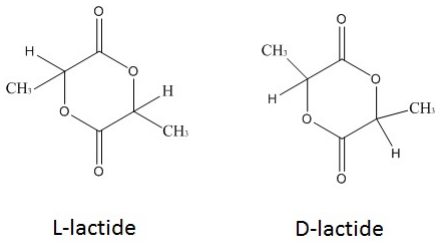

Figure 3: Chemical structure of the monomers L-lactide and D-lactide.

A summary of the main thermal and mechanical properties is presented in Table 1 and Table 2.

PLA can be synthesized by ring-opening polymerization of lactide. Copolymers of PLA and other polymers can be produced by ring-opening polymerization and condensation polymerization [37].

PLA is biodegradable, biocompatible, non-toxic and it has resorbable degradation products. Moreover, it is soluble in a wide variety of common industrial solvents, such as chloroform, dimethylformamide (DMF) and tetrahydrofuran (THF). So, it finds many applications in packaging and in biomedical engineering. As an example of the latter, PLA is one of the main components of scaffolds, stents, sutures and bone screws [32, 38]. PLLA is employed in bone fixation devices or to replace ligaments and non-degradable fibers. Instead, PDLA is more used in drug delivery systems and scaffolding for tissue engineering, because it has a faster degradation rate than PLLA [35].

Table 1: Summary of the main thermal and mechanical properties of PLLA and PDLA. T_m is the melting temperature, T_g is the glass transition temperature, E is the Young's modulus [39, 40].

Polymer	T_m (°C)	T_g (°C)	E (GPa)	Degradation rate (months)
PLLA	170-180	53-65	2.7-4	24
PDLA	Amorphous	55-60	1-3	12-16

Table 2: Tensile strength and elongation at break for PLLA and PDLA [35].

Polymer	Elongation at break (%)	Tensile strength (MPa)
PLLA	85-105	45-70
PDLA	2-10	27-50

3.1.2 *Poly(ϵ-caprolactone) (PCL)*

Poly(ϵ-caprolactone) (PCL) is a hydrophobic semicrystalline aliphatic polyester. It has good biocompatibility, is resorbable and it has high termal stability. So, it has been widely applied in the biomedical field. For instance, PCL is an important constituent of scaffolds for tissue engineering, it is used in drug release systems and to repair bone and cartilage. Because its degradation rate is slower than PLA (about two years), it is more suitable to be used for long-term implants. However, copolymers of ϵ-caprolactone with other monomers are preferably employed when faster degradation rate is needed [35, 33]. A summary of the main thermal and mechanical properties of PCL is presented in Table 3.

Table 3: Summary of the main thermal and mechanical properties of PCL [39, 40, 35].

Property	Value
Melting temperature T_m	58-65 °C
Glass transition temperature T_g	-(65-60) °C
Degradation rate	about 24 months
Young's modulus	0.2-0.4 GPa
Tensile strength	20-42 MPa
Elongation at break	700-1000 %

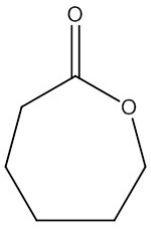

Figure 4: Chemical structure of the monomer ϵ-caprolactone.

3.1.3 *Poly(trimethylene carbonate) (PTMC)*

Poly(trimethylene carbonate) (PTMC) is a hydrophobic carbonate polyester and it has properties that make it suitable for medical applications, such as nontoxicity, biocompatibility, and biodegradability [41]. In comparison with polyesters, which are generally brittle and rigid, PTMC is softer and it has been used in copolymerization with different polyesters to improve their suitability in certain medical applications. For example, copolymers of TMC and D-lactide were studied [42].

On the other hand, the homopolymer PTMC cannot be directly implanted in the body because of its low mechanical properties [43]. As a matter of fact, it is amorphous, rubbery and with low tensile strength [42]. So, many studies have been conducted to copolymerize PTMC with other monomers, like L-lactide or ϵ – caprolactone [44, 45, 46], to enhance its physical properties.

The main thermal and mechanical properties of PTMC are summarized in Table 4.

Table 4: Summary of the main thermal and mechanical properties of PTMC [47, 48].

Property	Value
Melting temperature T_m	45-47 °C
Glass transition temperature T_g	-(12-17) °C
Young's modulus	about 2 GPa

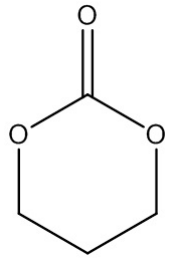

Figure 5: Chemical structure of the monomer TMC.

3.1.4 *Poly(ethylene glycol) (PEG)*

Poly(ethylene glycol) (PEG) is a synthetic hydrophilic polyether and it is often used in block copolymerization, in order to produce a more hydrophilic polymer [49].

In the native form, PEG does not allow cell adhesion, but it can be functionalized with different peptides, e.g. the Arginine-Glycine-

Aspartic acid (RGD) sequence. It is biocompatible, non-toxic and soluble in water. It is used to produce hydrogels and drug delivery systems. PEG is also employed in the pharmaceutical field, for enhancing the biocompatibility of certain biomaterials [33].

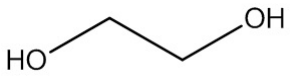

Figure 6: Chemical structure of the monomer ethylene glycol.

3.2 BACTERIAL POLYMERS: POLY(β-HYDROXYALCANOATE)S (PHAS)

Poly(β-hydroxyalcanoate)s (PHAs) is a family of degradable microbial polyesters with different properties and characteristics. They are accumulated by several types of bacteria as intracellular reserve materials. That is to say, by controlling the production organisms and the starting materials, it is possible to obtain a wide variety of PHA polymers and copolymers. As an example, the molecular mass of the PHAs depends on producing organisms and on the type of production [35, 33, 50]. Degradation of PHAs is caused by extracellular microbial enzymes and it takes place both in aerobic and anaerobic conditions.

3.2.1 *Poly(hydroxybutyrate)s (PHBs)*

The most important biopolymer among the PHAs is poly(hydroxybutyrate) (PHB). It is applied in vascular grafts, suture, and orthopedic fixture [35, 51, 33].

poly((R)-3-hydroxybutyrate) (P(3HB))

In the native form, P(3HB) is an amorphous polyester, with density around 1.18 g/cm^3, while in the crystalline form it has a density of about 1.28 g/cm^3. It can be obtained with high purity, that causes it to be highly crystalline, up to 55-80 %. From SEM analysis, Liang and co-workers [52] observed that PHB has a crystalline-like structure, because of its high tendency to crystallize. Other thermal and mechanical properties of P(3HB) are summarized in table 5.

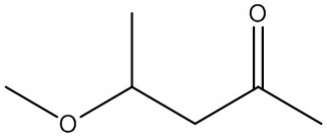

Figure 7: Chemical structure of the monomer 3HB.

Table 5: Thermal and mechanical properties of P(3HB) [53].

Property	Value
Crystallinity	up to 55-80 %
Melting temperature T_m	about 180 °C
Glass transition temperature T_g	about 4 °C
Tensile strength	about 40 MPa
Tensile modulus	about 3.5 GPa
Elongation at break	about 6 %

4

PROTEINS AND NANODIAMOND PARTICLES FOR SURFACE FUNCTIONALIZATION

4.1 FIBRONECTIN

Fibronectin is a glycoprotein very copious in extracellular matrix (ECM) and plasma and it has a molecular weight of about 450 kDa. Fibronectin has a dimer structure, being made up of two polypeptide chains. These chains are bonded by two disulphur bridges in the region of the C-terminals. Each of the chains is made up of about 2500 amino acids (Figure 8).

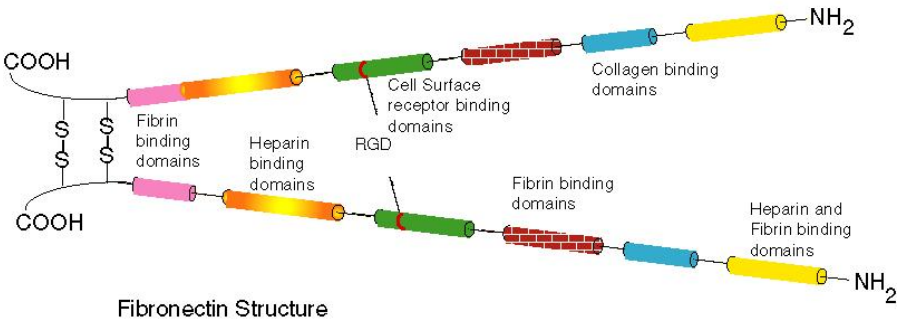

Figure 8: Dimer structure of fibronectin. Image from http://course1.winona.edu/sberg/308s10/Lecnote/Extracellular.htm

Fibronectin is an adhesion macromolecule that affects cell migration and organization. It has been proven to be one of the main adhesive components in plasma and ECM and to accelerate cell attachment and adhesion to the ECM [5]. As a matter of fact, it contains the sequence arginine-glycine-aspartic acid (RGD), which is a receptor for the integrins. Integrins are proteins situated in the cell membrane and they connect it to the cytoskeleton. When they bind to the RGD sequence on the fibronectin, they allow cell-ECM adhesion. The importance of the RGD sequence was proved by observing that synthetic peptides that include the RGD sequence can induce cell adhesion about as effectively as the native protein (fibronectin) [54, 55].

Moreover, fibronectin presents binding affinities for collagen, fibrinogen, fibrin, proteoglycans, cell membranes and actin [56]. For this reason, fibronectin has been widely applied for the functionalization of biomaterials in general and of polymers in particular. For instance, Dånmark et al. [6] demonstrated that the polymers PLA,

poly(LLA-co-CL), poly(LLA-co-DXO) and polystyrene could be effectively functionalized with fibronectin, to improve cell adhesion.

4.1.1 *Cell adhesion and interactions with fibronectin*

Cell adhesion, to a substrate or to the extracellular matrix, includes a sequence of four steps: cell attachment to the substrate, cell spreading, reorganization of the actin cytoskeleton, and formation of focal adhesions. In particular, considering a single detached cell, e.g. a single fibroblast, that encounters an adhesive glycoprotein, e.g. fibronectin, the four steps are [54]:

1. *Cell attachment to the substrate.* The cell contacts the fibronectin and it attaches to the substrate;

2. *Cell spreading.* The second phase of cell adhesion starts when the fibroblast body begins to flatten. The cell membrane spreads over the surface until it gets a shape that depends on the cell type;

3. *Reorganization of the actin cytoskeleton.* The cell organizes the actin to form microfilaments and it remodels its cytoskeleton;

4. *Formation of focal adhesions.* Eventually, special entities called focal adhesions are formed. They effectively link molecules of the extracellular matrix to the microfilaments of the cell actin cytoskeleton. Moreover, they also affect the cytoskeleton reorganization and the transmembrane signaling between the inner and the outer environment of the cell.

4.2 GROWTH FACTORS

The growth factors are proteins that regulate several cell functions. They can affect different kinds of cells and induce different effects according to the cell type. In general, the growth factors govern cell proliferation, migration and differentiation [57]. In the biological tissues, these proteins are attached to the ECM and they transmit signals to build up complex cellular structures [58].

In this work, a specific type of growth factors was considered: the Bone Morphogenetic Protein-2 (BMP-2).

4.2.1 *Bone Morphogenetic Protein-2 (BMP-2)*

BMP-2 is a growth factor of the family of the Bone Morphogenetic Proteins (BMP). It is osteoinductive, meaning that it stimulates osteoblasts differentiation and development. In general, the BMP proteins have the role of inducing migration, proliferation and differentiation of bone cells [59].

BMP2 is used as an adding agent to heal bone defects and to regenerate bone tissue. Some drawbacks of this method are the rapid diffusion of BMP-2 from the site of the defect, the decrease of its bioactivity in time and the fast degradation in vivo. So, several strategies have been developed to guarantee a longer-term duration of the BMP2 effect. For example, BMP2 can be either adsorbed onto collagen on polymer scaffolds, or covalently coupled to degradable polymers. However, the second method has some disadvantages, being the degradable polymers instable, subject to degradation and sensitive to solvent effects [60].

4.3 NANODIAMOND PARTICLES (NDP)

Nanodiamond particles (nDP), are single crystals of diamond particles. A subclass of nDP are the Detonation NanoDiamonds (DND), which are originated from a detonation of a TNT/hexogen composition, in absence of oxygen and carbon sources. After detonation, three main events occur. First of all, the diamond growth process begins. Then, the surface of the diamond particle starts to convert into graphite. Eventually, diamond particles start to aggregate in soot-like structures. The nanodiamonds produced have a diameter of about 4-5 nm [61].

Nanodiamond particles present good mechanical and chemical properties, such as hardness, thermal conductivity, dopability, optical transparency, inertness, small size and surface structure, as well as non-cytotoxicity [62]. For this reason, biomedical applications of nanodiamonds, e.g. drug delivery and labeling, are being studied [63]. Nanodiamond particles can also be employed for surface functionalization of artificial joints, for instance for hip replacement [64].

Moreover, it is possible to functionalize effectively the nanodiamonds surface with growth factors, fibronectin, DNA or other proteins and biomolecules. In particular, Steinmueller et al. [65] stated that the bonding between nDP and BMP2 is stable, effective, and that it enhances osseointegration in the living tissues. Grafting can be performed by either covalent or non-covalent attachment of functional groups on the surfaces. Furthermore, Lechleitner at al. [66] proved that the presence of nanodiamonds on a surface enhances cell adhe-

sion and that the surface itself is non-cytotoxic. Another study proved that a coating of apatite and nanodiamonds on a stainless steel surface ehnances the adsorption of fibronectin and osteoblast adhesion. This effect was more relevant at low concentrations of fibronectin (about 1 $\mu g/mL$) rather than at high concentrations (e.g. 30 $\mu g/mL$) [67].

5 MATERIALS

5.1 CHEMICALS

The following products were purchased from *Sigma-Aldrich* (Steinheim, Germany) and used as received:

- (3-aminopropyl)triethoxysilane;
- (3-aminopropyl)trimethoxysilane;
- (3-mercaptopropyl)trimethoxysilane;
- Acetic acid;
- Chloromethylsilane;
- Diethyl ether;
- Dimethyl sulfoxide (DMSO);
- Dulbecco's Modified Eagle's Medium (DMEM);
- Hydrogen peroxide;
- Polyethylene glycol (PEG), molecular weight 2000 Da;
- Polyethylene glycol (PEG), molecular weight 35000 Da;
- Stannnous octoate;
- Tryethylamine (TEA);
- Tween 80;

The following products were purchased from *Fisher scientific* (Leics, UK) and used as received:

- Chloroform;
- Dimethylformamide (DMF);
- Toluene;

The following products were purchased from *VWR* (Leuven, Belgium) and used as received:

- Dichloromethane (DCM);
- Ethanol;

- Hexane;
- Methanol;

The following products were purchased from *Scharlab* (Sentmenant, Spain) and used as received:

- Tetrahydrofuran (THF);

The following products were purchased from *Cambridge Isotope Laboratories* (Andover, USA) and used as received:

- Deuteron-chloroform;

The following products were purchased from *PAA Laboratories* (Pasching, Austria) and used as received:

- Phosphate-Buffered Saline (PBS);

The following products were purchased from *BASF* (Ludwigshfen, Germany) and used as received:

- Polyvinylamine (PVAm);

L-lactide was purchased from *Boehringer* (Ingelheim, Germany) and recrystallized according to a previously published method [68].

Poly(LLA-co-CL) was prepared by ring-opening polymerization following the method previously described [69].

Polystyrene was collected from cell tissue culture plates purchased from *Thermo Scientific*.

Colloidal nano-diamond particles were prepared as described in [70].

5.2 MATERIALS FOR QCM EXPERIMENTS AND PREPARATION

Silicon wafers, with silicon oxide on the surface, were purchased from *MEMC Electronics Materials* (Novara, Italy).

The air plasma cleaner employed for this thesis, model PDC 002, was purchased from *Harrick Scientific Corporation* (NY, USA).

The spin coater was purchased from *Pi-KEM* (Staffs, UK).

The QCM apparatus, model E4, and the sensors XQ303 coated in silicon dioxide were purchased from *Q-Sense AB* (Västra Frölunda, Sweden).

5.3 CHARACTERIZATION METHODS

The contact angle equipment, a KSV 200 CAM goniometer, was purchased from *KSV Instruments* (Helsinki, Finland). The data were processed with a CAM 2008 software (version 4.0, KSV).

The Scanning Electron Microscopes, model Tabletop TM-1000 and model S-4800, were purchased from *Hitachi*.

NMR spectra were recorded with a Bruker Advanced Nuclear Magnetic Resonance Spectrometer, operating at 400 MHz.

DSC analysis of the polymers was perfomed using DSC 820 from *Mettler-Toledo* (Switzerland) .

For size-exclusion chromatography measurements a Verotech PL-GPC 50 Plus system from *Varian Inc* (MA, USA) was used.

6 METHODS

6.1 POLYMERIZATION OF PLA-PEG-PLA

In order to synthesize and test the triblock copolymer PLA-PEG-PLA, five reactions were prepared, with different molar ratios of reactants and different molecular weights of PEG (Table 6). This was done with the purpose of testing different molecular weights and degrees of polymerization. Polymerization was made by ring-opening of L-lactide and stannous octoate $Sn(oct)_2$ was used as catalyst. The molecular weight of L-lactide was 144 g/mol for all the reactions, while for PEG were employed two different molecular weights: 35000 g/mol for reaction (1) and 2000 g/mol for the other reactions.

The design of the reactions was made according to the following criteria:

- Reaction (2) had the same feeding ratio as reaction (1), but the PEG employed had a different molecular weight: $PLA-PEG_{35000}-PLA$ = 1:1:1 for reaction (1); $PLA-PEG_{2000}-PLA$ = 1:1:1 for reaction (2);
- Reaction (3), i.e. $PLA-PEG_{2000}-PLA$ = 20:1:20, was designed to produce a polymer with a similar molecular weight of the product of reaction (1). As a matter of fact, a theoretical molecular weight of 161000 g/mol was expected for the product of reaction (1) and a value of 128000 g/mol for reaction (3);
- Reactions (2), (4) and (5) were designed to have a lower molecular weight than other reactions. In particular, Reaction (2) $PLA-PEG_{2000}-PLA$ = 1:1:1 was expected to give a molecular weight of 5600 g/mol; Reaction (4) $PLA-PEG_{2000}-PLA$ = 2:1:2 was expected to give a molecular weight of 5240 g/mol; Reaction (5) $PLA-PEG_{2000}-PLA$ = 1:1:1 was expected to give a molecular weight of 5600 g/mol;
- The difference between reaction (2) and (5) was the reaction time: the fifth reaction was left to react for about 60 hours, while the second one only 30 hours.

The first step was flasks silanization. Without silanization, the catalyst stannous octoate would initiate a reaction by binding to the hydroxyl groups on the glass surface of the flask. So, the purpose of silanization is to bind the molecules of chloromethysilane to the hydroxyl groups that are on the glass surface (Figure 10).

Table 6: Inital feed ratios to obtain PLA-PEG-PLA.

Reaction number	Feed ratio LA:PEG:LA	Molecular weight of PEG (g/mol)	Reaction time (hours)
1	1:1:1	35000	168
2	1:1:1	2000	30
3	20:1:20	2000	18
4	2:1:2	2000	60
5	1:1:1	2000	60

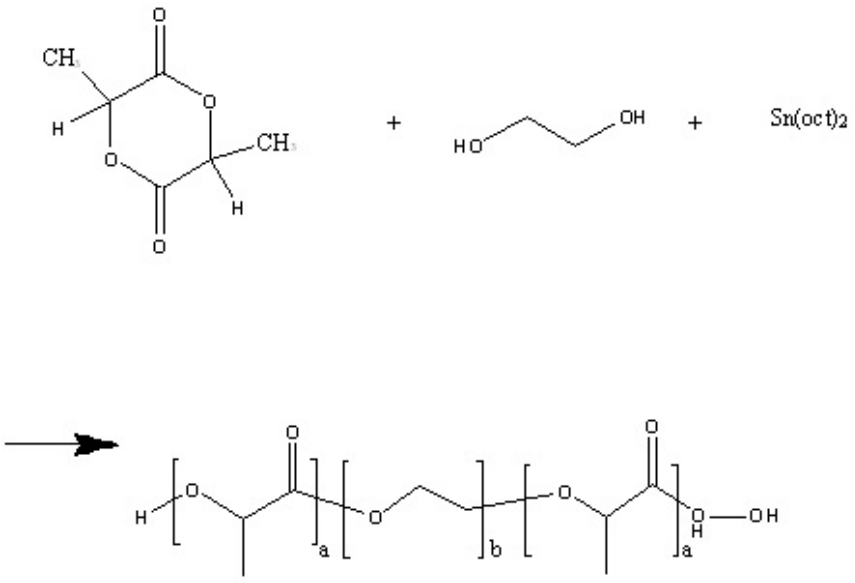

Figure 9: Reaction scheme for the triblock copolymer PLA-PEG-PLA.

the glasswares were filled with dichloromethane, 5 % v/v dichlorodimethylsilane and 10 % v/v triethylamine. Then, the solution was kept under stirring at room temperature for half an hour. The solution was then removed and the glasswares were rinsed with acetone and dried in oven at 100 °C. After flasks silanization, pure PEG, L-lactide, $Sn(oct)_2$ were placed in the flasks and kept at a constant temperature of 120 °C. The reactions were then terminated at room temperature, by adding 30 mL of chloroform. Later, to purify the reaction product, unreacted L-lactide was dissolved a solution of 90 % hexane and 10 % methanol, while for unreacted ethylene glycol diethyl ether was employed. The number of precipitations and the yield obtained for each copolymer are summarized in table 7. After each precipitation, ^1H NMR was employed to analyze the percentage of impurities (see Section 6.2.1).

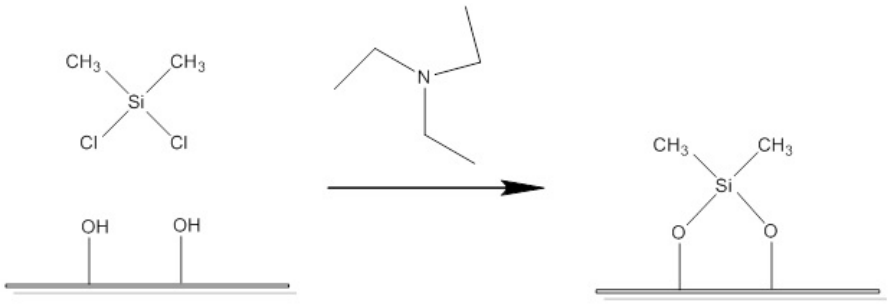

Figure 10: Reaction of silanization

Table 7: Numer of precipitations after each of the reactions to obtain PLA-PEG-PLA.

Reaction number	Feed ratio LA:PEG:LA	Molecular weight of PEG (g/mol)	Nr. of lactide precipitations	Nr. of ehtylene glycol precipitations	Yield (%)
1	1:1:1	35000	4	1	33
2	1:1:1	2000	1	1	0.04
3	20:1:20	2000	2	1	68
4	2:1:2	2000	2	1	24
5	1:1:1	2000	2	1	65

6.2 CHARACTERIZATION METHODS

6.2.1 *Nuclear Magnetic Resonance (NMR)*

During the phase of purification of PLA-PEG-PLA, ^1H NMR spectra were acquired after each precipitation, for each of the reactions summarized in table 6. Also, all the other polymers tested were analyzed in the same manner.

The $^1H - NMR$ analysis was performed at room temperature and about 1mm of chloroform-D ($CDCL_3$) was employed to dissolve the samples in 5 mm samples tubes.

6.2.2 *Size Exclusion Chromatography (SEC)*

Since the yield of the triblock copolymer PLA-PEG-PLA obtained with reaction (2) of Table 6 was too low to allow further investigations and employment for QCM. So, only reactions (1), (3), (4), (5) were further analyzed. First of all, they were analyzed with the size-exclusion chromatography (SEC) for determining their molecular

weights. Size-exclusion chromatography is a chromatographic method to characterize the size and molecular weight of large molecules such as proteins and polymers.

In general, the main components of the SEC apparatus are one or more columns. These are made up of a hollow tube that contains a filter. The filter is a set of porous beads and the pores have different sizes. The polymer solution is eluted through the column and the main idea is that molecules of different size are filtered at different rates. In fact, molecules having wider dimensions go faster through the column, passing in the empty spaces between the beads. Instead, smaller molecules go inside the pores of the beads and their passage through the column is delayed (11).

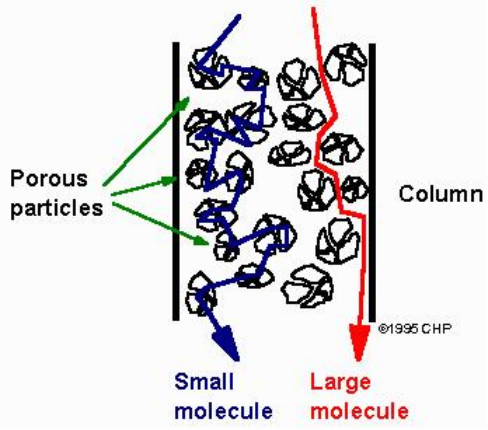

Figure 11: Schematic representation of a SEC column. Image from http://www.files.chem.vt.edu/chem-ed/sep/lc/size-exc.html

This technique allows to obtain a distribution of the molecular weights included in the sample. In particular, different values are provided to express the average molecular weight:

1. The number average molecular weight M_n represents the arithmetic average of the single molecular weights of the sample's molecules and it is calculated as

$$M_n = \frac{\sum_i N_i M_i}{\sum_i N_i} = \frac{\sum_i h_i}{\sum_i h_i / M_i} \tag{6.1}$$

   where N_i is the number of molecules having molecular weight M_i, h_i is the height of the SEC curve, calculated from the baseline, and the summation takes into account all the molecular weights present in the polymer solution;

2. The weight average molecular weight M_w is obtained as

$$M_w = \frac{\sum_i N_i M_i^2}{\sum_i N_i M_i} = \frac{\sum_i h_i M_i}{\sum_i M_i} \tag{6.2}$$

3. The z-average molecular weight is defined as

$$M_z = \frac{\sum_i N_i M_i^3}{\sum_i N_i M_i^2} = \frac{\sum_i h_i M_i^2}{\sum_i h_i M_i} \tag{6.3}$$

From these values, it is also possible to calculate the polydispersity index PDI as:

$$PDI = \frac{M_w}{M_n} \tag{6.4}$$

During this work, about 9 mg of polymers were dissolved in 3 mL of chloroform and prepared in SEC-vials. A Verotech PL-GPC 50 Plus system equipped with a PL-RI Detector and two PLgel 5 µm MIXED-D (300 × 7.5 mm) columns from *Varian* were employed to analyze the samples. The samples were injected with a PL-AS RT Autosampler for PL-GPC 50 Plus and chloroform was used as the mobile phase (1 mL/min, 30 °C). Polystyrene standards with a narrow molecular weight distribution were used to calibrate the system and toluene was employed to make corrections for flow-rate fluctuations. Eventually, the data were processed with Cirrus™ GPC Software.

6.2.3 *Contact angle*

To evaluate surface hydrophilicity, static contact angle measurements were performed with a KSV 200 CAM goniometer from *KSV Instruments*.

In general, the contact angle is a measure of the ability of a liquid to spread on a surface. This technique consists of measuring the outline tangent of the drop on the surface and the surface itself. From these measurements, it is possible to quantify surface hydrophilicity and energy [71, 72].

When a drop of liquid lays on a solid surface, three interfacial tensions must be taken into consideration (Figure 12):

1. Solid-vapor tension γ_{sv};
2. Solid-liquid tension γ_{sl};
3. Liquid-vapor tension γ_{lv}.

The Young's equation defines the equilibrium relation [73]:

$$\gamma_{lv}\cos\theta_\gamma = \gamma_{sv} - \gamma_{sl} \tag{6.5}$$

where θ_γ is the Young's contact angle.

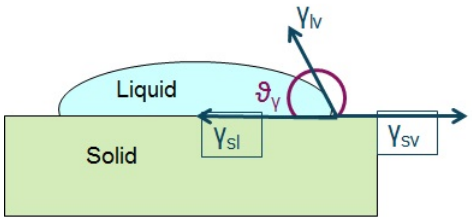

Figure 12: Schematic representation of a contact angle system (Image from [71]).

In practice, contact angles present hysteresis, ranging from an advancing contact angle θ_a (upper limit) to a receding contact angle θ_r (lower limit). The hysteresis H is given by the difference between these two angles [71]:

$$H = \theta_a - \theta_r \tag{6.6}$$

From the measure of the hysteresis, it is also possible to gain information about the surface homogeneity and roughness. As a matter of fact, contact angles are wider on rough surfaces than on smooth surfaces. So, for smooth surfaces θ_a can be considered a good approximation of θ_γ, while for rough surfaces the Young's equation does not hold any more. In general, for smooth surfaces, values of contact angle $\theta_\gamma < 90\,^\circ$ are associated to surface hydrophilicity, while for $\theta_\gamma > 90\,^\circ$ the surface is considered hydrophobic (Figure 13).

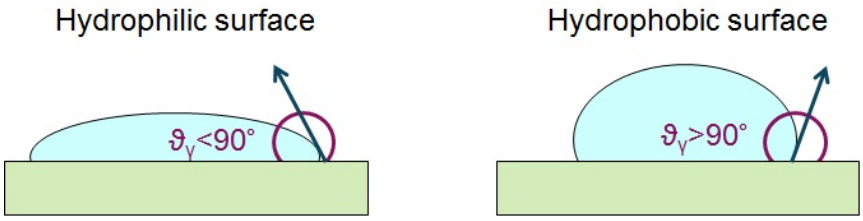

Figure 13: Schematic representation of the contact angle for hydrophilic and hydrophobic surfaces.

To evaluate the polymers employed for this project, the samples were prepared by dissolving 0.12 g of polymer in 15 mL of chloroform. Then, thin polymer films were obtained by solvent casting and dried in vacuum. The samples were stored at 20 °C and 50 % humidity for 24 hours. Within the contact angle system, 5 µL drops of MilliQ water were placed on the films of samples. An optical camera recorded the frames from four independent drops for every sample. At the end, the contact angle values were calculated by the CAM 2008 software as an average of the four measurements.

6.2.4 *Differential Scanning Calorimetry (DSC)*

Differential Scanning Calorimetry (DSC) is a thermal analysis method, which measures how the physical properties of a sample are modified if the temperature increases or decreases in time. In particular, it monitors the temperature and heat flow associated to material transitions, such as glass transition and melting. The heat flow is calculated on the basis of temperature difference between the sample and the reference material in the same conditions [74, 75]. This technique can be used to analyze polymeric samples, in order to obtain information such as crystallinity, melting temperature and glass transition temperature.

DSC analysis of the polymers considered in this work was perfomed using Mettler-Toledo DSC 820. Standard 40 µL alluminium cups enclosed about 3 mg of each sample. The samples were then subjected to the following thermal cycles:

1. The temperature was increased from -50 °C to 200 °C, at a rate of 10 °C/min;
2. The temperature was kept constant at 200 °C for 5 minutes;
3. The temperature was decreased until -50 °C at 10 °C/min;
4. Eventually, the temperature was kept constant at -50 °C for 5 minutes;
5. The temperature was raised until 200 °C at a rate of 10 °C/min.

The whole process took place under a nitrogen gas flow of 80 mL/min. Glass transition temperature T_g and melting temperature T_m were measured from the second thermal cycle. The degree of crystallinity χ_c was calculated as

$$\chi_c = \frac{\Delta H_f}{\Delta H_f^0} 100\% \tag{6.7}$$

where ΔH_f is the heat of fusion of the sample and ΔH_f^0 is the corresponding value for a 100 % crystalline polymer. The reference values used for ΔH_f^0 were 93 J/g for PLA [76], 139.5 J/g for PCL [77], 180 J/g for PEG [78], 139 J/g for PGA [79].

6.2.5 *Scanning Electron Microscopy (SEM)*

A table-top Scanning Electron Microscopy (SEM) was employed to observe the conditions of polymer layers on silicon oxide surfaces. The accelerating voltage was 15 kV and the polymer layers were observed at magnifications ranging from 40x and 3000x. Instead, a S-4800 SEM

Hitachi was used to observe the surfaces of QCM crystals flushed with nanodiamond particles. The acceleration voltage was set to 1.5 kV and the samples were coated with a 5 nm layer of Au/Pd by a Cressington 208 HR High Resolution Gold/Palladium sputter.

6.2.6 *Atomic force microscopy (AFM)*

The Atomic Force Microscopy (AFM) is a high-resolution microscope. It provides a resolution of the order of magnitude of a nanometer and it is used to obtain information about the topography of a surface. The Atomic Force Microscopy sensor consists of a cantilever with a tip, which scans the sample surface. Due to the interaction forces between the tip and the sample surface, the cantilever is deflected. The images are obtained from the vertical movement of the cantilever as a function of the lateral movement in the horizontal plane [80, 81].

In general, there are three imaging modes:

1. *Contact mode.* The tip of the cantilever is always in contact with the sample surface. The force between the tip and the sample is kept constant by a feedback loop. The main drawback of this imaging mode is that it provokes the damage of the sample. However, it provides high vertical resolution.

2. *Non-contact mode.* The cantilever oscillates at its resonance frequency, a few nanometers above the sample. The amplitude or the frequency of the oscillations is kept constant by a feedback loop that adjusts the distance between the tip and the sample. This imaging mode does not damage the sample, but it does not provide as high resolution as the contact mode.

3. *Tapping mode.* The cantilever oscillates at its resonance frequency and at some points it taps the sample. The variation of oscillation amplitude is measured and the image of the specimen surface is reconstructed. This method does not damage soft samples, while providing a high vertical resolution.

6.3 PREPARATION OF QCM CRYSTALS

6.3.1 *Preparation of silicon oxide surfaces*

Since the QCM crystals used for this project were coated in silicon oxide, tests for evaluating the polymers behavior in contact with

silicon oxide were performed. For these tests, silicon wafers naturally coated with silicon didioxide were employed. Small squares of about 1 cm^2 area were cut from bigger wafers and used for the tests. In the following text, the term *silicon dioxide surface* will refer both to silicon wafers and to QCM crystals.

Before performing any modification on silicon dioxide surfaces, both the QCM crystal and the silicon wafers were cleaned according to the following procedure:

1. The silicon dioxide surfaces were rinsed with water, ethanol and water;
2. They were dried under a stream of nitrogen;
3. They were placed in an air plasma cleaner at reduced air pressure at 30 W for 2 minutes.

6.3.2 *Spin coating of silicon dioxide surfaces*

Spin coating is a technique employed to cover flat substrates with thin films.

The QCM quartz crystals and silicon wafers were then coated by dropping 100 µL of polymer solution (Figure 14). The crystals were made to spin at 1500 rpm for 15 seconds and, then, at 3000 rpm for 30 seconds by the spin coater. In this way, the centrifugal force caused a spreading of the solution on the surface, the ejection of the excess of solution off the substrate and the evaporation of the solvent [82]. Later, the silicon dioxide surfaces were dried in vacuum for at least one hour, to guarantee complete solvent evaporation.

In some experiments, when a thinner polymer layer was needed, the spin coating rates were raised to 2500 rpm for 15 seconds followed by 5000 rpm for 30 seconds.

6.3.3 *Choice of the solutions for spin coating*

In order to choose the most suitable solvent for spin coating, the first tests were performed on silicon wafers covered in silicon dioxide.

In general, the layers obtained must be as even, homogeneous and thin (about 30 nm for polymers) as possible, without superficial defects. An important factor that affects the result is the solvent evaporation rate. This parameter is proportional to spin speed and depends on other factors such as air flow conditions and solvent saturation of the spin environment [83].

The wafer surfaces were cleaned as explained in Section 6.3.1. Different solutions of polymers, varying solvents and concentrations, were

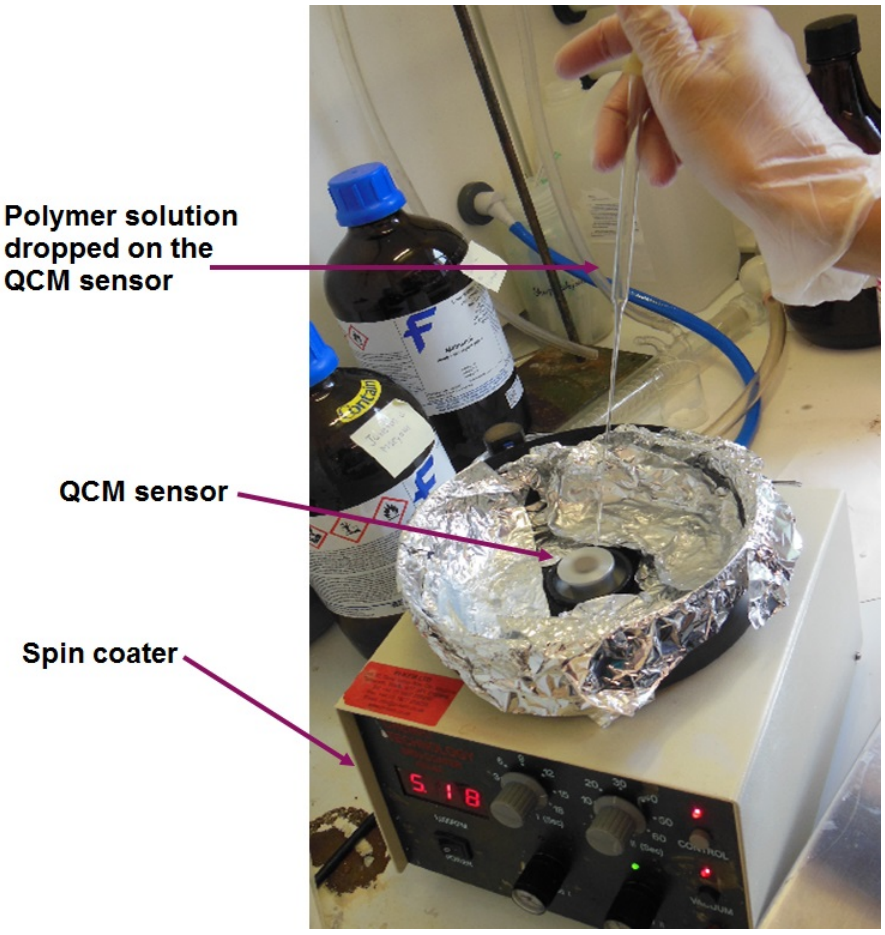

Figure 14: Spin coating equipment employed for this project.

prepared. In particular, the solvents chloroform ($CHCl_3$), dichloromethane (CH_2Cl_2), dimethylformamide (DMF) and tetrahydrofuran (THF) were tested. For each solvent, different solutions of polymers were prepared, with concentrations 0.1 mg/mL, 1 mg/mL, 2 mg/mL, 5 mg/mL and 10 mg/mL. The polymers poly(LLA-co-CL), PLA-PEG-PLA (3) and P(3HB), 5HV, PLA, PCL, poly(TMC-D-LA), PS and PGA were tested.

6.3.4 *Pre-coating methods*

Pre-coating with polyvinylamine (PVAm)

Some researches employed polyvinylamine (PVAm) as a pre-coating for QCM crystals, in order to stregthen the adesion of different materials to the crystal surface [84, 85]. Before spin coating, for some tests the silicon dioxide surfaces were pre-coated with PVAm, with molecular weight 340 kDa, according to the following procedure:

1. The silicon dioxide surfaces were cleaned as explained in Section 6.3.1;
2. They were submerged in a solution of PVAm for 15 minutes;
3. Eventually they were dried in vacuum.

Later, they were spin coated as explained in section 6.3.2. All the polymers solutions selected in Section 7.2 were tested.

Amino functionality

Morrill et al. [86] proposed a method to introduce amino functionality on silicon dioxide surfaces. A similar method was employed by Atthoff and Hilborn [**?**] for treating QCM crystals, before spin coating PLA, in order to avoid polymer detachment during the QCM measurements. In this thesis, the procedure was applied to the silicon wafers, for testing its validity for the chosen polymers, according to the following protocol:

1. The silicon wafers were prepared as in Section 6.3.1;
2. The silicon wafers were submerged in a solution of (3-aminopropyl)triethoxysilane (APTES) 1 wt % dissolved in ethanol at room temperature for 24 hours;
3. The silicon wafers were dried in vacuum for one hour;
4. The silicon wafers were spin coated as illustrated in Section 6.3.2.

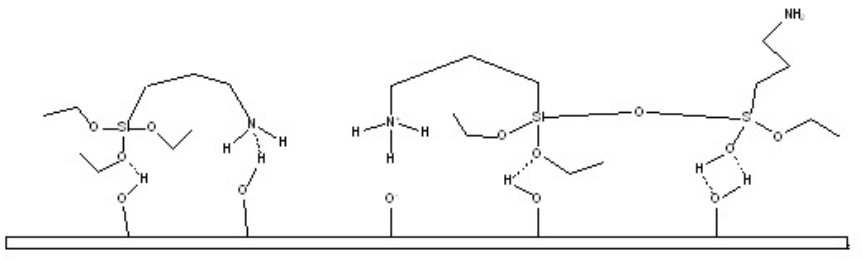

Figure 15: Schematic representation of the amino functionality on silicon dioxide surfaces. Image adapted from [87].

6.3.5 *Reuse of QCM crystals*

The QCM crystals were reused up to ten times. After each experiment, they were cleaned according to the following procedure:

1. The crystals were submerged in chloroform for one hour;

2. They were rinsed with MilliQ water;
3. They were rinsed with hydrogen perdioxide;
4. They were rinsed with MilliQ water;
5. The crystals were submerged in a solution of Sodium Dodecyl Sulfate (SDS) 2 wt % in MilliQ water for 30 minutes;
6. They were rinsed with MilliQ water;
7. They were dried in vacuum for one hour.

6.4 COATING TESTS WITH SILICON DIOXIDE WAFERS

6.4.1 *Evaluation of polymer layer conditions*

For checking the condition of the polymer layer on the silicon dioxide surface after contact with water, tests were performed on silicon dioxide wafers. Several silicon wafers were spin coated with polymer solutions and submerged in deionized water for 24 hours, either at room temperature or at 37 °C. In some cases, the tests were repeated with submersion in Phosphate-Buffered Saline (PBS) or Dulbecco's Modified Eagle's Medium (DMEM) for comparison. After submersion, the wafers were dried in vacuum for one hour.

For some tests, additional treatments on silicon wafers were performed before submersion in water. For instance, pre-coating with PVAm (Section 6.3.4), amino functionality (Section 6.3.4), coating stabilization at 37 °C (Section 6.4.1), coating stabilization above the glass transition temperature (Section 6.4.1).

The polymers employed for these tests were:

- PLA;
- Poly(LLA-co-CL);
- PLA-PEG-PLA (3) of Table 6;
- PLA-PEG-PLA (4) of Table 6;
- PLA-PEG-PLA (5) of Table 6;
- PCL;
- poly(TMC-D-LA);
- PGA;
- PS;

- P(3HB);
- 5HV;
- Double coating: first layer of PLA, followed by a layer of poly(LLA-co-CL);
- Double coating: first layer of PLA, followed by a layer of PLA-PEG-PLA;

and they were dissolved in chloroform, or in DMF in some cases, in concentrations:

- 0.1 mg/mL;
- 1 mg/mL;
- 2 mg/mL;
- 2.5 mg/mL;
- 5 mg/mL;
- 10 mg/mL;

The polymer layer conditions were assessed with a visual naked-eye analysis and with further SEM observations. SEM images were recorded at different magnifications.

Coating stabilization in incubator

An idea to make the polymer layers more strongly attached to the silicon dioxide surfaces was to leave the silicon wafers and the QCM crystals to adapt to the high temperature after spin coating and before submersion in water. The following procedure was applied to the silicon wafers:

1. The silicon wafers were prepared as in Section 6.3.1;
2. The silicon wafers and the solutions for spin coating were kept in the incubator at 37 °C for 24 hours;
3. The silicon wafers were spin coated as in Section 6.3.2;
4. The silicon wafers were dried in vacuum at room temperature for one hour;
5. The silicon wafers were kept in incubator at 37 °C for 2 hours;
6. The silicon wafers were submerged into water and kept in incubator at 37 °C for 24 hours.

Coating stabilization above the glass transition temperature

As proposed by Oliveira et al. [10], after spin coating the silicon wafers were placed in oven at 62 °C for 48 hours. This temperature is 5 °C higher than the glass transition temperature measured for the polymers considered (T_g = 57.09 °C for PLA). Then, the same procedure adopted for the previous tests was followed:

1. Submersion in water and incubation at 37 °C for 24 hours;
2. Drying in vacuum for one hour;
3. SEM and visual naked-eye analysis.

6.4.2 *Evaluation of the effect of air plasma treatment on silicon dioxide surfaces and on the polymer layers*

The air plasma treatment introduces free radicals on silicon dioxide surfaces, i.e. on silicon wafers and QCM crystals surfaces. So, it enhances surface hydrophilicity. For evaluating the effectiveness and the consequences of this treatment, several tests were performed.

First of all, contact angle measurements were performed on silicon wafers before and after air plasma treatment. The duration of plasma treatment was also varied.

Then, silicon wafers, without being previously treated with air plasma, were spin coated with different polymer solutions. Then, they were submerged in water and kept in incubator at 37 °C for 24 hours. To make a comparison, a control set of silicon wafers were pre-treated with air plasma and subjected to the same procedure of the other silicon wafers. All the surfaces were also observed with a Scanning Electron Microscope.

This test was performed to investigate whether an increase in surface hydrophilicity of the silicon dioxide surfaces could guarantee a stronger adhesion of hydrophilic polymers such as, for example, PLA-PEG-PLA.

6.4.3 *Effect of the polymer layer thickness*

For evaluating the effect of the polymer film thickness, silicon wafers with thinner polymeric films were prepared. 0.1 mg/mL solutions of polymers dissolved in chloroform were employed and the wafers were spin coated at a rate of 2500 rmp for 15 seconds, followed by 5000 rmp for 30 seconds. The surfaces were analyzed with SEM before and after submersion in water at 37 °C for 24 hours.

6.4.4 *Summary of coating tests on silicon dioxide wafers*

A summary of the coating tests performed on silicon dioxed wafers, applying the methods explained in section 6.4, is presented in Figure 16.

Temperature	Plasma treatment	Pre-coating method	Coating stabilization	Polymer	Polymer concentration
24 °C	Plasma treatment	No pre-coating; PVAm; Amino functionality;	No coating stabilization	poly(LLA-co-CL)	1 wt % 5 wt % 10 wt %
				PLA-PEG-PLA (3)	2 wt % 10 wt %
				P(3HB)	2.5 wt %
				5HV	2.5 wt %
37 °C	Plasma treatment	No pre-coating; PVAm; Amino functionality; PLA;	No coating stabilization; Coating stabilization in incubator; Coating stabilization above Tg.	PLA	0.1 wt % 5 wt %
				poly(LLA-co-CL)	0.1 wt % 1 wt % 5 wt % 10 wt %
				PLA-PEG-PLA (3)	0.1 wt % 2 wt % 10 wt %
				PLA-PEG-PLA (4)	2 wt % 10 wt %
				PLA-PEG-PLA (5)	2 wt % 10 wt %
	No plasma treatment	No pre-coating; PVAm; Amino functionality		PCL	5 wt %
				TMC-D-LA	0.1 wt % 5 wt %
				PGA	0.1 wt % 5 wt %
				PS	0.1 wt % 5 wt %
				P(3HB)	2.5 wt %
				5HV	2.5 wt %

Figure 16: Summary of coating tests on silicon dioxide wafers.

6.5 QCM TESTS

6.5.1 *Setup of the Quartz Crystal Microbalance*

QCM-D tests were performed with a QCM instrument model E4 from *Q-Sense*. In general, in order to start a QCM-D experiment, a QCM sensor must be placed inside a chamber. The sensors used for this project are made up of a quartz crystal coated in silicon dioxide and golden electrodes (Figure 17). Two hollow plastic tubes are then connected to the chamber: one for the input solution, that must flow above the crystal, and the other to collect the solution from the chamber and moving it in a waste container (Figure 18). The flow of the solution is achieved thanks to a pump, that allows to select the rate of flow. For this project, the flow rate was set to 50 $\mu L/min$ for evaluating proteins and nDP behavior. This value of flow rate was chosen because it was in the range of values used by other authors to investigate cell adhesion (i.e. about 30-60 $\mu L/min$ [8, 19]. As a matter of fact, higher flow rates would prevent cell adhesion onto the surface by flushing them away from the sensor chamber.

The sensor chamber is then mounted inside a machine, that allows to apply a voltage to the electrodes of the sensor and to modify the temperature inside the chamber. In this thesis, it was chosen to evaluate polymer, nDP and proteins behavior at 37 °C, in order to establish a procedure that can be applied for researches involving cells as well.

The machine is connected to a processor that records frequency shift and dissipation energy (Figure 19). The odd harmonics of the crystal resonance frequency were monitored, up to the 13th overtone. Later, the 3rd, 5th, 7th and 9th overtones were considered to extract information about mass changes on the material surface. In particular, the first overtone was neglected because it did not provide consistent results with the other overtones, as previously done by other authors [16].

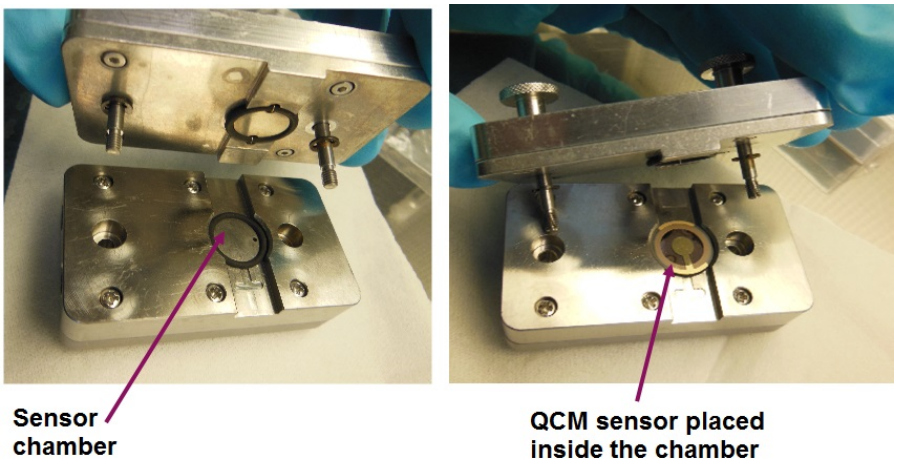

Figure 17: QCM crystal placed inside the chamber of a QCM apparatus, model E4 from *Q-Sense*.

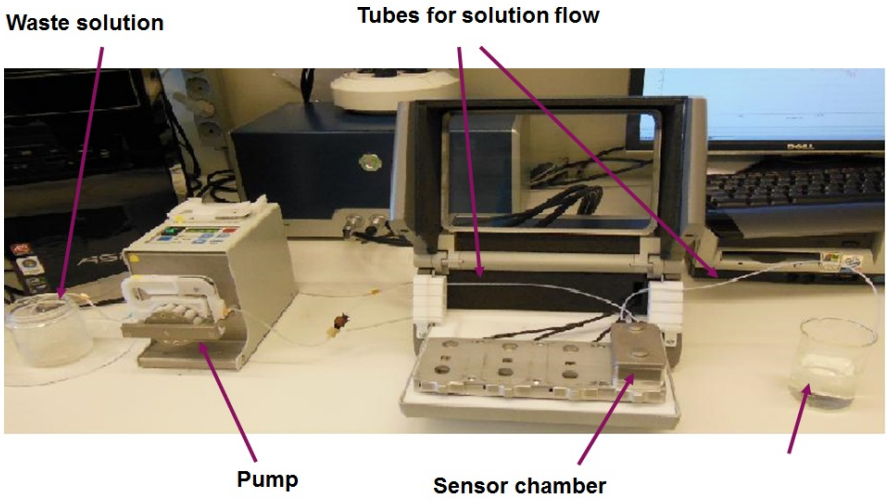

Figure 18: Setup of a QCM experiment: the crystal chamber connected to two tubes and a pump for the flow of solutions. QCM apparatus model E4 from *Q-Sense*.

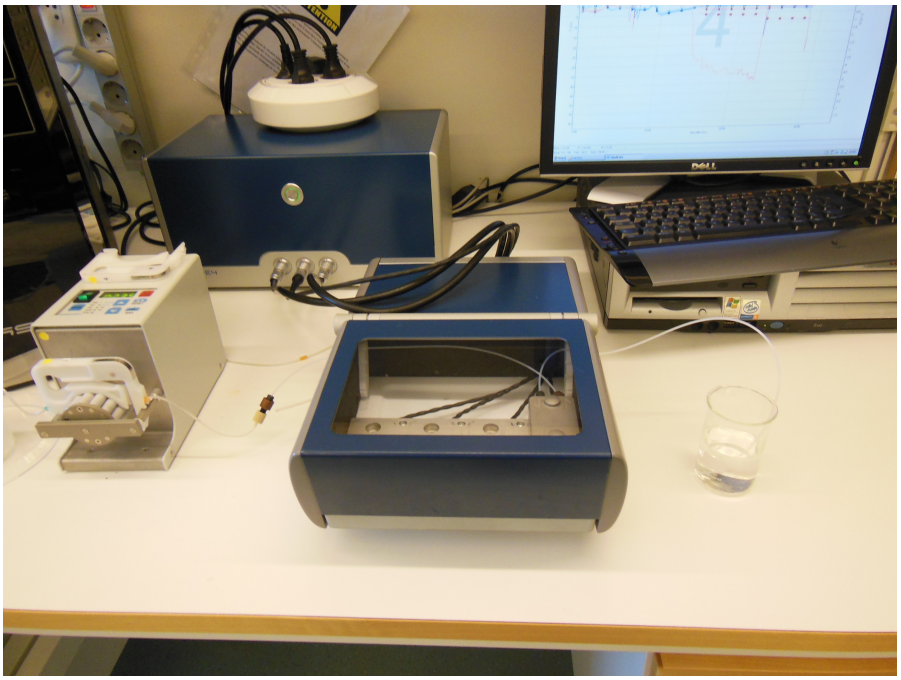

Figure 19: Setup of a QCM experiment: the instrument is ready to acquire frequency shift and dissipation energy. QCM apparatus model E4 from *Q-Sense*.

6.5.2 *First step: obtaining a stable baseline with polymer coating*

To obtain reliable QCM measurements, the first step is to have a stable baseline in the curves of frequency shift and dissipation energy, after positioning the crystal coated with polymer and flushing MilliQ water over the crystal, through the machine. In other words, the frequency shift must remain approximately constant in a range 0 ± 2 Hz. The first measurements with the QCM machine were run flowing MilliQ water over the crystals coated with the polymer layer, at a temperature of 24 °C.

Obtain a stable baseline with PVAm pre-coating at 24 °C

QCM tests were performed to check if the PVAm pre-coating allowed to obtain a stable baseline in the frequency shift and dissipation energy curves. PLA-PEG-PLA (3) and poly(LLA-co-CL) were used as polymer layers, MilliQ water was flushed at 200 $\mu L/min$ at a constant temperature of 24 °C.

First tests to obtain a stable baseline at 37 °C

QCM tests were performed to evaluate if the films of PLA-PEG-PLA 2 mg/mL, poly(LLA-co-CL) 5 mg/mL and 5HV 2.5 mg/mL were stable enough to allow the QCM measurements at 37 °C. PVAm and amino functionality pre-coating method were used for PLA-PEG-PLA and poly(LLA-co-CL), while for 5HV no pre-coating method was employed. MilliQ water was flushed at a constant flow rate of 100 $\mu L/min$.

PLA as a layer and as a pre-coating

Since PLA layers did not detach from the silicon wafers, even after incubation at 37 °C and submersion in water, this polymer was employed for the next QCM experiments. A QCM crystal was coated with a solution 5 mg/mL of PLA dissolved in chloroform, without any pre-coating. Once setting the temperature at 37 °C, MilliQ water was flushed over the crystal, through the QCM. If a flow rate of 200 $\mu L/min$ was employed, the baseline was stable after three hours.

Since PLA seemed to maintain adhesion to the QCM crystal throughout the whole experiments, an idea was to spin coat PLA on the silicon dioxide surfaces before spin coating a second polymer layer. This method was tested both with PLA-PEG-PLA (3) and with poly(LLA-co-CL). Two different QCM tests were run at 37 °C, but none of them allowed to obtain the stability of the baseline. In these tests, PBS was flushed at 50 $\mu L/min$ and frequency shift and dissipation energy were monitored for 15 and 8 hours, respectively.

Crystals coated with 0.1 mg/mL polymer solutions

Several QCM crystals were prepared following the procedure explained in Section 6.4.3. They were spin coated with 0.1 mg/mL polymer solutions at high speed rates. QCM tests were performed flushing MilliQ water as a buffer solutions at 50 µL/min, at a constant temperature of 37 °C. The polymers tested were PLA, PGA, TMA-D-LA, poly(LLA-co-CL), PS, PLA-PEG-PLA (3). Only the crystals coated with PLA were subjected to air plasma treatment before spin coating, while all the other crystals were not treated with air plasma. This choice was based on previous tests performed on silicon wafers (Section 7.3.3).

6.5.3 *First QCM tests to evaluate the absorption of nanodiamond particles (nDP) at 24 °C*

Different tests were performed to assess the interactions between the polymers and nanodiamond particles (nDP). PLA-PEG-PLA (3) and poly(LLA-co-CL) with PVAm pre-coating were employed as polymer layers and the temperature was set to 24 °C. As a buffer solution to flush over the crystal, MiliQ water was employed. Solutions of nDP in different concentrations (e.g. 5 µg/mL, 10 µg/mL, 20, µg/mL, 50 µg/mL) were used and they were flushed at different flow rates, e.g. 50 µL/min, 100 µL/min, 150 µL/min, 200 µL/min.

After the QCM measurements, SEM and AFM images were acquired from the crystals, to compare the QCM curves with the effect observed on the surface at the end of the experiment.

6.5.4 *QCM tests performed with PLA 5 % at 37 °C*

Adsorption of nDP onto PLA 5 mg/mL

Further QCM tests were performed to investigate adsorption of nanodiamond particles onto PLA. The crystals were treated with air plasma and spin coated with a solution of PLA 5 mg/mL. The temperature was set to 37 °C and the flow rate was varied from test to test (e.g. 50 µL/min, 100 µL/min). MilliQ water was used as a buffer solution and nanodiamond particles were diluted in MilliQ water in different concentrations. For every test, the areal mass of the adsorbed nDP layer was calculated with the Sauerbrey equation 2.2. Exploiting the same relationship, it was also possible to obtain the thickness and the density of the adsorbed layer.

Adsorption of Bone Morphogenetic Protein-2 (BMP-2) onto PLA 5 mg/mL

Several QCM tests were aimed to study the adsorption of BMP-2 onto PLA. The growth factor was dissolved in PBS in different concentrations (e.g. 10 µg/mL, 20 µg/mL) and it was flushed over the crystal at 50 µL/min. In some experiments, solutions of nDP were flushed before BMP-2, to evaluate if the presence of nDP enhanced the physisorption of the growth factor. From the Sauerbrey equation, areal mass, thickness and density of the adsorbed BMP-2 were calculated as well.

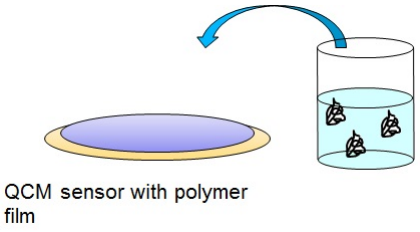

(a) *Solution of BMP-2 flushed directly onto the polymer layer*

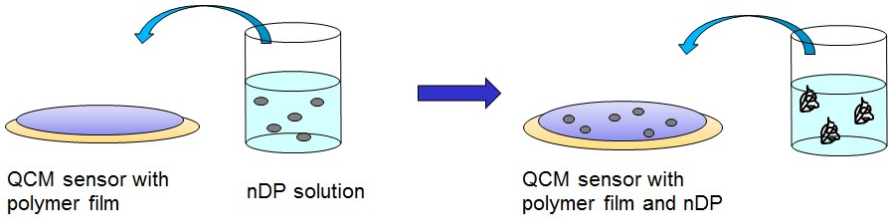

(b) *Solution of nDP flushed onto the polymer layer before flushing BMP-2*

Figure 20: Schematic representation of the solutions flushed onto the polymer film to evaluate BMP-2 adsorption onto PLA 5 mg/mL.

Adsorption of fibronectin onto PLA 5 mg/mL

Other tests were run employing PLA layers obtained from a 5 mg/mL solutions, 37 °C, PBS as buffer solution, flushed at 50 µL/min. When the baseline was stable, a solution of fibronectin dissolved in PBS was flushed. Different concentrations of fibronectin were employed: 6.6 µg/mL, 10 µg/mL, 20 µg/mL, 30 µg/mL. In addition, other tests were performed in the same conditions, flushing a solution of nDP before the flow of fibronectin. In particular, the concentrations of nDP considered were 5 µg/mL, 10 µg/mL, 20 µg/mL, 30 µg/mL, 50 µg/mL and 100 µg/mL. These tests were performed in order to evaluate if the physisorption of nDP affects the adsorption of fibronectin. Also in this case, areal mass, thickness and density values were obtained.

6.5.5 *QCM tests performed with PLA and poly(LLA-co-CL) 0.1 mg/mL at 37 °C*

Once the optimal conditions of coating, temperature, flow rate, buffer solution and range of concentrations were determined, a precise experimental procedure was established. In particular:

1. Air plasma treatment was performed only for the crystals with PLA 0.1 mg/mL coating;
2. Solutions of PLA 0.1 mg/mL and poly(LLA-co-CL) 0.1 mg/mL were used for spin coating;
3. The temperature of the QCM chamber was set to 37 °C;
4. PBS was chosen as buffer solution and flushed at 50 $\mu L/min$ through the QCM chamber.

Solutions of nDP dissolved in water in different concentrations were analyzed: 1 $\mu g/mL$, 5 $\mu g/mL$, 10 $\mu g/mL$, 20 $\mu g/mL$, 50 $\mu g/mL$. Higher concentrations were avoided because in tests performed with PLA 5 mg/mL they did not provide any advantage, in comparison with lower concentrations.

As for BMP-2, it was dissolved in PBS to make solutions of concentrations 1 $\mu g/mL$, 5 $\mu g/mL$, 10 $\mu g/mL$. The same concentrations and solvent were used to make solutions of fibronectin. These were flushed into the QCM chamber with and without pre-absorption of nanodiamonds.

For all the tests, the Sauerbray relationship was employed to obtain information about areal mass, thickness and density of the adsorbed nDP and protein layers.

7

RESULTS AND DISCUSSION

7.1 CHARACTERIZATION METHODS

7.1.1 *NMR analysis*

During the synthesis of PLA-PEG-PLA, ^1H NMR analysis of the polymers was performed after each precipitation. From the spectra, it was possible to calculate the ratio of monomer conversion and chemical composition of the copolymer. These values were obtained from a comparison between relative monomer peak intensities and the corresponding monomer and copolymer peak intensities from the spectra.

In particular, for reaction (1) of Table 6, i.e. $PLA_1 - PEG_{35000,1} - PLA_1$, the spectrum showed a value of 73 % of lactide conversion, meaning that 73 % of lactide monomer was converted into polymer. So, PLA precipitations were necessary to purify completely the sample. Moreover, the composition of lactide was 99.7 % (Figure 21). This means that the reaction did not provide the expected results and there was not any PEG in the product obtained.

As for reaction (2) $PLA_1 - PEG_{2000,1} - PLA_1$, the NMR spectrum revealed 53 % of lactide conversion and a composition of lactide of 59 %. The value of lactide conversion is rather low, meaning that probably the reaction time was too short to allow full polymerization. So, it was decided to prepare another reaction (i.e. reaction (5) of Table 6) with the same feeding ratio, same reactants and longer reaction time.

Instead, the spectrum for reaction (3) $PLA_{20} - PEG_{2000,1} - PLA_{20}$ showed an initial value of 93 % of lactide conversion and a composition of lactide of 84 %. The lactide conversion obtained was high, so the polymer obtained from this reaction was considered for being employed in further tests as well.

The results from NMR analysis for the PLA-PEG-PLA reactions are summarized in Table 8.

7.1.2 *Size-Exclusion Chromatography (SEC)*

As for PLA-PEG-PLA, the number average molecular weight obtained for reaction (1) $PLA_1 - PEG_{35000,1} - PLA_1$ was $M_n = 27$ kDa, that is even lower than the molecular weight of the PEG used for the reaction (35 kDa). The polydispersity index (PDI) was 2.3, mean-

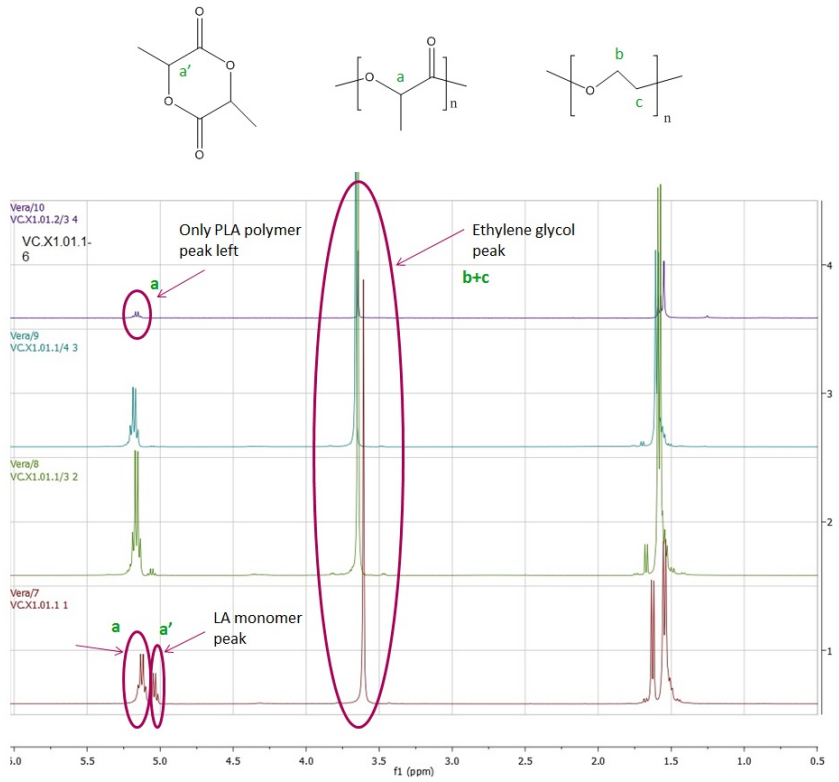

Figure 21: NMR spectrum for $PLA_1 - PEG_{35000,1} - PLA_1$ (1) of table 6. The lower spectrum refers to the original sample, while the spectra above refer to the samples obtained after each precipitation. The spectrum at the top refers to the final copolymer.

ing that the molar mass distribution was broad. So, the copolymer obtained from this reaction was not used further for the QCM tests.

For reaction (3) $PLA_{20} - PEG_{2000,1} - PLA_{20}$, the number average molecular weight was $M_n = 134$ kDa. This value was similar to the expected molecular weight obtained from the theoretical calculations (i.e 128 kDa). So, this copolymer seemed promising to be employed for QCM experiments and it was selected to be used in the following tests (e.g. coating tests on silicon wafers).

On the contrary, the low molecular weight obtained from the reactions (4) $PLA_2 - PEG_{2000,1} - PLA_2$ and (5) $PLA_1 - PEG_{2000,1} - PLA_1$ did not allow to make films by solvent casting from these polymers and powders were produced. Nevertheless, it was decided to employ these polymers for further tests (e.g. coating tests on silicon wafers) to assess their suitability to be used with QCM and to compare their behavior with the higher molecular weight polymer obtained from reaction (3) $PLA_{20} - PEG_{2000,1} - PLA_{20}$.

To make a comparison, other polymers considered for this project were also analyzed with SEC. The results from SEC analysis are summarized in Table 9.

Table 8: Summary of NMR analysis for PLA-PEG-PLA.

Reaction number	Molar ratio LA:PEG:LA	Molecular weight of PEG (g/mol)	L-lactide monomer conversion (%)	Composition of lactide (%)
1	1:1:1	35000	73	99.7
2	1:1:1	2000	53	59
3	20:1:20	2000	93	84
4	2:1:2	2000	95	87.3
5	1:1:1	2000	61	75.3

Table 9: Summary of SEC analysis for PLA-PEG-PLA and bacterial polymers.

Polymer	M_n (kDa)	PDI
$PLA_2 - PEG_{2000,1} - PLA_2$ (4)	10	1.6
$PLA_1 - PEG_{35000,1} - PLA_1$ (1)	27	2.3
$PLA_1 - PEG_{2000,1} - PLA_1$ (5)	39	1.2
5HV	63	1.4
PS	77	3.4
Poly(LLA-co-CL)	96	1.8
$PLA_{20} - PEG_{2000,1} - PLA_{20}$ (3)	134	1.4
poly(TMC-D-LA)	154	1.7
PCl	180	1.4
PLA	219	1.2
P(3HB)	507	1.2

7.1.3 *Contact angle*

In order to assess polymer hydrophilicity, contact angle measurements of the materials considered were performed. The results are summarized in Table 10 and it is possible to see that the most hydrophilic polymer is PLA-PEG-PLA (3), while the more hydrophobic is 5HV.

It was not possible to make contact angle measurements for the copolymers $PLA_2 - PEG_{2000,1} - PLA_2$ (4) and $PLA_1 - PEG_{2000,1} - PLA_1$ (5), because they did not allow to obtain films by solvent casting.

Table 10: Results of contact angle measurements.

Polymer	Contact Angle (°)
$PLA_{20} - PEG_{2000,1} - PLA_{20}$ (3)	73.2 °± 1.2 °
PLA	75.0 °± 1.0 °
poly(LLA-co-CL)	81.5 °± 2.5 °
P(3HB)	83.7 °± 4.0 °
PCL	86.4 °± 6.2 °
poly(TMC-D-LA)	87.5 °± 2.6 °
PS	90.1 °± 2.6 °
5HV	99.0 °± 1.5 °

7.1.4 *Differential Scanning Calorimetry (DSC)*

The Differential Scanning Calorimetry (DSC) was performed as illustrated in 6.2.4 and the results of the DSC analysis are summarized in Table 11.

Table 11: Differential Scanning Calorimentry measurements: glass transition temperature T_g, melting temperature T_m, crystallinity.

Polymer	T_g (°C)	T_m (°C)	Crystallinity (%)
PLA	57.1	175.2	53
$PLA_1 - PEG_{35000,1} - PLA_1$ (1)	45.0 and 140.3	-	11.9 and 35.1
$PLA_{20} - PEG_{2000,1} - PLA_{20}$ (3)	50.4	174.1	48.6
$PLA_2 - PEG_{2000,1} - PLA_2$ (4)	-1.9	139.1	-
$PLA_1 - PEG_{2000,1} - PLA_1$ (5)	-	161.7	68.5
poly(LLA-co-CL)	9.7	amorphous	amorphous
PCL	-	55.8	52.3
poly(TMC-D-LA)	54.2	170.9	31.2
PGA	-	83.2	60.9
PEG35000	-	61.5	63.6
PEG2000	-	61.5	63.7
P(3HB)	8.0	173.6	53.9

From these measurements, some observations can be made. First of all, the polymer with the highest glass transition temperature is PLA. Moreover, the glass transition temperature of poly(TMC-D-LA) and PLA-PEG-PLA (3) is similar to the value obtained for PLA. It is worth noticing that these values are higher than the human body temper-

ature of 37 °C. On the contrary, the glass transition temperatures of poly(LLA-co-CL) and P(3HB) are very low. Furthermore, PLA, P(3HB) and PLA-PEG-PLA (3) have also similar values of melting temperature and crystallinity, while other polymers have lower values of melting temperature.

7.2 CHOICE OF THE SOLUTIONS FOR SPIN COATING

In general, an appropriate coating is achieved if the layer of polymer is uniform, homogeneous, as thin as possible (maximum 30 nm for polymer coating of QCM crystals) and without visible defects. After the tests performed, the 5 mg/mL solution with chloroform was chosen as the best solution for the polymers poly(LLA-co-CL), PLA, PCL, poly(TMC-D-LA) and PS, because the polymer layers produced with this solvent best fulfilled the requirements. Also, in the literature could be found some examples of concentrations used for spin coating and, for instance, 5 mg/mL solutions of PLA and PGA were employed by some researchers [11]. Lower concentrations were initially avoided, because it was not easy to assess whether the polymer layer was present or not and to evaluate its conditions.

However, after the synthesis of PLA-PEG-PLA, further spin coating tests were performed using a solution of 5 mg/mL of this polymer dissolved in chloroform. A naked-eye analysis revealed that the chosen solution caused some defects and inhomogeneities on the polymer layer. So, the 2 mg/mL solution was preferred for PLA-PEG-PLA.

As for bacterial polymers, 5HV and P(3HB) were found to dissolve in chloroform and the 2.5 mg/mL solutions were proved to produce good coating layers.

To sum up, chloroform was used as a solvent and the chosen solutions were:

1. Solution of poly(LLA-co-CL) 5 mg/mL;
2. Solution of PLA-PEG-PLA (3) 2 mg/mL;
3. Solution of PLA 5 mg/mL;
4. Solution of PCL 5 mg/mL;
5. Solution of poly(TMC-D-LA) 5 mg/mL;
6. Solution of PS 5 mg/mL;
7. Solution of P(3HB) 2.5 mg/mL;
8. Solution of 5HV 2.5 mg/mL.

7.3 COATING TESTS WITH SILICON OXIDE WAFERS

7.3.1 *Submersion in water at room temperature*

After submersion in deionized water for 24 hours at room temperature, the coated silicon wafers were observed with a visual naked-eyes analysis and with SEM. This revealed a detachment of the polymer films from many of the samples, with evident cracks and additional defects. The same samples were observed before submersion in water as well, to compare the polymer layers conditions before and after submersion in water. Eventually, some observations could be made:

- In general, for the polymer solutions in concentrations higher than 1 mg/mL, before submersion in water the layers were approximately even, with a few small point-like defects but without cracks. The only main defects in the films were close to the borders, where the films had a wave-like structure (Figure 22a). These defects are acceptable for the purposes of this project, because they do not alter excessively the QCM measures and the geometry of the QCM crystals reduces the formation of these imperfections. However, after submersion in water many cracks on the polymers layers were visible, of different extensions and width, not only on the borders but also in the central part of the wafers (Figure 22b);
- With a naked-eye visual analysis, it was not possible to assess if the absence of apparent defects in the 1 mg/mL solutions was reliable or if the film was too thin to be distinguished, even before submersion in water. Instead, from the SEM images it was possible to see that before submersion in water the polymer film was very thin and visible only at high magnifications (e.g. 500x) (Figure 23a). Then, after the contact with water, the polymer layer was almost not visible any more, even at high values of magnification (Figure 23b);
- The samples coated with poly(LLA-co-CL) revealed wider detachment than samples with PLA-PEG-PLA (Figure 24e and 24f). This was coherent with the QCM results, that showed a larger frequency shift for poly(LLA-co-CL) than PLA-PEG-PLA;
- Among the poly(LLA-co-CL) samples, the film obtained from the 5 mg/mL and 10 mg/mL solutions in chloroform showed the largest detachment (Figure 24f).
- As for the bacterial polymers, the P(3HB) film presented some cracks after submersion in water (Figure 24g);
- Only the silicon wafers coated with 5HV did not show significant differences before and after submersion in water. As a matter of

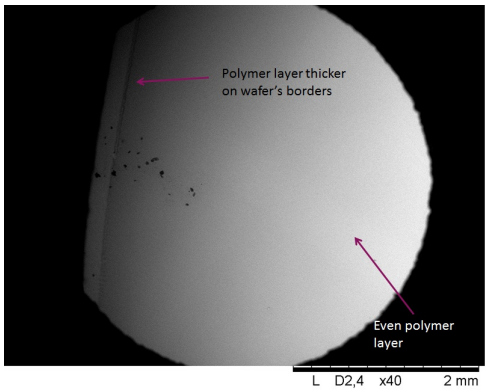

(a) *Before submersion in water.*

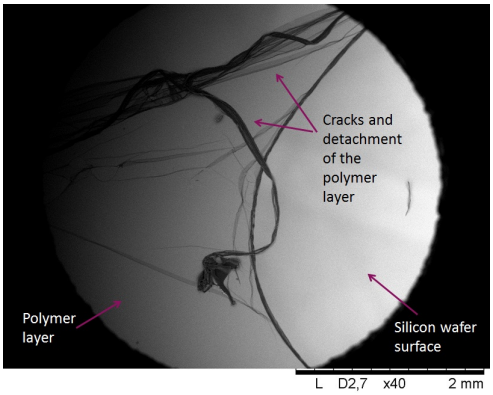

(b) *After submersion in water.*

Figure 22: SEM image of a silicon wafer coated with a solution of poly(LLA-co-CL) 5 mg/mL dissolved in chloroform, before and after submersion in water for 24 hours at room temperature.

fact, the layer observed was even, without important defects in the central part of the wafer and with small defects only close to the borders, both before and after contact with water (Figure 24d and 24h).

These detachments and defects on the polymer films meant that the bond between the silicon dioxide surface and the polymer was weaker than the bond of the polymer with water. So, the following experiments made during this project were aimed to strengthen this bond.

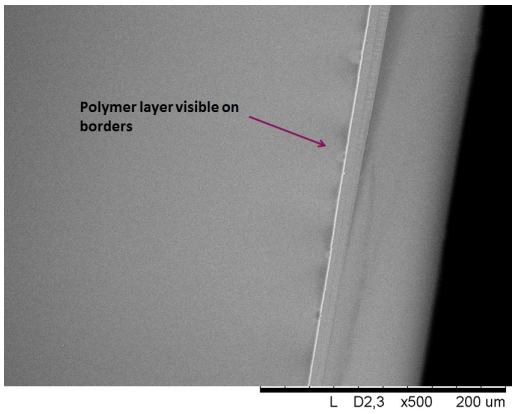

(a) *Before submersion in water.*

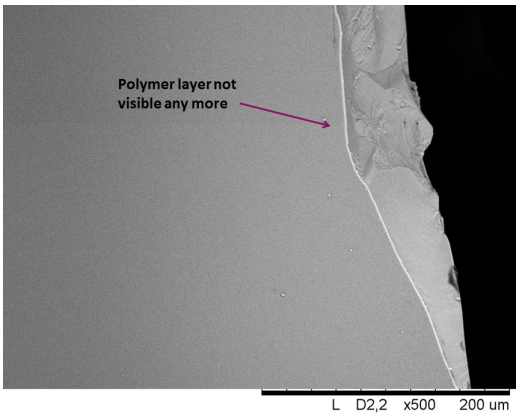

(b) *After submersion in water.*

Figure 23: Examples of SEM images of a silicon wafer coated with a solution of poly(LLA-co-CL) 1 mg/mL dissolved in DMF, before and after submersion in water at room temperature for 24 hours.

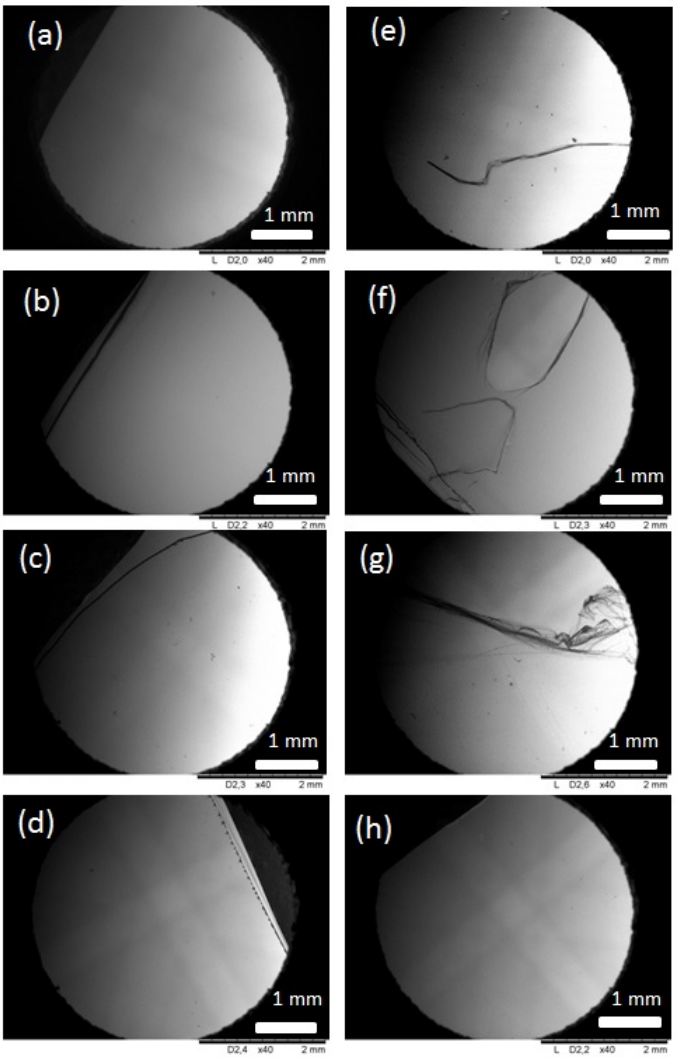

Figure 24: SEM images of silicon wafers before (images from (a) to (d)) and after (images from (e) to (h)) submersion in water at room temperature. The polymer layers are obtained by spin coating solutions of PLA-PEG-PLA 2 mg/mL in figure (a) and (e), poly(LLA-co-CL) 10 mg/mL in figure (b) and (f), P(3HB) 2.5 mg/mL in figure (c) and (g), 5HV 2.5 mg/mL in figure (d) and (h)

Pre-coating methods

In order to understand the behavior of the polymer layers and of the pre-coating layers, further tests were performed, employing silicon wafers. To make a comparison, they were divided in two groups and pre-coated either with PVAm or with the amino functionality as explained in Section 6.3.4.

PRE-COATING WITH POLYVINYLAMINE The silicon wafers were pre-coated with polyvinylamine (PVAm) as illustrated in Section 6.3.4, spin coated with the polymer solutions and then submerged in water at room temperature for 24 hours.

After that, a naked-eye visual analysis did not reveal any visible additional defects. A further SEM analysis was performed and it confirmed the first visual observations. All the layers were proved to be even, without cracks nor wide damages. However, some waves were visible close to the wafers edges (Figure 25 from (a) to (d)).

AMINO FUNCTIONALITY When the silicon wafers were treated with amino functionality, spin coated with the polymer solutions and submerged in water for 24 hours at room temperature, SEM images were acquired from the samples (Figure 25 from (e) to (h)). .

For wafers coated with PLA-PEG-PLA 2 mg/mL, poly(LLA-co-CL) 5 mg/mL , P(3HB) 2.5 mg/mL and 5HV 2.5 mg/mL the films were even, thin, with very few point-like defects, or some small lines, bubbles or waves close to the borders. Instead, the wafer coated with poly(LLA-co-CL) 10 mg/mL showed big dark stains, not only close to the borders but also far away from the edges, in the central part of the wafer. These stains were visible with naked eyes as well. Moreover, the film obtained from a 1 mg/mL solution of poly(LLA-co-CL) dissolved in DFM was very thin, but it was still visible.

So, this demonstrated the effectiveness of this method to guarantee polymer adhesion to the silicon wafers even after submersion in water at room temperature, but defects were present on the sample surfaces all the same. Furthermore, these defects appeared deeper than the ones visible on the surfaces pre-treated with PVAm.

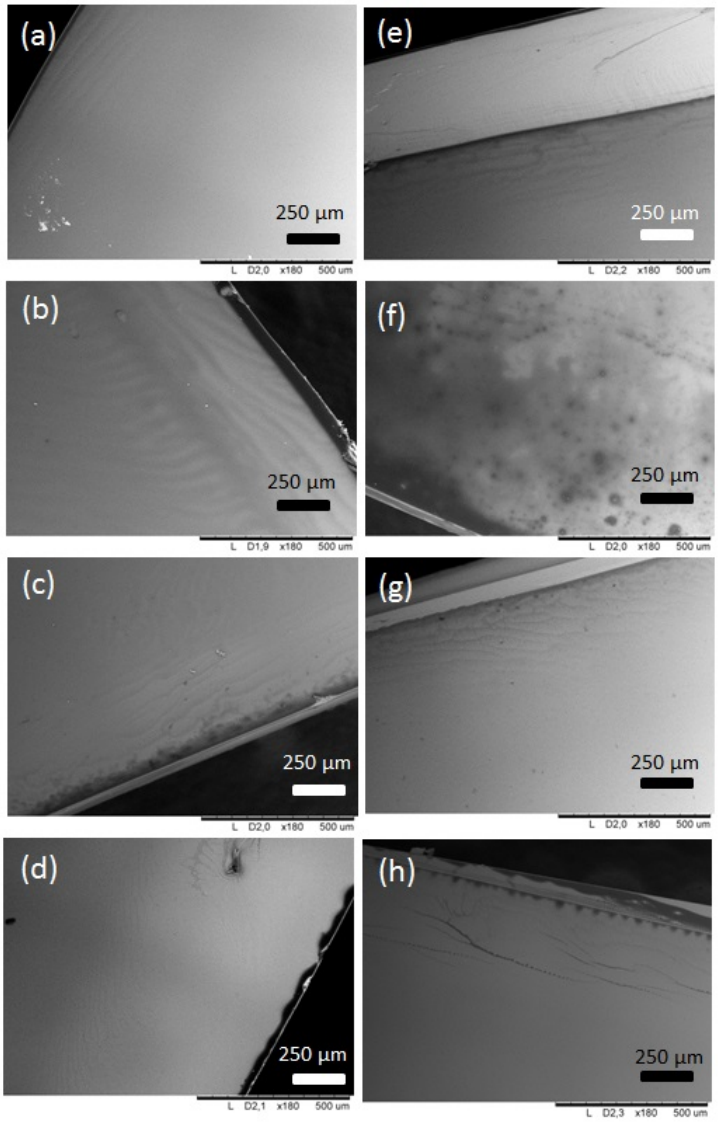

Figure 25: SEM images of silicon wafers with PVAm pre-coating (images from (a) to (d)) and amino functionality (images from (e) to (h)), after submersion in water at room temperature. The polymer layers are obtained by spin cotaing solutions of PLA-PEG-PLA 2 mg/mL in figure (a) and (e), poly(LLA-co-CL) 10 mg/mL in figure (b) and (f), P(3HB) 2.5 mg/mL in figure (c) and (g), 5HV 2.5 mg/mL in figure (d) and (h)

7.3.2 *Assessing polymer coating conditions after submersion in water at 37 °C*

To evaluate the effectiveness of pre-coatings employing PVAm and amino functionality, silicon wafers were pre-coated, spin coated and submerged in water at 37 °C for 24 hours. After that, a visual analysis did not allow to perceive any difference between the polymer layers before and after submersion in water, except in some cases. For example, in the wafers pre-coated with PVAm and coated with PLA-PEG-PLA 2 mg/mL, the pre-coating in PVAm was non-uniform before submersion in water, and it was possible to see big stains of PVAm. Anyway, after submersion in water and incubation at 37 °C these stains and inhomogeneities were not visible any more. Instead, the films coated after amino functionality pre-treatment appeared thick but opaque, for all the polymers tested. A SEM analysis revealed that, in general, the polymer films were thinner than before incubation and submersion in water.; in some cases the film was barely visible. This can be due to an increase in swelling of the polymer layers when submerged in water at 37 °C. The swelling provokes movements of the polymer chains, that are also more likely to detach from the silicon dioxide surface.

Some exceptions were:

- The silicon wafers pre-coated with PVAm and coated with poly(LLA-co-CL) 10 mg/mL, PLA-PEG-PLA (3) and 5HV 2.5 mg/mL. In these cases, the film was still present, but it showed many wide cracks and defects, revealing extensive film detachment, that was visible with naked eyes as well (Figure 26);

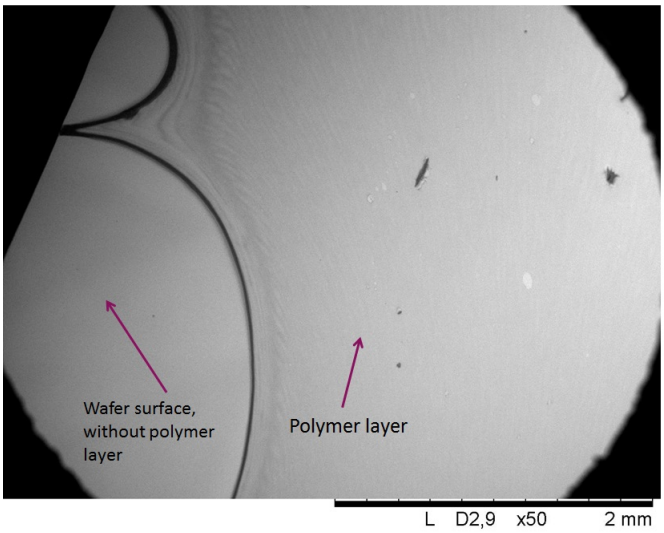

Figure 26: SEM image of a silicon wafer with PVAm pre-coating and spin coated with a solution of poly(LLA-co-CL) 10 mg/mL dissolved in chloroform, after submersion in water and incubation at 37 °C.

- The wafers with amino functionality allowed to see the thick polymer films, even if they had some superficial cracks and defects, such as small bubble-like defects, evenly distributed on the surface (Figure 27).

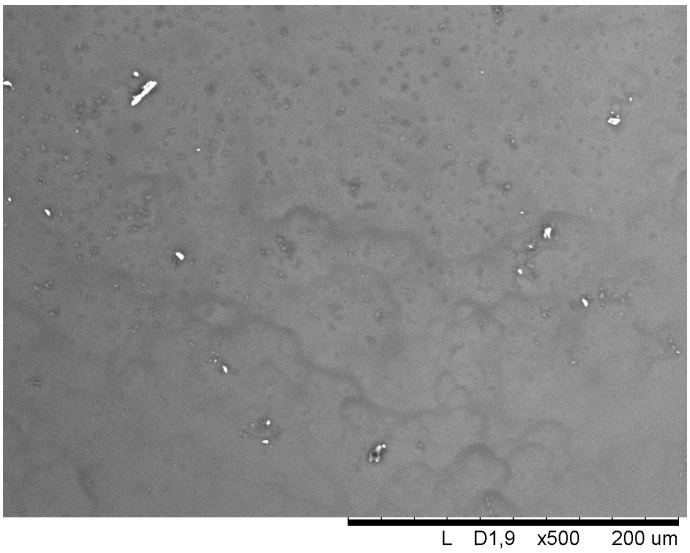

Figure 27: SEM image of a silicon wafer with amino functionality and spin coated with a solution of PLA-PEG-PLA (4) 2 mg/mL dissolved in chloroform, after submersion in water and incubation at 37 °C. Small bubbles and waves are visible on the polymer layer.

These observations lead to the conclusion that neither PVAm precoating nor amino functionality allowed to guarantee a strong adhesion of the polymer layer to the silicon wafers when in contact with water at 37 °C. This was probably caused by the fact that these precoating methods did not create as many binding sites for the polymer as expected. So, both of these procedures were dismissed.

Coating stabilization in incubator

For other tests, the silicon wafers were kept in incubator at 37 °C for 2 hours before submersion in water at 37 °C. This type of test was designed to evaluate if the problems of layer detachment were related to the the rapid change in temperature, from 24 °C to 37 °C, that took place together with the submersion in water. If this was the case, allowing the polymer film to adapt to higher temperatures before submersion in water could have brought some improvements in terms of film adhesion and uniformity.

Polymer films were obtained by spin coating polymer solutions on wafers either without any pre-coating, or pre-treated with PVAm or amino functionality. After submersion in water and incubation at 37 °C for 24 hours, from a visual naked-eye analysis all the wafers appeared to have the coating, but they all showed dense dots as well. SEM images allowed to see that all the polymer films showed defects like streaks and waves, but they did not reveal any layer detachment (Figure 28). So, it was decided to perform QCM tests employing this technique as well, to evaluate its effectiveness with higher accuracy.

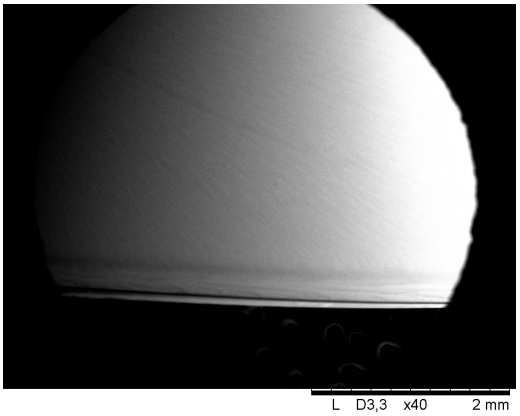

Figure 28: SEM image of a silicon wafer with a poly(LLA-co-CL) 5 mg/mL layer, kept in incubator incubation 37 °C and later submerged in water at 37 °C. Streaks and waves are visible on the polymer layer.

Coating stabilization above the glass transition temperature

From the DSC data (Section 7.1.4), it was observed that there was a relationship between the glass transition temperature T_g and the behavior of the polymeric films in water at 37 °C. In particular, if the glass transition temperature of a polymer was higher than 37 °C, then the film was still attached to the wafer after submersion in water and incubation. So, several silicon wafers were placed in oven at 62 °C for 48 hours after spin coating and before submersion in water and incubation.

Later, neither a visual naked-eye nor SEM observations could detect any remarkable difference on the layer conditions, in comparison to the set of wafers submerged directly after spin coating.

A QCM crystal was also subjected to the same procedure, including storage in oven at 62 °C after being spin coated with a solution of PLA 5 mg/mL. No difference with other QCM tests were detected, except that the baseline of the frequency shift and dissipation energy curves required longer time to be stable. So, this procedure was dismissed.

Tests employing PLA

In the literature can be found some applications of the QCM technique for evaluating the behavior of PLA at 37 °C [10]. So, further tests were performed on silicon wafers spin coated with a 5 mg/mL solution of PLA dissolved in chloroform, for comparing the results with the previous tests. The wafers were divided in four groups, according to the pre-coating method adopted:

1. Without any pre-coating;
2. Pre-coating with PVAm;
3. PVAm only, without polymer coating;
4. Amino functionality.

After being spin coated, the wafers were submerged in water and kept at 37 °C for 24 hours. Then, the surfaces were evaluated with a visual naked-eye analysis and SEM.

All these analyses lead to the same conclusions:

- Without any pre-coating method, the PLA film was still present and visible even with naked-eyes;
- The PVAm layer detached at 37 °C, both with and without PLA coating;
- The amino functionality pre-coating guaranteed PLA adhesion, even if the PLA film was thinner after submersion in water and incubation and it presented tiny bubble-like defects were visible.

As a conclusion, since the pre-coating procedures did not seem to provide any advantage or improvement in comparison to the layer spin coated directly on the wafer surface, it was chosen to perform a QCM trial employing PLA without any pre-coating.

7.3.3 *Tests to evaluate the effect of plasma treatment on silicon oxide surfaces*

First of all, contact angle measurements were performed on silicon wafers as explained in section 6.4.2, to assess the presence and the magnitude of changes in hydrophilicity. Four different silicon wafers was tested, after being subjected to 0, 2, 4 and 6 minutes of plasma treatment, respectively. The results of contact angle measurements are summarized in table 12. These measurements confirmed that the plasma treatment actually enhanced surface hydrophilicity. Besides, since the larger decrease in contact angle was achieved with 2 minutes of treatment, this duration was considered sufficient to induce this surface modification. So, in the following experiments, both for QCM sensors and silicon wafers, the duration of air plasma treatment was maintained to two minutes.

Table 12: Results of contact angle measurements of silicon wafers after different durations of plasma treatment.

Duration of plasma treatment (min)	Contact Angle (°)
0 min	51.0 °± 3.9 °
2 min	24.0 °± 0.7 °
4 min	16.2 °± 0.5 °
6 min	24.2 °± 0.4 °

After spin coating the silicon wafers with different polymers, without previous air plasma treatment, the surfaces were submerged in water and kept in incubator at 37 °C for 24 hours. To make a comparison, another set of silicon wafers was subjected to the same procedure, but pre-treated with air plasma before spin coating. This test was performed to investigate whether an increase in surface hydrophilicity of the silicon wafer could guarantee a stronger or weaker adhesion of hydrophilic polymers such as PLA-PEG-PLA. Later, a visual and a SEM analysis allowed to make the following observations:

- The films of PLA-PEG-PLA, PS and P(3HB) were even and thin, without remarkable defects (Figure 29d). This means that the polymer layers were more stable, if compared to the results obtained with silicon wafers with previous plasma treatment (Figure 29a). In that case, the polymer layers presented much wider cracks after submersion in water;

- The surfaces coated with poly(LLA-co-CL) presented some cracks and detachments (Figure 29e), but these were fewer and less wide than the defects obtained with plasma pre-treatment (Figure 29b);

- The PLA film was even and without defects (Figure 29f). Only some waves close to the borders were visible, but no other relevant differences with the PLA layer obtained after air plasma treatment could be detected (Figure 29c);
- The layer of poly(TMC-D-LA) was thin, but still visible and even (Figure 30d). Instead, with pre-treatment with air plasma, the film was thinner and with small defects (Figure 30a);
- The layer of PCL showed cracks and detachment from the surface both with and without plasma treatment. However, the defects were wider if the silicon oxide surface were not treated with air plasma (Figure 30e);
- Without air plasma treatment, the film of PGA was even and thicker than the film coated on the plasma treated surface (Figures 30c and 30f).

So, it is possible to sum up saying that for a few polymer layers (i.e. PLA, PCL) the plasma treatment allows a better adhesion to the silicon oxide surface, while for the majority of the polymers it causes more extensive detachment from the wafers.

From one point of view, this phenomenon can be explained with polymer hydrophilicity. If these results are compared with the values of contact angle obtained from the polymers (Table 10), it is possible to observe that PLA, that shows stronger adhesion if silicon hydrophilicity is enhanced with air plasma treatment, is one of the less hydrophobic polymers. Instead, poly(TMC-D-LA) and PS are the most hydrophobic and they adhere better if the silicon wafers are not treated with air plasma. However, this relationship holds for semi-crystalline polymers, because their structure is tighter and prevents water to pass through the polymer layer. If the polymer is amorphous, water can penetrate more easily through the film and reach the wafer surface, which may cause film detachment. In this case, if the surface is not treated with air plasma, it is less hydrophilic and it blocks water penetration into the polymer film.

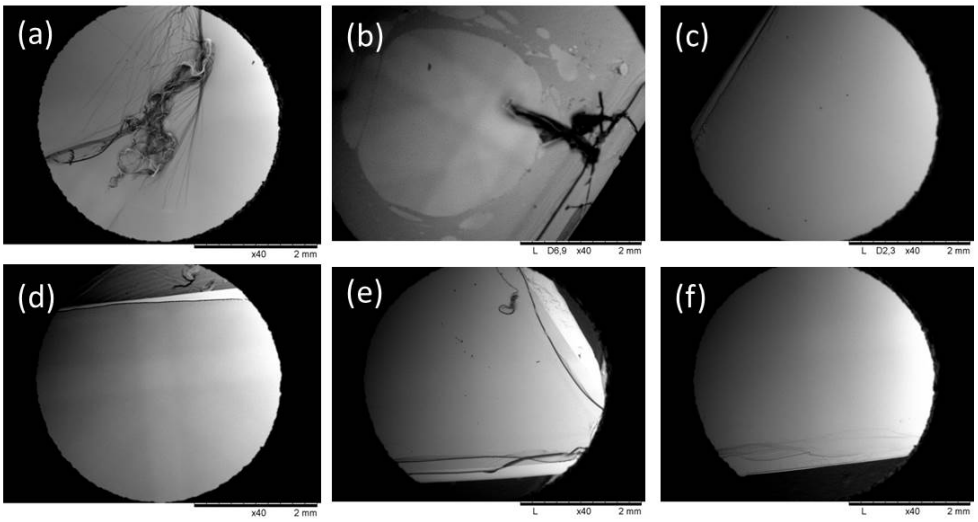

Figure 29: SEM images of silicon wafers with plasma air treatment (images from (a) to (c)) and without it (images from (d) to (f)), after submersion in water at 37 °C. The polymer layers were obtained by spin coating solutions of PS 5 mg/mL in figure (a) and (d), poly(LLA-co-CL) 5 mg/mL in figure (b) and (e), PLA 5 mg/mL in figure (c) and (f).

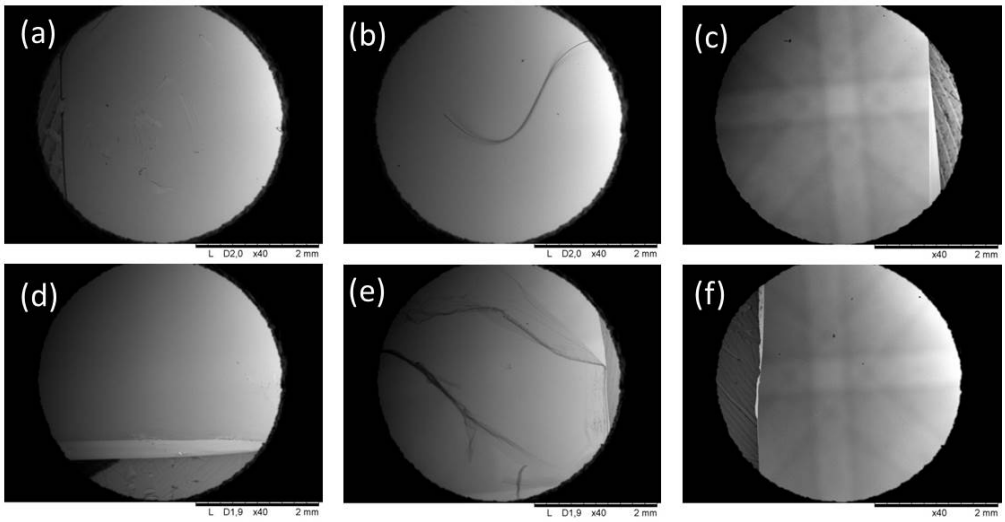

Figure 30: SEM images of silicon wafers with plasma air treatment (images from (a) to (c)) and without it (images from (d) to (f)), after submersion in water at 37 °C. The polymer layers were obtained by spin cotaing solutions of poly(TMC-D-LA) 5 mg/mL in figure (a) and (d), PCL 5 mg/mL in figure (b) and (e), PGA 5 mg/mL in figure (c) and (f).

7.3.4 *Effect of different coating concentrations*

First of all, the silicon wafers spin coated with 0.1 mg/mL polymer solutions were analyzed with SEM before submersion in water. This was done to be sure that the polymer films were actually present on the surfaces, since they were not visible with naked eyes. These tests demonstrated that all the layers of the polymers considered (i.e. PLA, poly(LLA-co-CL), PGA, PS, poly(TMC-D-LA), PLA-PEG-PLA (3)) were present, even if thin, on the wafers surfaces (Figure 31).

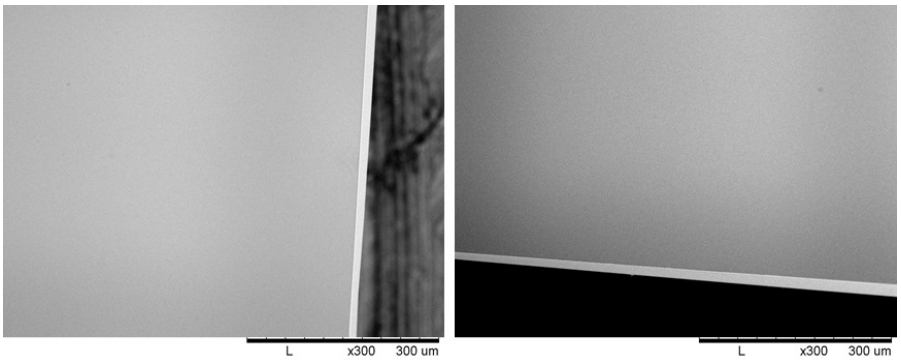

Figure 31: SEM images of silicon wafers coated with PLA 0.1 mg/mL (a) and poly(LLA-co-CL) 0.1 mg/mL (b), before submersion in water.

Instead, after submersion in water at 37 °C, all the films were present, but extremely thin and visible only at high magnifications (e.g. 1000x) (Figure 32). Besides, on the poly(TMC-D-LA) and PLA-PEG-PLA (3) layers there were some light and superficial defects such as lines, dots, and stains (Figure 33). The PS film also showed wave-like defects, although not deep.

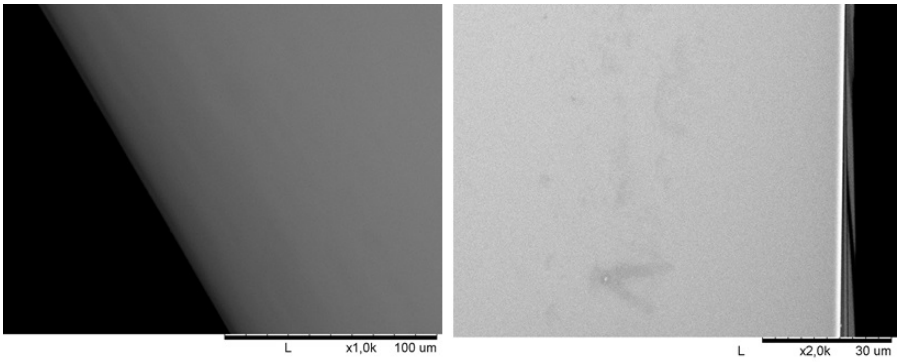

Figure 32: SEM images of silicon wafers coated with PLA 0.1 mg/mL (a) and poly(LLA-co-CL) 0.1 mg/mL (b), after submersion in water at 37 °C for 24 hours.

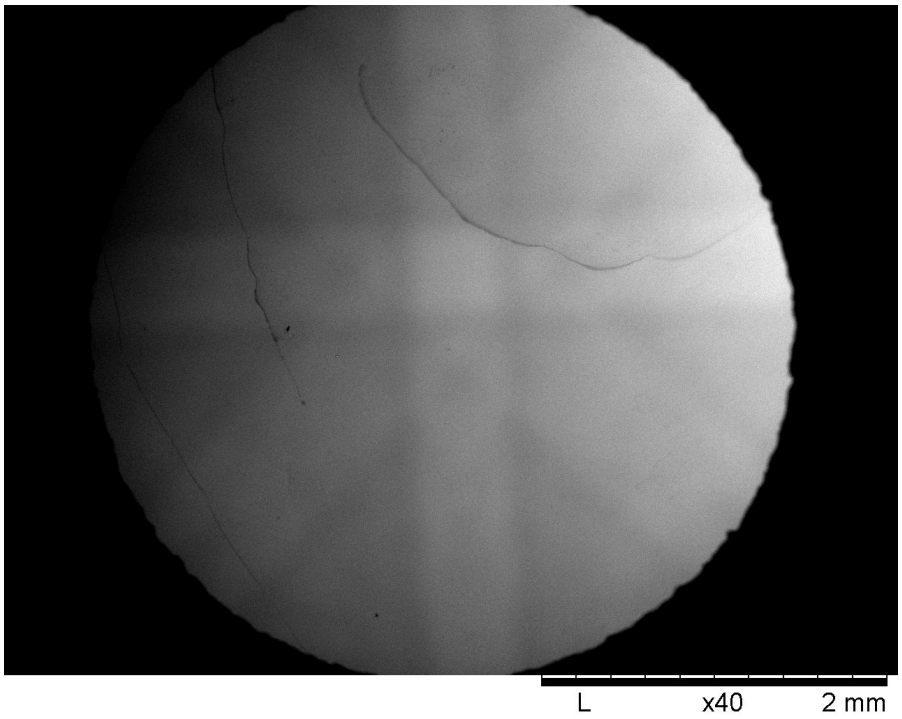

Figure 33: SEM image of a silicon wafers coated with PLAPEG-PLA (3) 0.1 mg/mL, after submersion in water at 37 °C for 24 hours.

7.4 QCM TESTS

7.4.1 *Stability of the baseline*

The first polymer layers tested with the QCM were PLA-PEG-PLA (3) and poly(LLA-co-CL), without any pre-coating of the crystals, for verifying if they allowed to obtain a stable baseline for the frequency shift and dissipation energy curves at 24 °C. The graphs obtained did not show the expected constant baseline. On the contrary, the frequency shifts appeared to increase, suggesting a detachment of the polymer from the crystal. This effect was more relevant for the poly(LLA-co-CL) layer than for the PLA-PEG-PLA film (Figure 34). A possible explanation is that the polymer detached from the crystal because of the interaction with water.

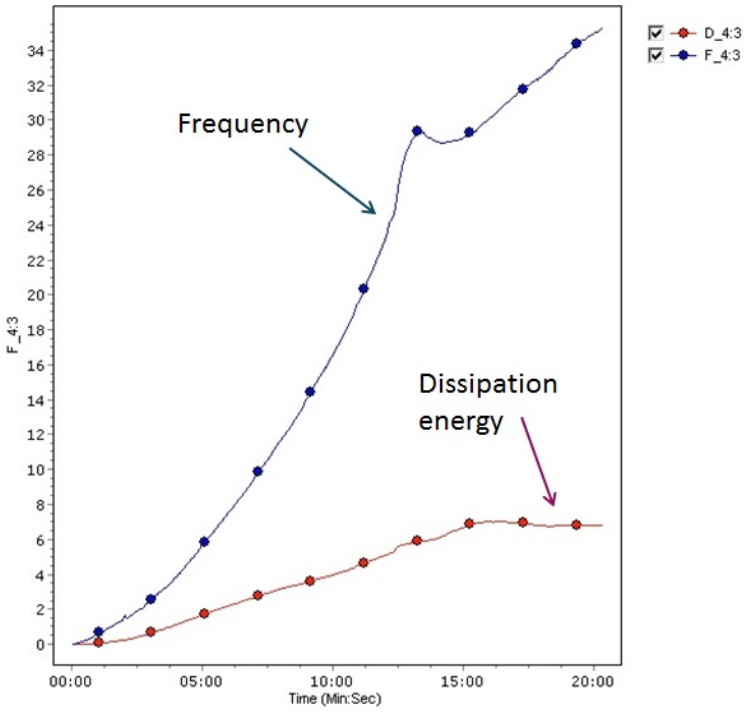

Figure 34: Frequency shift and dissipation energy curves for a crystal coated with PLA-PEG-PLA (3); MilliQ water was flushed at 100 µL/min at 24 °C.

Obtain a stable baseline with PVAm pre-coating at 24 °C

The QCM tests performed employing PVAm pre-coating and both PLA-PEG-PLA (3) and poly(LLA-co-CL) polymer layers, at 24 °C,

allowed to obtain a stable baseline in the frequency and dissipation energy curves within twenty minutes (Figure 35).

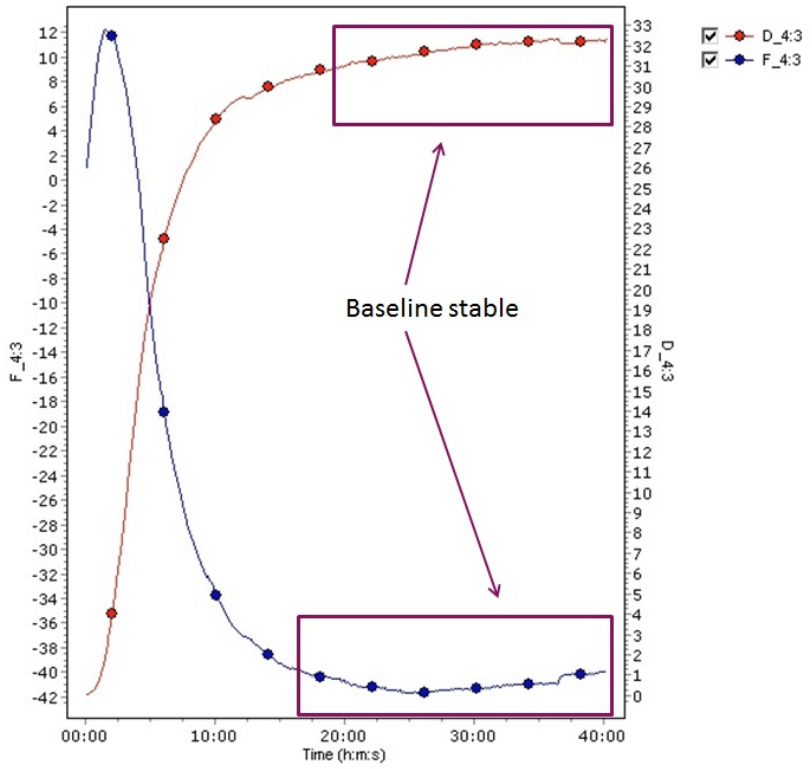

Figure 35: Frequency shift and dissipation energy curves for a crystal pre-coated with PVAm and coated with PLA-PEG-PLA (3); MilliQ water was flushed at 180 μL/min at 24 °C.

First tests to obtain a stable baseline at 37 °C

QCM tests were performed to evaluate if the films of poly(LLA-co-CL) 5 mg/mL, PLA-PEG-PLA 2 mg/mL , with PVAm and amino functionality pre-coating, and 5HV without any pre-coating, were stable enough to allow the QCM measurements at 37 °C. These tests showed that the polymer films obtained were not stable enough to allow QCM measurements at 37 °C. As a matter of fact, after three hours the baseline of the frequency shift curve was not stable yet and the frequency was still increasing.

PLA as a layer and as a pre-coating

Other tests were run, employing PLA as polymer layer and as a pre-coating for PLA-PEG-PLA (3) and with poly(LLA-co-CL). Using only

PLA coating, without any other pre-coating method, it was possible to obtain a stable baseline in the Δf and ΔD of the QCM graphs.

Instead, the crystals pre-coated with PLA and coated with PLA-PEG-PLA (3) or poly(LLA-co-CL) did not allow to obtain a stable baseline at 37 °C.

Thinner polymer layers obtained from 0.1 mg/mL polymer solutions

After running the QCM tests with crystals spin coated with 0.1 mg/mL polymer solutions, it was possible to observe that:

- PLA (with previous plasma treatment) allowed to reach the stability of the baseline in about 30 minutes;
- poly(TMC-D-LA), poly(LLA-co-CL), PS (without previous plasma treatment) guaranteed the stability of the baseline after about 30 minutes;
- With PLA-PEG-PLA (3) and PGA, the Δf and ΔD curves were not stable, even if the process was monitored for two hours.

So, the choice of a thinner polymer layer for QCM measurements allowed to reduce dramatically the time required for the stability of the baseline when testing PLA. Furthermore, it also permitted to test other polymers such as poly(TMC-D-LA) and PS, that did not provide a stable frequency shift curve when the layer was thicker.

A possible explanation of this phenomenon is that polymer layers are likely to produce swelling when in contact with water. If the layer is thick, it can gain much water. The amount of liquid gained by the polymer increases slowly with time and it provokes swelling. This means that the interaction forces between the sensor and the outer polymer chains become weaker. Also, some polymer chains can detach from the film and be flushed away by the flow of buffer solution. All these processes are reflected by the increase in the crystal's resonance frequency, because the mass of the polymer that is directly in contact with the crystal increases.

On the other hand, if the polymer layer is thinner, it can gain less water. Less polymer chains will change and adapt their position when in contact with water. So, the time needed for the film to reach a stable conformation is strongly reduced.

Summary of QCM tests for monitoring the stability of the baseline

In conclusion, the QCM tests aimed to evaluate the stability of the baseline in the frequency and dissipation energy curves are summed up in Figure 36 and the results obtained can be summarized as follows:

- At 24 and 37 °C, without any pre-coating method, the polymer layers obtained from PLA-PEG-PLA (3), poly(LLA-co-CL),

P(3HB) and 5HV isolutions in concentrations higher than 1 mg/mL did not lead to the stability of the baseline. Instead, the PLA layer did allow to have a stable baseline in the Δf and ΔD curves;

- At 24 °C, the PVAm pre-coating permitted to the PLA-PEG-PLA (3) and poly(LLA-co-CL) layers to adhere more strongly to the crystal. So, the QCM graphs showed a stable baseline. Anyway, the same layers did not lead to the stability of the baseline at 37 °C, but the PVAm layer shows extensive detachment from the cystal;
- At 37 °C, a PLA pre-coating did not guarantee the adhesion of PLA-PEG-PLA (3) and poly(LLA-co-CL) to the crystal;
- At 37 °C, the amino-functionality pre-coating did not strengthen enough the bonds between polymer layers and QCM crystal. So, the stability of the baseline could not be obtained in these conditions;
- At 37 °C, a thinner layer obtained with 0.1 mg/mL solutions of PLA, poly(TMC-D-LA), poly(LLA-co-CL) or PS allowed to get a stable baseline within 30 minutes. Instead, this was not possible with PLA-PEG-PLA (3) nor PGA.

So, it is possible to conclude that the temperature significantly affects the stability of the baseline. This can be related to the swelling of the polymer layer, due to water uptake. Swelling is related to glass transition temperature T_g. As a matter of fact, swelling is more likely for polymers with lower T_g. Increasing the temperature, the hydrogen bonds within the polymer layer become weaker and water penetrates more easily through the film. So, swelling is also enhanced and the conditions of the polymer film will require more time to be stable. On the other hand, if the thickness of the polymer layer is reduced, swelling diminishes as well, and the temperature increase has a more limited effect on the stability of the baseline.

A summary of the decisional process that lead to define the successful coating conditions for obtaining a stable baseline with the QCM is presented in Figure 37.

Temperature	Plasma treatment	Pre-coating method	Coating stabilization	Polymer	Polymer concentration
24 °C	Plasma treatment	No pre-coating	No	PLA-PEG-PLA (3)	2 mg/mL
				Poly(LLA-co-CL)	5 mg/mL
		PVAm	No	PLA-PEG-PLA (3)	2 mg/mL
				Poly(LLA-co-CL)	5 mg/mL
37 °C	Plasma treatment	PVAm	No	PLA-PEG-PLA (3)	2 mg/mL
				Poly(LLA-co-CL)	5 mg/mL
		Amino functionality	No	PLA-PEG-PLA (3)	2 mg/mL
				Poly(LLA-co-CL)	5 mg/mL
		No pre-coating	No	5HV	2.5 mg/mL
				PLA	5 mg/mL 0.1 mg/mL
			37 °C	PLA	5 mg/mL
			62 °C (above Tg)	PLA	5 mg/mL
		PLA	No	PLA-PEG-PLA (3)	2 mg/mL
				Poly(LLA-co-CL)	5 mg/mL
				P(3HB)	2.5 mg/mL
	No plasma treatment	No pre-coating	No	PLA-PEG-PLA (3)	2 mg/mL 0.1 mg/mL
				Poly(LLA-co-CL)	0.1 mg/mL
				TMC-D-LA	5 mg/mL 0.1 mg/mL
				PS	0.1 mg/mL

Figure 36: Summary of the QCM tests to obtain a stable baseline in the frequency and dissipation energy curves.

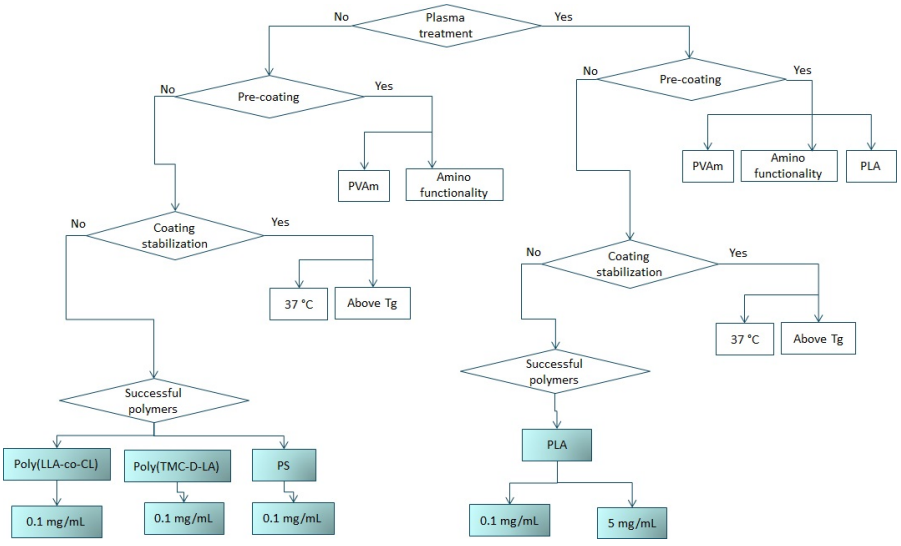

Figure 37: Summary of the decisional process that lead to define the successful coating conditions for QCM sensors.

7.4.2 *First QCM tests to evaluate the absorption of nanodiamond particles (nDP)*

The first tests were performed at 24 °C, with PVAm pre-coating and PLA-PEG-PLA 2 mg/mL and poly(LLA-co-CL) 5 mg/mL as polymer layers, in the experimental conditions illustrated in Section 6.5.3.

From the tests employing PLA-PEG-PLA, the following observations and hypothesis could be made:

- As soon as a solution of nDP was flushed over the crystal, an increase in frequency was recorded, suggesting a detachment of matter from the crystal;
- If the concentration of nDP is increased during the experiment (e.g. flushing consequently solutions of nDP in concentrations 5 μg/mL, 10 μg/mL, 20, μg/mL, 50 μg/mL) the frequency continued to increase, until it reached a saturation (Figure 38). These tests suggested the hypothesis of a continuous detachment of matter due to the flow of solution. This effect happened both at high and low flow rates;
- The flow rate did not affect the trend of the frequency and dissipation energy curves, but it affected the amplitude and the steepness of the curve variations.

After the QCM measurements, SEM images were acquired from the crystal (Figure 39). They revealed the presence of particles on the surface, with an even and homogeneous distribution, forming aggregates having diameter in the range 11 -165 nm.

AFM images were also acquired from the same crystal and they confirmed the presence of particles on the surface and they pointed out that holes were present as well (Figure 40). Since the deepness and wideness of these holes look similar to the dimensions of the elevations representing adhered nDP, a hypothesis is that nDP initially bind to the polymer film and they detach it from the QCM sensor. This phenomenon happens if the strength of the bond between PLA and nDP is greater than the strength of the PLA-silicon dioxide surface bond. However, as highlighted by the SEM and AFM images, nanodiamonds were likely to adhere to the surface, either onto PLA or on the silicon dioxide surface of the QCM sensor.

Tests employing poly(LLA-co-CL) with PVAm pre-coating were also performed and it could be observed that:

- When the first solution of nDP in water was flushed over the crystal, the frequency decreased and this pointed out that nDP were likely to be absorbed onto the polymer layer, because the mass of the oscillating system was increasing;

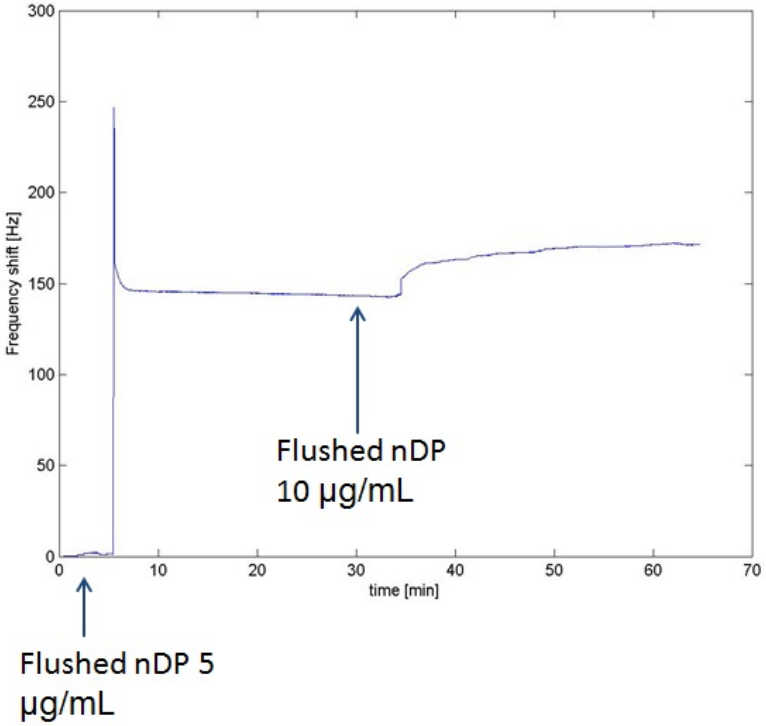

Figure 38: Frequency shift for a crystal pre-coated with PVAm and coated with PLA-PEG-PLA (3) 2 mg/mL at 24 °C.

- If a second solution of nDP, with a higher concentration, was flushed, it provoked an increase in frequency. This could mean that a continuous flow of nDP solution at high flow rate (200 $\mu L/min$) lead to a detachment either of nDP from the polymer, or of the polymer itself from the underlaying PVAm, or of the PVAm from the crystal (Figure 41);
- A possible explanation is that at first the nDP adhere to the polymer, but then a higher flow rate does not allow further nDP attachment and, on the contrary, it flushes away matter from the oscillating system (either nDP, or PVAm, or polymer). It seems likely that nDP are flushed away, because it is known that the inter-particle interactions are stronger than the attractive forces between nDP and the substrate [88].

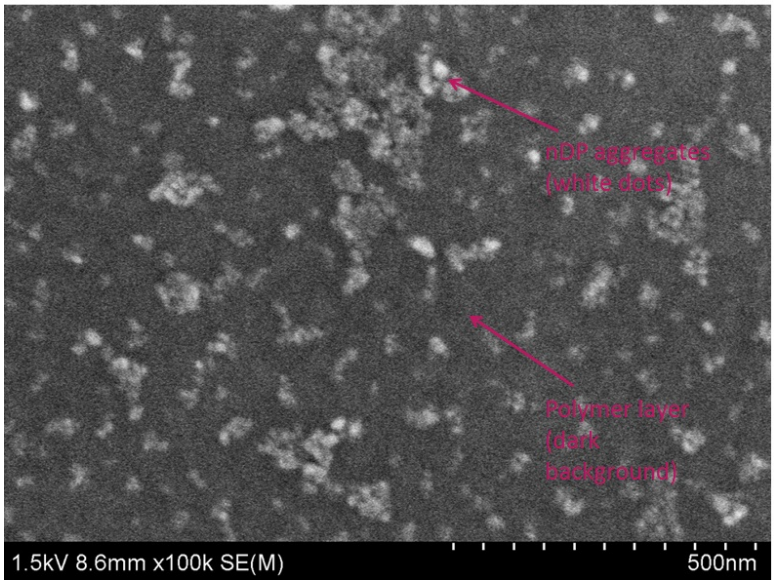

Figure 39: SEM image of QCM crystal pre-coated with PVAm and coated with PLA-PEG-PLA (3) 2 mg/mL, after the QCM measurement involving nDP at 24 °C.

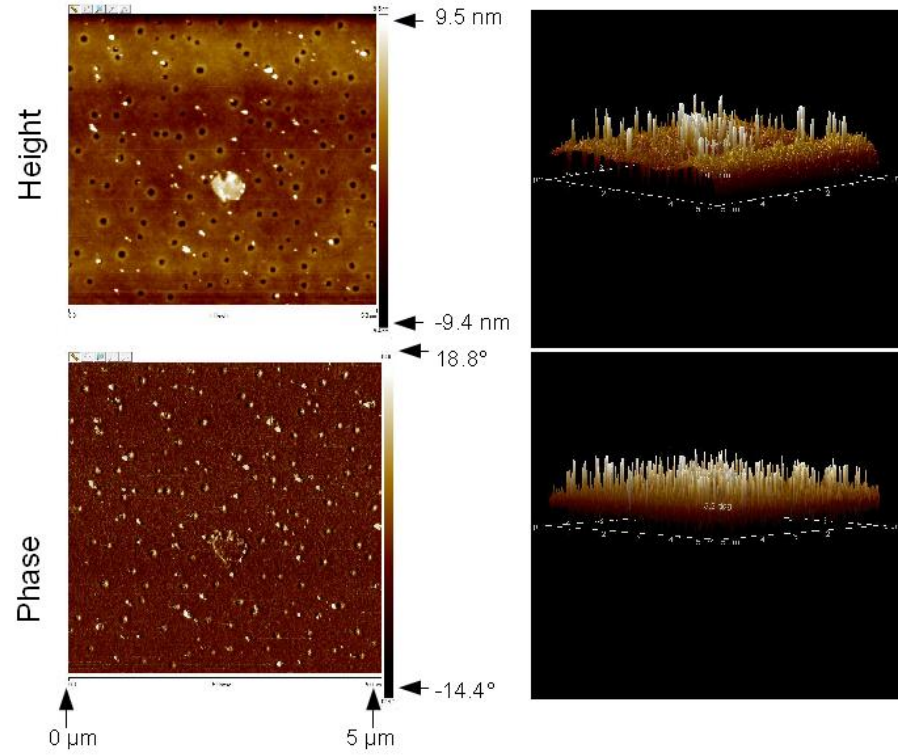

Figure 40: Height and phase AFM images of QCM crystal pre-coated with PVAm and coated with PLA-PEG-PLA (3) 2 mg/mL, after the QCM measurement involving nDP at 24 °C.

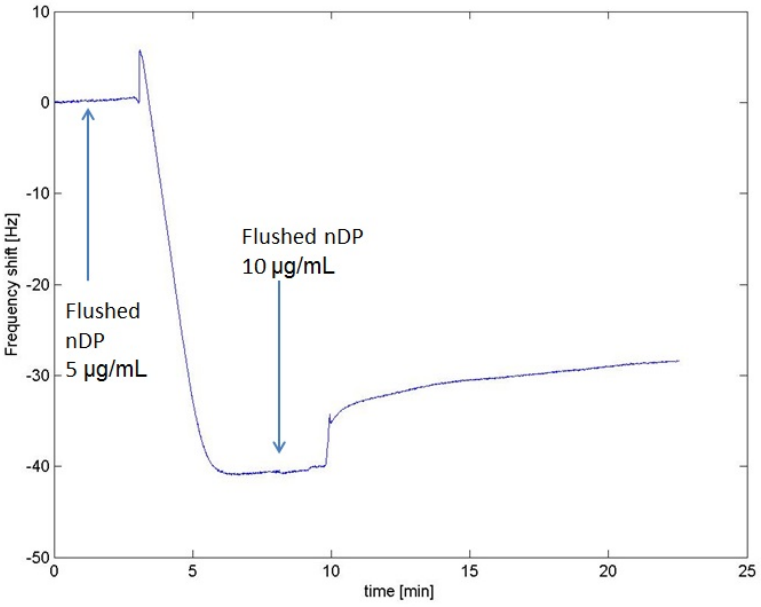

Figure 41: Frequency shift for a crystal pre-coated with PVAm and coated with poly(LLA-co-CL) 5 mg/mL at 24 °C.

7.4.3 *QCM tests performed with PLA 5 mg/mL at 37 °C*

Adsorption of nDP onto PLA 5 mg/mL

In general, when flushing nDP, the frequency curves obtained showed a common trend. As an example, during a test a 20 µg/mL solution of nDP was flushed over the crystal coated with PLA, at a flow rate of 100 µL/min. The frequency at first showed a tiny decrease, followed by a huge increase (Figure 42). A possible explanation of this behavior is that at first nanodiamonds adhere to the PLA, covering all the polymer surface. The effect is reflected by the initial brief decrease in frequency. Then the curve increase can be explained with a detachment of nDP, due to the continuous flow of more nDP solution. As a matter of fact, the strong interactions among nDPs can lead to the formation of aggregates of these particles and to their detachment from the polymeric matrix. However, the detachment of these aggregates can also cause a detachment of PLA from the crystals, that is monitored by the wide increase in the frequency curve.

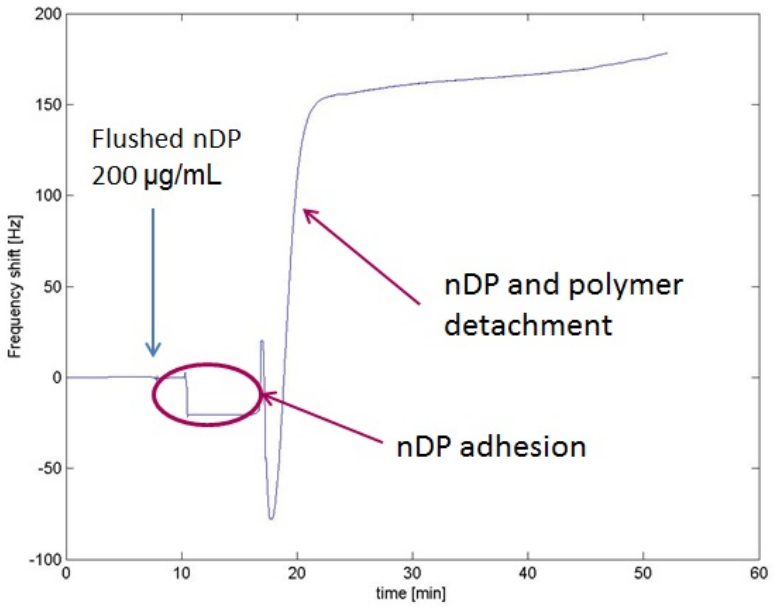

Figure 42: Frequency shift for a crystal coated with PLA 5 mg/mL and flushed with nDP 200 µg/mL, at 37 °C.

In order to find the optimal concentration of nDP to obtain the maximum frequency shift, further QCM tests were performed, in the same experimental conditions of coating (i.e. PLA 5 mg/mL) and temperature (i.e. 37 °C), flowing PBS at a rate of 50 µL/min. For every crystal, a different concentration of nDP was used, in particular 5 µg/mL, 10 µg/mL, 20 µg/mL, 50 µg/mL and 200 µg/mL. Then, the maximum increase in frequency was measured. The results are

summarized in Figure 43 and it is possible to see that the concentration of nDP that aloows to obtain the higher maximum frequency shift by the QCM in this case is 10 µg/mL.

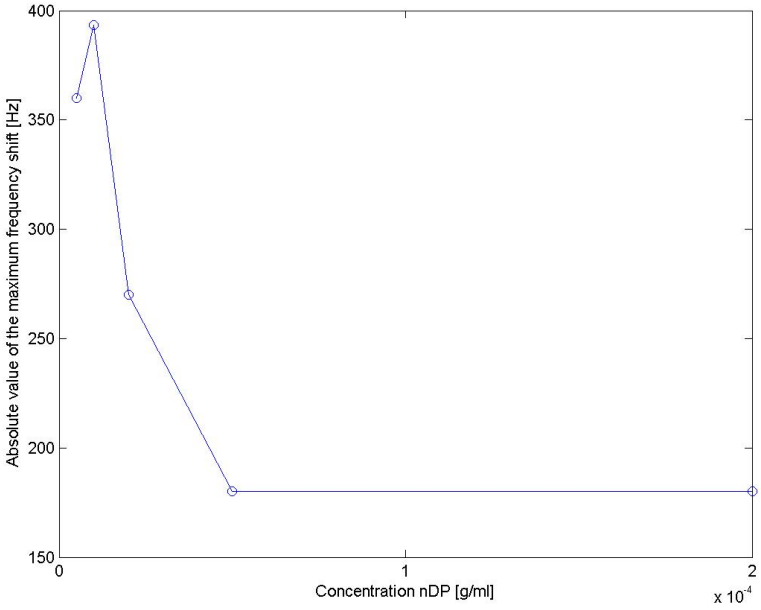

Figure 43: Maximum frequency shift (absolute value) for a crystal coated with PLA 5 mg/mL and flushed with nDP solutions.

Adsorption of Bone Morphogenetic Protein-2 (BMP-2) onto PLA 5 mg/mL

Several QCM experiments were performed with crystals coated in PLA 5 mg/mL, flushing solutions of nanodiamond particles and, later, of BMP-2.

In general, the trend of the frequency shift curves was similar to the graph shown in Figure 44. In this example, a 5 μg/mL solution of nDP was flushed over the crystal. Initially, a brief and limited decrease in frequency was monitored, while later there was a wide increase of the curve. After waiting for the curve stabilization, a 10 μg/mL solution of BMP-2 dissolved in PBS was employed. The QCM equipment monitored an even higher decrease in frequency.

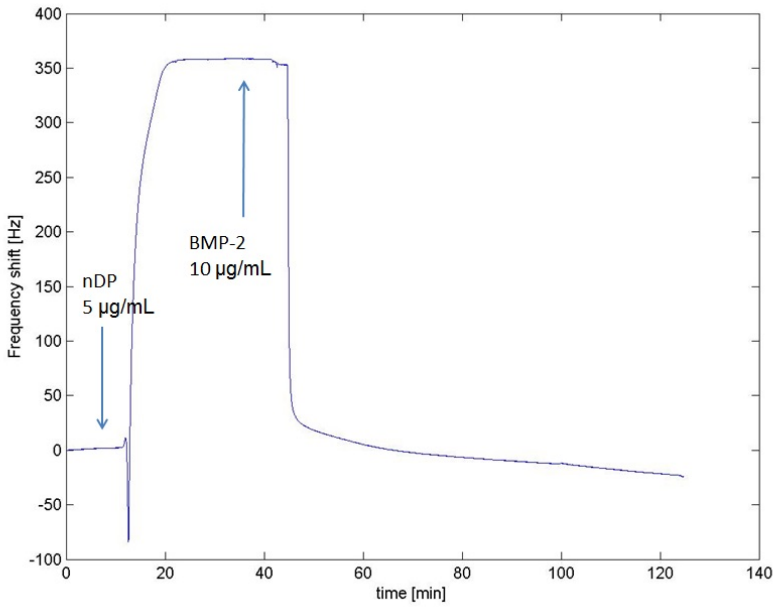

Figure 44: Frequency shift for a crystal coated with PLA and flushed with 5 μg/mL nDP and 10 μg/mL BMP-2 solutions at 50 μL/min, at 37 °C.

A possible explanation for this behavior of nDP and BMP-2 is that after the first adhesion of nDP and the consequent detachment of PLA and nanodiamonds, it is likely that some of the nDP are flushed away by the flow of solution, while others float above the crystal for a while. This can be due to the choice of employing a low value of flow rate (i.e. 50 μL/min) for the injected solutions. As a matter of fact, a slow flow of solution can be too weak to eject the nDP from the sensor chamber. To confirm this hypothesis, future researches could be aimed to evaluate the effect of flow rate on the interactions between PLA and nDP.

When the BMP-2 solution is flushed, the proteins bond to the nDP that are both on the QCM crystal surface and in solution in the sensor

chamber. This makes the nDP heavier, so that they will sit again on the PLA surface. So, this can be an interpretation of the relevant decrease in the frequency curve. Moreover, if the hypothesis of the dependence of this phenomenon on the flow rate is correct, a higher flow rate should provoke a decreased polymer detachment, because it would reduce the number of nDP floating above the crystal, in the sensor chamber.

At this point, one may wonder if the BMP-2 adhesion on PLA is enhanced by the presence of the nDP. So, additional QCM tests were run for comparison in the same experimental conditions, flushing BMP-2 directly above the crystal coated with PLA, without flushing nDP before. For example, if a 10 $\mu g/mL$ solution of BMP-2 was employed, the net decrease in frequency recorded was very limited, around 6 Hz (Figure 45).

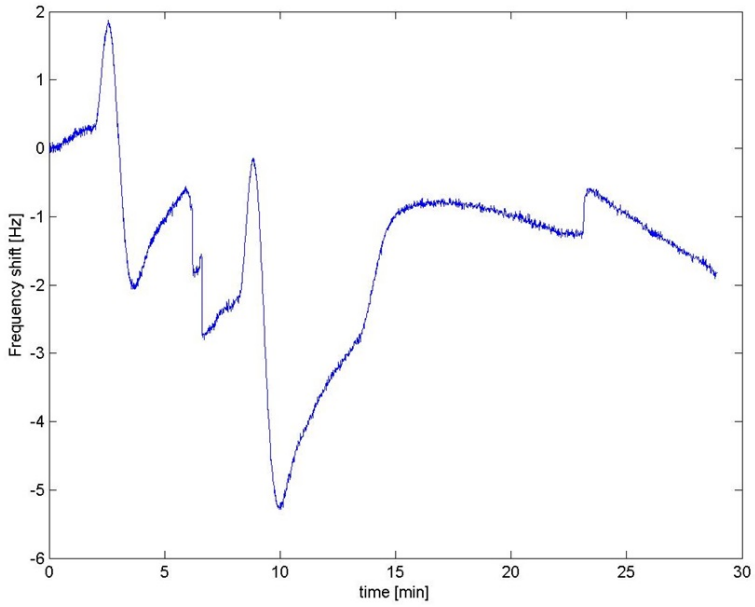

Figure 45: Frequency shift for a crystal coated with PLA and flushed with a 10 $\mu g/mL$ solution of BMP-2, at 37 °C. The variations in frequency recorded are very limited.

So, it seems likely that the presence of nDP increased BMP-2 adsorption on PLA. Other QCM tests were run in the same experimental conditions of crystal coating and temperature, flushing PBS at 50 $\mu L/min$. The results are summarized in Figure 46. The graph highlights how the presence of nDP allows to detect a greater frequency shift. This effect is more evident for a lower concentration of BMP-2 (i.e. 10 $\mu g/mL$) and for lower concentrations of nDP (i.e. 5 $\mu g/mL$).

This phenomenon could be explained with the small size of nDP. One aspect is that, because of their small size, nanodiamonds have a great surface area. So, BMP-2 is more likely to find binding sites

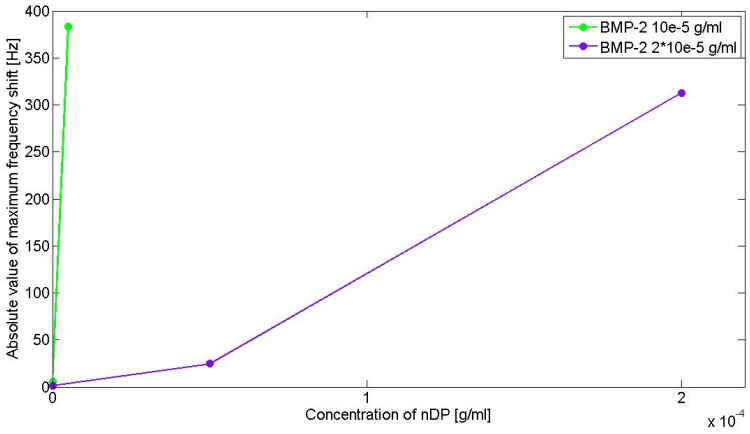

Figure 46: Maximum frequency shift for a crystal coated with PLA 5 % and flushed nDP and BMP-2 in concentration 10 µg/mL and 20 µg/mL, at 37 °C.

exposed on the nDP surface. Moreover, the physisorption of nDP onto PLA increases surface roughness and, as a consequence, surface area as well, augmenting the probability of BMP-2 binding. This also contributes to vary the orientation of the binding sites for BMP-2 on the surface. So, the proteins can reach the surface in different orientations and be likely to find binding sites and be adsorbed all the same.

Adsorption of fibronectin onto PLA 5 mg/mL

In the same experimental conditions, further tests were run flushing solutions of fibronectin in different concentrations, with and without pre-adsorption of nDP. Without pre-adsorption of nDP, a decrease in frequency was measured, reflecting protein adsorption onto PLA (Figure 47).

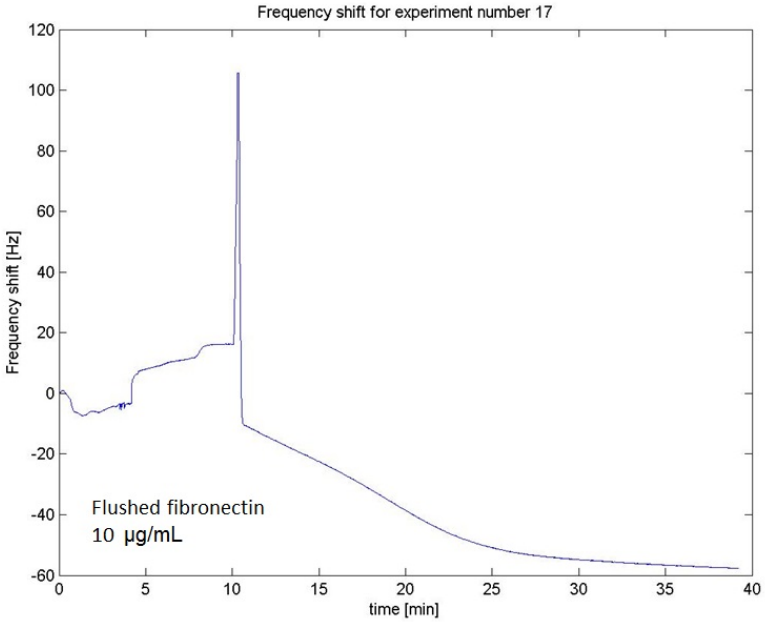

Figure 47: Frequency shift for a crystal coated with PLA and flushed with a 10 µg/mL solution of fibronectin dissolved in PBS, at 37 °C.

Instead, when a solution of nanodiamonds was flushed before fibronectin, the frequency shift due to fibronectin was much higher and the curve behavior was similar to the trend described for BMP-2 (Section 7.4.3).

7.4.4 *QCM tests performed with PLA 0.1 mg/mL and poly(LLA-co-CL) 0.1 mg/mL at 37 °C*

Several QCM tests were performed employing crystals coated with thinner polymer layers. These films were obtained from 0.1 mg/mL polymer solutions spin coated at higher spin rates (i.e. 2500 rpm and 5000 rpm), as explained in Section 6.3.2. Among the polymers that were proved to allow obtaining a stable baseline (i.e. PLA, poly(TMC-D-LA), poly(LLA-co-CL) and PS), PLA and poly(LLA-co-CL) were selected to be used for further extensive tests. PLA was chosen to assess if the layer thickness affected the results. Instead, poly(LLA-co-CL) was employed because it differed from PLA in terms of crystallinity:

while PLA is semi-crystalline, poly(LLA-co-CL) is amorphous. Besides, both of these materials were proven to be a good choice in bone regeneration.

Behavior of nDP onto PLA 0.1 mg/mL and poly(LLA-co-CL) 0.1 mg/mL

When flushing solutions of nanodiamonds in concentrations 1 µg/mL, 5 µg/mL, 10 µg/mL and 50 µg/mL on PLA and poly(LLA-co-CL), the frequency shift curves showed the same trend for both the polymers tested: an abrupt increase was followed by a slower decrease (Figure 48).

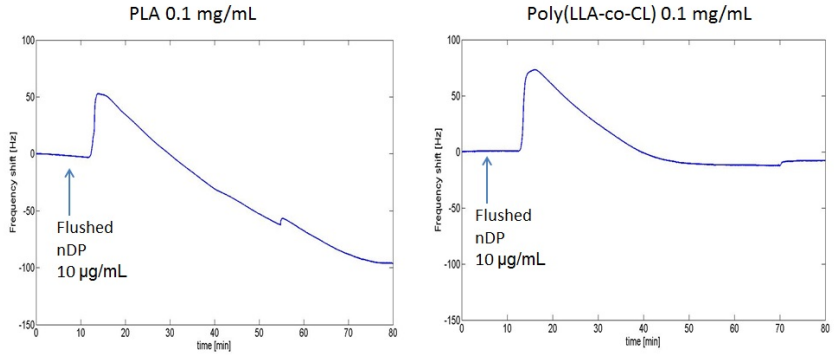

Figure 48: Frequency shift for crystals coated with PLA 0.1 mg/mL and poly(LLA-co-CL) 0.1 mg/mL and flushed with nDP 10 µg/mL, at 37 °C.

This trend might reflect a first detachment of the polymer layer, followed by an adhesion of nDP onto the polymer or onto the crystal itself. One possibility is that the first polymer detachment is due to the change from the buffer solution (PBS) and the water of the nDP solution, which involve a change in viscosity and concentration of diluted substances. The same trend was obtained when employing Milli-Q water as a buffer solution as well. Another possible explanation is that the bonds between the nDP and the polymer are stronger than the bonds between the polymer and the crystal. So, the first nanodiamonds flushed capture and remove the polymer chains, or some of the chains. Then, according to this hypothesis, the following adhesion of nDP takes place onto the quartz crystal, onto some spare polymer chains that are still attached to the crystal and on nDP already attache to the crystal, because of the tendency of nDP to form aggregates.

Furthermore, the relationship between maximum frequency shift and concentration of nDP, for crystals coated with PLA 0.1 mg/mL and poly(LLA-co-CL) 0.1 mg/mL is summarized in Figure 49a. In Figure 49b, the same data are compared with the results obtained for PLA 5 mg/mL.

First of all, it is possible to observe that for PLA the frequency shift increases considerably at lower concentrations of nDP (e.g. 10

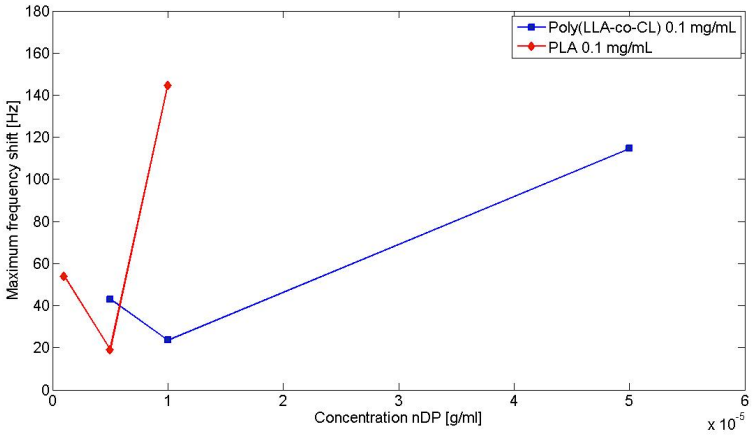

(a) *PLA 0.1 mg/mL (red curve), poly(LLA-co-CL) 0.1 mg/mL (blue curve)*

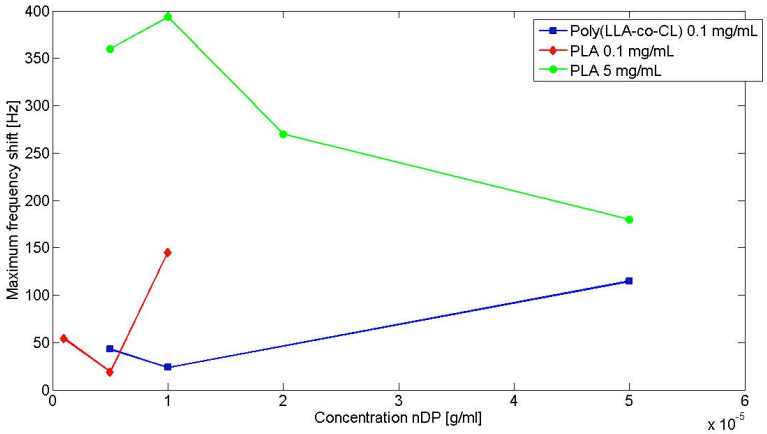

(b) *PLA 5 mg/mL (green curve), PLA 0.1 mg/mL (red curve), poly(LLA-co-CL) 0.1 mg/mL (blue curve)*

Figure 49: Relationship between maximum frequency shift and concentration of nDP, at 37 °C. Crystals coated with PLA 0.1 mg/mL, poly(LLA-co-CL) 0.1 mg/mL and PLA 5 mg/mL.

µg/mL), while poly(LLA-co-CL) requires higher concentrations (e.g. 50 µg/mL). This reveals a stronger affinity of nDP for PLA rather than for poly(LLA-co-CL), which can be due to the polymers structure. As a matter of fact, PLA is semi-crystalline while poly(LLA-co-CL) is amorphous. Probably, the semi-crystalline polymer structure provides more binding sites for nDP. Also, if nDP have a crystalline structure as well, it is likely that a more organized polymer structure enhances nDP binding. Another point is that the nDP employed for this thesis are hydrophilic [89], fact that makes them more affine to PLA than to poly(LLA-co-CL), because the former is slightly less hydrophobic than the latter (see Table 10).

This difference in behavior between the two polymers PLA and poly(LLA-co-CL) probably means that the initial detachment of poly-

mer film due to the presence of nDP is not complete, but only the most weakly bonded polymer chains detach from the crystal.

Both the films of PLA 5 mg/mL and PLA 0.1 mg/mL present a maximum frequency shift when flushed with nDP in concentration 10 µg/mL. This means that this concentration is high enough to flush an adequate number of particles that can bind to PLA. At the same time, this value is low enough to allow the nDP to bind PLA and not to other nanodiamonds that are in the chamber. In fact, with higher concentrations there might be many more nDP in the chamber at the same time and they can bind to each other rather than with PLA and be flushed away by the flow of solution.

From Figure 49b, it is immediate to notice that the frequency shift obtained for PLA 5 mg/mL is significantly higher than for PLA 0.1 mg/mL, meaning that for PLA 5 mg/mL there is much more polymer detachment. This is because in a thicker layer there are more polymer chains that can be easily detached. The swelling of the PLA 5 mg/mL film due to the water uptake can also contribute, reducing the number and strength of bonds between polymer chains and making the chains easier to detach.

Adsorption of Bone Morphogenetic Protein-2 (BMP-2) onto PLA 0.1 mg/mL and poly(LLA-co-CL) 0.1 mg/mL

Whan a BMP-2 solution was flushed over crystals coated with PLA 0.1 mg/mL and poly(LLA-co-CL) 0.1 mg/mL, in some cases it was possible to observe a net frequency decrease, while in other tests only tiny frequency oscillations around 0 Hz were recorded (Figure 50).

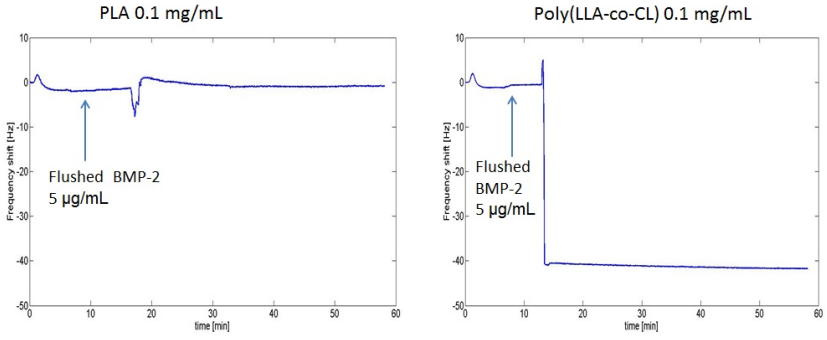

Figure 50: Frequency shift for crystals coated with PLA 0.1 mg/mL and poly(LLA-co-CL) 0.1 mg/mL and flushed with BMP-2 5 µg/mL, at 37 °C.

Moreover, Figure 51 points out that for PLA the BMP-2 concentration needed to increase protein adsorption (i.e. 1 µg/mL) is lower than the value required by poly(LLA-co-CL) (i.e. 5 µg/mL).

On the other hand, both the polymer layers present a minimum in BMP-2 adsorption when the protein concentration in solution was 10 µg/mL. A possible explanation for this result is related to protein

folding. In general, the adsorption process of proteins on a surface involves protein adhesion and unfolding, to create as many bonds with the surface as possible. If the concentration of proteins in solution is too high, there is not space enough for all the proteins to be adsorbed on the surface. So, some of the proteins are completely adsorbed onto the surface, while others cannot unfold properly and they can only create a few bonds with the surface. In this case, the flow of solution in the QCM might detach these loosely tightened proteins (Figure 52).

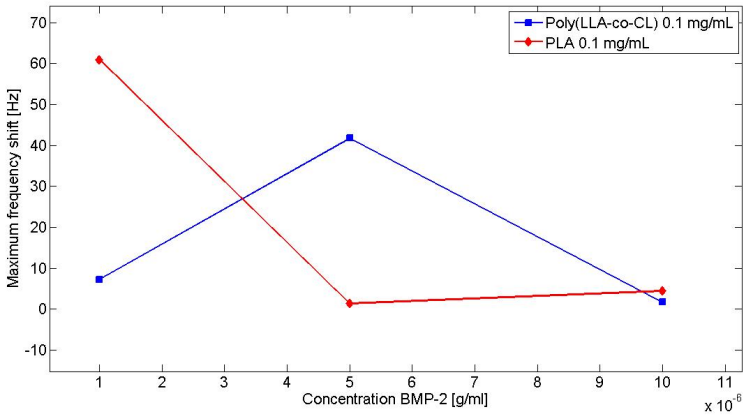

Figure 51: Absolute value of the maximum frequency shift for crystals coated with PLA 0.1 mg/mL and poly(LLA-co-CL) 0.1 mg/mL, flushed with BMP-2, at 37 °C.

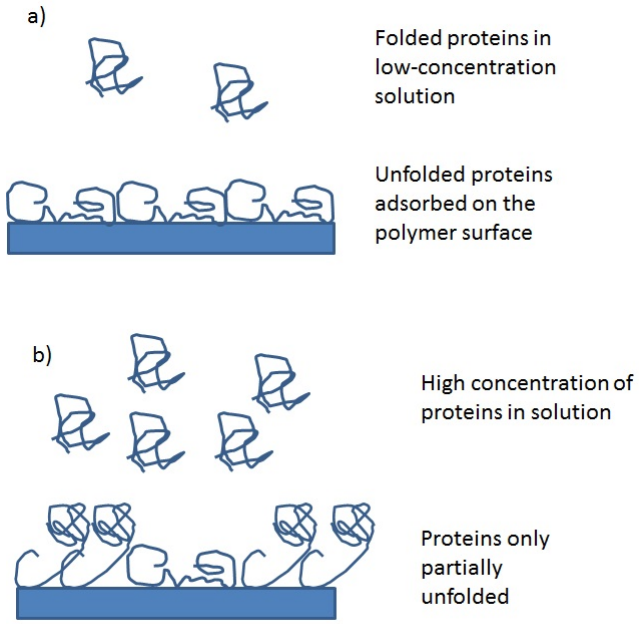

Figure 52: Schematic representation of protein adsorption on a surface.

If a solution of BMP-2 was flushed after nDP, a high decrease in frequency was monitored, both for PLA 0.1 mg/mL and poly(LLA-co-CL) 0.1 mg/mL (Figure 53). The trend of the recorded curve was the same for the two polymers and it represented BMP-2 adhesion onto nDP and polymer films.

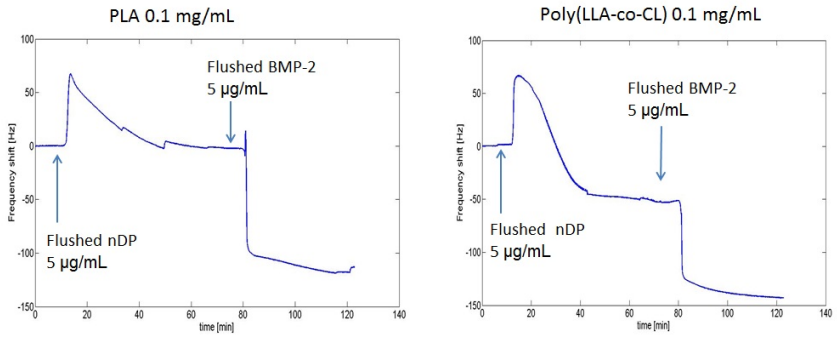

Figure 53: Frequency shift for crystals coated with PLA 0.1 mg/mL and poly(LLA-co-CL) 0.1 mg/mL and flushed with nDP 5 µg/mL and BMP-2 5 µg/mL, at 37 °C.

Instead, when BMP-2 was flushed directly onto the crystal, without flushing nDP before, the decrease in frequency was smaller, for both the polymers tested. For PLA the presence of nDP significantly increased the frequency shift, while for poly(LLA-co-CL) the difference in frequency shift was more limited (Figure 54). This can be related to the fact that low nDP concentrations were chosen for these tests (i.e. up to 20 µg/mL). For these concentration values, there is more nDP adhesion onto PLA than on poly(LLA-co-CL). So, the higher BMP-2 adsorption onto the crystals coated with PLA and flushed with nDP is a further confirm of the greater affinity of BMP-2 for nDP than for the polymer film, being it PLA or poly(LLA-co-CL). This is also proved by the higher frequency shift measured with pre-adsorption of nDP than without, for both the polymers tested.

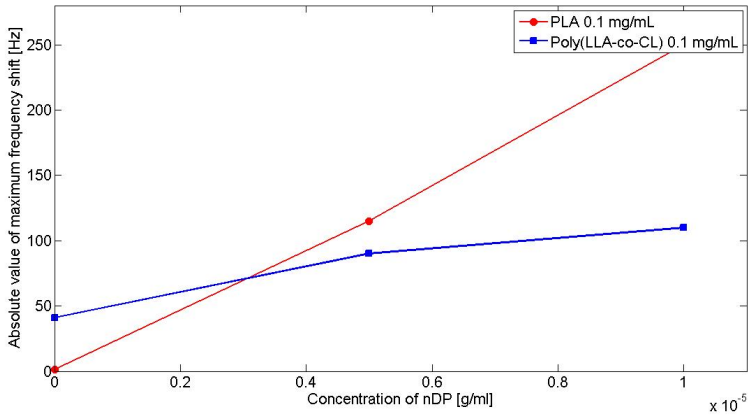

Figure 54: Maximum frequency shift for crystals coated with PLA 0.1 mg/mL and poly(LLA-co-CL) 0.1 mg/mL, flushed with nDP in varying concentrations and BMP-2 5 µg/mL, at 37 °C

Adsorption of fibronectin onto PLA 0.1 mg/mL and poly(LLA-co-CL) 0.1 mg/mL

Both for PLA 0.1 mg/mL and poly(LLA-co-CL) 0.1 mg/mL, if a solution of fibronectin was flushed before pre-adsorption of nanodiamonds, the frequency shift showed a first small increase, followed by a slower and gradual decrease (Figure 55).

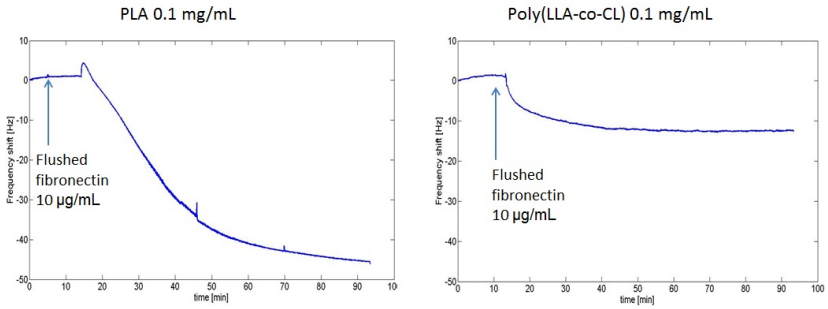

Figure 55: Frequency shift for crystals coated with PLA 0.1 mg/mL and poly(LLA-co-CL) 0.1 mg/mL and flushed with fibronectin 10 µg/mL, at 37 °C.

Comparing the maximum frequency shift obtained for the two polymer layers (Figure 56), it seems clear that the value 1 µg/mL is the optimal concentration of fibronectin to enhance protein adsorption. This effect can be explained as previously illustrated for BMP-2: higher concentrations prevent some proteins to bind to the polymer layer and some of the proteins are flushed away from the crystal chamber.

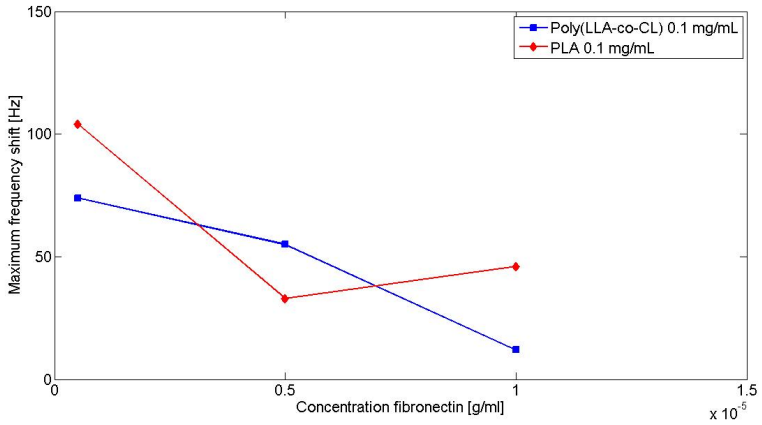

Figure 56: Maximum frequency shift (absolute value) for crystals coated with PLA 0.1 mg/mL and poly(LLA-co-CL) 0.1 mg/mL and flushed with fibronectin, at 37 °C.

Instead, if nDP were pre-adsorbed on the surfaces, a definite decrease in frequency was monitored (Figure 57).

If compared to the magnitude of the frequency shift obtained without pre-adsorption of nDP, these variations in frequency are much

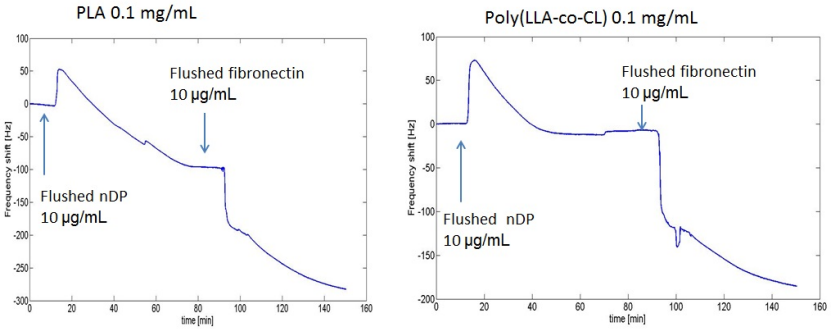

Figure 57: Frequency shift for crystals coated with PLA 0.1 mg/mL and poly(LLA-co-CL) 0.1 mg/mL and flushed with nDP 10 µg/mL and fibronectin 10 µg/mL, at 37 °C.

higher (Figure 58). So, this if an additional prove of the fact that nDP can be functionalized with fibronectin and that nanodiamonds enhance fibronectin adsorption onto PLA and poly(LLA-co-CL).

Furthermore, the frequency shifts recorded when flushing fibronectin after nDP is not considerably different for the two polymer films. This means that fibronectin has a similar affinity for PLA and poly(LLA-co-CL) when they are enriched with nDP.

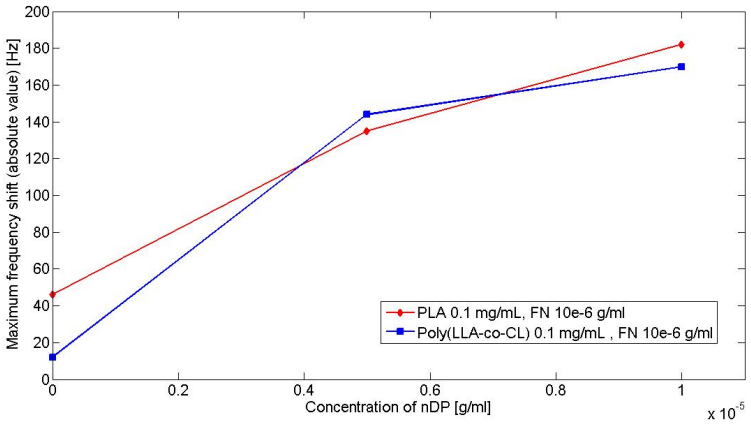

Figure 58: Maximum frequency shift for crystals coated with PLA 0.1 mg/mL and poly(LLA-co-CL) 0.1 mg/mL, flushed with nDP in varying concentrations and fibronectin 10 µg/mL, at 37 °C

8

CONCLUSIONS

Quartz Crystal Microbalance (QCM) is a technique that exploits the changes in the resonance frequency of a quartz crystal to evaluate the mass changes at the interface with the crystal surface. In the present Master thesis, QCM was proven to be a suitable technique for analyzing the interactions between selected degradable polymers and nanodiamond particles (nDP), fibronectin and the growth factor BMP-2.

During the first part of the project, great effort was aimed to guarantee polymers adhesion on quartz crystal surfaces in contact with water at 37 °C, to allow QCM measurements. In particular, different strategies of crystals treatments were tested and the polymer films behavior was found to be dependent on temperature, film thickness and quartz crystal surface treatments, such as air plasma treatment. Then, particular conditions of polymer film and crystal surface treatment that allowed to perform QCM measurements were defined. However, these conditions held only for a selection of degradable polymers, such as PLA, poly(LLA-co-CL), poly(TMC-D-LA) and PS. Further researches should be undertaken in the future to identify a strategy that permits the analysis of other degradable polymers, like PLA-PEG-PLA, PGA and PHAs with QCM.

Once the first selection of suitable polymers and conditions for QCM measurements was concluded, the attention was focused on PLA and poly(LLA-co-CL), for investigating and comparing the relationships of these materials with nDP, fibronectin and BMP-2. In particular, these interactions were proven to be dependent on polymer thickness and concentration of nDP and proteins in solution. As an example of the former, a thick and a thinner film of PLA revealed an opposite behavior in terms of nDP absorption and detachment. These differences can be explained with the swelling of the thicker layer when in contact with water and by the strong interactions between nDP.

As for the concentration of nDP and protein solutions, for every material and protein there is a different optimal concentration that maximizes protein and nDP adsorption. This value of concentration must be high enough to allow sufficient interaction between proteins or nDP and the material. On the other hand, it also has to be low enough to limit the formation of nDP aggregates and the flow of proteins and nDP outside the QCM crystal chamber. As a matter of fact, these events would prevent an optimal adsorption of nDP and proteins onto the polymer. Moreover, these optimal concentrations are dependent on the material considered. For instance, poly(LLA-co-CL) was proven to

require higher values of concentrations of nDP and BMP-2 to maximize the adsorption, in comparison with the concentrations needed for PLA. This effect can be explained with the difference in degree of crystallinity of the two polymers. In the future, a wider variety of polymers, protein types and concentrations should be analyzed, in order to find the optimal concentration for every protein and material. Furthermore, QCM measurements also confirmed that the presence of nDP enhances the adsorption of fibronectin and BMP-2 onto PLA and poly(LLA-co-CL). This phenomenon can be related to the small size of nanodiamonds, that increases polymer surface roughness.

Eventually, a future development of the work performed for this Master thesis could be the evaluation of the interactions of cells with proteins, nanodiamonds and degradable polymers, to determine the conditions that enhance cell adhesion. As a matter of fact, many of the choices made for this project, in particular about the experimental setup of the QCM, were aimed to allow future progresses in cell adhesion analysis.

ABBREVIATIONS

AFM	Atomic Force Microscope
BMP-2	Bone Morphogenetic Protein-2
DCM	Dichloromethane
DMEM	Dulbecco's Modified Eagle's Medium
DMF	Dimethylformamide
DMSO	Dimethyl sulfoxide
DSC	Differential Scanning Calorimetry
ECM	Extracellular Matrix
FN	Fibronectin
MSCs	Mesenchymal Stem Cells
nDP	NanoDiamond Particles
P(3HB)	poly((R)-3-hydroxybutyrate)
PBS	Phosphate-Buffered Saline
PCL	Poly(ϵ-caprolactone)
PDLA	Poly(D-lactide)
PEG	Polyethylene glycol
PET	Polyethylene terephthalate
PGA	Polyglycolide
PLA	Polylactide
PLLA	Poly(L-lactide)
Poly(LLA-co-CL)	Poly(L-lactide-co-ϵ-caprolactone)
Poly(TMC-D-LA)	Trimethylene carbonate-co-D-lactide
PS	Polystyrene
PVA	Polyvinyl acetate
PVAm	Polyvinylamine
QCM	Quartz Crystal Microbalance
QCM-D	Quartz Crystal Microbalance with Dissipation monitoring
QCM/HCC	Quartz Crystal Microbalance Heat Conduction Calorimeter
RGD	Arginine-Glycine-Aspartic acid
SEC	size-exclusion chromatography
SEM	Scanning Electron Microscope
TEA	Tryethylamine
THF	Tetrahydrofuran
TMC	trimethylene carbonate
VEGF	Vascular Endothelial Growth Factor

BIBLIOGRAPHY

[1] G. Sauerbrey, "Verwendung von schwingquarzen zur wägung dünner schichten und zur mikrowägung," *Zeitschrift für Physik*, vol. 155, no. 2, pp. 206–222, 1959.

[2] K. K. Kanazawa and J. G. Gordon, "Frequency of a quartz microbalance in contact with liquid," *Analytical Chemistry*, vol. 57, no. 8, pp. 1770–1771, 1985.

[3] M. A. Cooper and V. T. Singleton, "A survey of the 2001 to 2005 quartz crystal microbalance biosensor literature: applications of acoustic physics to the analysis of biomolecular interactions," *Journal of Molecular Recognition*, vol. 20, no. 3, pp. 154–184, 2007.

[4] S. Dånmark, A. Finne-Wistrand, M. Wendel, K. Arvidson, A.-C. Albertsson, and K. Mustafa, "Osteogenic differentiation by rat bone marrow stromal cells on customized biodegradable polymer scaffolds," *Journal of Bioactive and Compatible Polymers*, vol. 25, no. 2, pp. 207–223, 2010.

[5] C. Moseke and A. Ewald, "Cell and protein adsorption studies using . quartz crystal microgravimetry with dissipation monitoring," *Materialwissenschaft Und Werkstofftechnik*, vol. 40, pp. 36–42, 2009.

[6] S. Dånmark, A. Finne-Wistrand, A.-C. Albertsson, M. Patarroyo, and K. Mustafa, "Integrin-mediated adhesion of human mesenchymal stem cells to extracellular matrix proteins adsorbed to polymer surfaces," *Biomedical Materials*, vol. 7, no. 3, p. 035011, 2012.

[7] M. Tagaya, T. Ikoma, T. Takemura, N. Hanagata, M. Okuda, T. Yoshioka, and J. Tanaka, "Detection of interfacial phenomena with osteoblast-like cell adhesion on hydroxyapatite and oxidized polystyrene by the quartz crystal microbalance with dissipation," *Langmuir*, vol. 27, no. 12, pp. 7635–7644, 2011.

[8] T.-W. Chung, T. Limpanichpakdee, M.-H. Yang, and Y.-C. Tyan, "An electrode of quartz crystal microbalance decorated with cnt/-chitosan/fibronectin for investigating early adhesion and deforming morphology of rat mesenchymal stem cells," *Carbohydrate Polymers*, vol. 85, no. 4, pp. 726 – 732, 2011.

[9] J. Wegener, A. Janshoff, and H.-J. Galla, "Cell adhesion monitoring using a quartz crystal microbalance: comparative analysis

of different mammalian cell lines," *European Biophysics Journal*, vol. 28, pp. 26–37, 1998.

[10] N. Oliveira, J. Oliveira, T. Gomes, A. Ferreira, J. Dorgan, and I. Marrucho, "Gas sorption in poly(lactic acid) and packaging materials," *Fluid Phase Equilibria*, vol. 222-223, no. 0, pp. 317 – 324, 2004. Proceedings of the Fifteenth Symposium on Thermophysical Properites.

[11] B. Atthoff and J. Hilborn, "Protein adsorption onto polyester surfaces: Is there a need for surface activation?," *Journal of Biomedical Materials Research Part B: Applied Biomaterials*, vol. 80B, no. 1, pp. 121–130, 2007.

[12] A.-S. Andersson, K. Glasmästar, D. Sutherland, U. Lidberg, and B. Kasemo, "Cell adhesion on supported lipid bilayers," *Journal of Biomedical Materials Research Part A*, vol. 64A, no. 4, pp. 622–629, 2003.

[13] E. Karabulut and L. Wagberg, "Design and characterization of cellulose nanofibril-based freestanding films prepared by layer-by-layer deposition technique," *Soft Matter*, vol. 7, pp. 3467–3474, 2011.

[14] C. Modin, A.-L. Stranne, M. Foss, M. Duch, J. Justesen, J. Chevallier, L. K. Andersen, A. G. Hemmersam, F. S. Pedersen, and F. Besenbacher, "Qcm-d studies of attachment and differential spreading of pre-osteoblastic cells on ta and cr surfaces," *Biomaterials*, vol. 27, no. 8, pp. 1346 – 1354, 2006.

[15] M. S. Lord, C. Modin, M. Foss, M. Duch, A. Simmons, F. S. Pedersen, B. K. Milthorpe, and F. Besenbacher, "Monitoring cell adhesion on tantalum and oxidised polystyrene using a quartz crystal microbalance with dissipation," *Biomaterials*, vol. 27, no. 26, pp. 4529 – 4537, 2006.

[16] M. E. Alf, T. A. Hatton, and K. K. Gleason, "Insights into thin, thermally responsive polymer layers through quartz crystal microbalance with dissipation," *Langmuir*, vol. 27, no. 17, pp. 10691–10698, 2011.

[17] N. Weber, H. P. Wendel, and J. Kohn, "Formation of viscoelastic protein layers on polymeric surfaces relevant to platelet adhesion," *Journal of Biomedical Materials Research Part A*, vol. 72A, no. 4, pp. 420–427, 2005.

[18] F. Hook, J. Voros, M. Rodahl, R. Kurrat, P. Boni, J. Ramsden, M. Textor, N. Spencer, P. Tengvall, J. Gold, and B. Kasemo, "A comparative study of protein adsorption on titanium oxide surfaces using in situ ellipsometry, optical waveguide lightmode

spectroscopy, and quartz crystal microbalance/dissipation," *Colloids and Surfaces B: Biointerfaces*, vol. 24, no. 2, pp. 155–170, 2002.

[19] T.-W. Chung, Y.-C. Tyan, R.-H. Lee, and C.-W. Ho, "Determining early adhesion of cells on polysaccharides/pcl surfaces by a quartz crystal microbalance," *Journal of Materials Science: Materials in Medicine*, vol. 23, pp. 3067–3073, 2012.

[20] K. Marx, "Quartx crystal microbalance. a useful tool for studying thin polymer films and complex biomolecular systems at the solution-surface interface.," *Biomacromolecules*, vol. 4, no. 5, pp. 1099–1120, 2003. PMID: 12959572.

[21] J. Redepenning, T. K. Schlesinger, E. J. Mechalke, D. A. Puleo, and R. Bizios, "Osteoblast attachment monitored with a quartz crystal microbalance," *Analytical Chemistry*, vol. 65, no. 23, pp. 3378–3381, 1993. PMID: 8297027.

[22] C. Fredriksson, S. Khilman, B. Kasemo, and D. Steel, "In vitro real-time characterization of cell attachment and spreading," *Journal of Materials Science: Materials in Medicine*, vol. 9, pp. 785–788, 1998.

[23] M. Tagaya, T. Ikoma, T. Takemura, N. Hanagata, T. Yoshioka, and J. Tanaka, "Effect of interfacial proteins on osteoblast-like cell adhesion to hydroxyapatite nanocrystals.," *Langmuir*, vol. 27, no. 12, pp. 7645–53, 2011.

[24] R. Cairncross, J. Becker, S. Ramaswamy, and R. O'Connor, "Moisture sorption, transport, and hydrolytic degradation in polylactide," in *Twenty-Seventh Symposium on Biotechnology for Fuels and Chemicals* (J. McMillan, W. Adney, J. Mielenz, and K. Klasson, eds.), ABAB Symposium, pp. 774–785, Humana Press, 2006.

[25] H. Fujisaki and S. Hattori, "Keratinocyte apoptosis on type i collagen gel caused by lack of laminin 5/10/11 deposition and akt signaling," *Experimental Cell Research*, vol. 280, no. 2, pp. 255 – 269, 2002.

[26] M. Yamada, S. Takahashi, Y. Okahata, Y. Doi, and K. Numata, "Monitoring and kinetic analysis of the molecular interactions by which a repressor protein, phar, binds to target dnas and poly[(r)-3-hydroxybutyrate]," *AMB Express*, vol. 3, no. 6, 2013.

[27] K. Yamashita, M. Yamada, K. Numata, and S. Taguchi, "Nonspecific hydrophobic interactions of a repressor protein, phar, with poly[(r)-3-hydroxybutyrate] film studied with a quartz crystal microbalance," *Biomacromolecules*, vol. 7, no. 8, pp. 2449–2454, 2006.

[28] A. J. Svagan, A. Åkesson, M. Cárdenas, S. Bulut, J. C. Knudsen, J. Risbo, and D. Plackett, "Transparent films based on pla

and montmorillonite with tunable oxygen barrier properties," *Biomacromolecules*, vol. 13, no. 2, pp. 397–405, 2012.

[29] S. Utsel, E. E. Malmstrom, A. Carlmark, and L. Wagberg, "Thermoresponsive nanocomposites from multilayers of nanofibrillated cellulose and specially designed n-isopropylacrylamide based polymers," *Soft Matter*, vol. 6, pp. 342–352, 2010.

[30] A. Marais and L. Wågberg, "The use of polymeric amines to enhance the mechanical properties of lignocellulosic fibrous networks," *Cellulose*, vol. 19, pp. 1437–1447, 2012.

[31] J. Li, C. Thielemann, U. Reuning, and D. Johannsmann, "Monitoring of integrin-mediated adhesion of human ovarian cancer cells to model protein surfaces by quartz crystal resonators: evaluation in the impedance analysis mode," *Biosensors and Bioelectronics*, vol. 20, no. 7, pp. 1333 – 1340, 2005.

[32] U. Edlund, M. Källrot, and A.-C. Albertsson, "Single-step covalent functionalization of polylactide surfaces," *Journal of the American Chemical Society*, vol. 127, no. 24, pp. 8865–8871, 2005.

[33] C. Vasile and G. E. Zaikov, eds., *Environmentally Degradable Materials Based on Multicomponent Polymeric Systems*. VSP - An imprint of BRILL, 2009.

[34] M. Källrot, U. Edlund, and A.-C. Albertsson, "Surface functionalization of degradable polymers by covalent grafting," *Biomaterials*, vol. 27, no. 9, pp. 1788 – 1796, 2006.

[35] I. Vroman and L. Tighzert, "Biodegradable polymers," *Materials*, vol. 2, no. 2, pp. 307–344, 2009.

[36] P. Ouyang, Y.-q. Kang, G.-f. Yin, Z.-b. Huang, Y.-d. Yao, and X.-m. Liao, "Fabrication of hydrophilic paclitaxel-loaded pla-peg-pla microparticles via seds process," *Frontiers of Materials Science in China*, vol. 3, pp. 15–24, 2009.

[37] M. Ajioka, H. Suizu, C. Higuchi, and T. Kashima, "Aliphatic polyesters and their copolymers synthesized through direct condensation polymerization," *Polymer Degradation and Stability*, vol. 59, no. 13, pp. 137 – 143, 1998. Biodegradable Polymers and Macromolecules.

[38] U. Edlund and A. C. Albertsson, "Microspheres from poly(d,l-lactide)/poly(1,5-dioxepan-2-one) miscible blends for controlled drug delivery," *Journal of Bioactive and Compatible Polymers*, vol. 15, no. 3, pp. 214–229, 2000.

[39] J. Russias, E. Saiz, R. Nalla, K. Gryn, R. Ritchie, and A. Tomsia, "Fabrication and mechanical properties of pla/ha composites: A

study of in vitro degradation," *Materials Science and Engineering: C*, vol. 26, no. 8, pp. 1289 – 1295, 2006. Proceedings of the First TMS Symposium on Biological Materials Science.

[40] E. Bozza, "Matrici autofilate di peptidi auto-assemblanti per l'ingegneria del tessuto osseo. master thesis in biomedical engineering. universitá degli studi di padova," 2012.

[41] L.-Q. Yang, D. Yang, Y.-M. Guan, J.-X. Li, and M. Li, "Random copolymers based on trimethylene carbonate and ϵ-caprolactone for implant applications: Synthesis and properties," *Journal of Applied Polymer Science*, vol. 124, no. 5, pp. 3714–3720, 2012.

[42] B. Buchholz, "Analysis and characterization of resorbable dl-lactide-trimethylene carbonate copolyesters," *Journal of Materials Science: Materials in Medicine*, vol. 4, no. 4, pp. 381–388, 1993.

[43] I. Engelberg and J. Kohn, "Physico-mechanical properties of degradable polymers used in medical applications: A comparative study," *Biomaterials*, vol. 12, no. 3, pp. 292 – 304, 1991.

[44] N. Andronova and A.-C. Albertsson, "Resilient bioresorbable copolymers based on trimethylene carbonate, l-lactide, and 1,5-dioxepan-2-one," *Biomacromolecules*, vol. 7, no. 5, pp. 1489–1495, 2006.

[45] A.-C. Albertsson and M. Eklund, "Influence of molecular structure on the degradation mechanism of degradable polymers: In vitro degradation of poly(trimethylene carbonate), poly(trimethylene carbonate-co-caprolactone), and poly(adipic anhydride)," *Journal of Applied Polymer Science*, vol. 57, no. 1, pp. 87–103, 1995.

[46] A.-C. Albertsson and M. Eklund, "Synthesis of copolymers of 1,3-dioxan-2-one and oxepan-2-one using coordination catalysts," *Journal of Polymer Science Part A: Polymer Chemistry*, vol. 32, no. 2, pp. 265–279, 1994.

[47] Q. Y. Liu, L. Q. Zhang, and R. Shi, *Handbook of Applied Biopolymer Technology - Synthesis, Degradation and Applications. Degradable Bioelastomers: Synthesis and Biodegradation*. 2011.

[48] R. Chapanian, M. Y. Tse, S. C. Pang, and B. G. Amsden, "The role of oxidation and enzymatic hydrolysis on the in vivo degradation of trimethylene carbonate based photocrosslinkable elastomers," *Biomaterials*, vol. 30, no. 3, pp. 295 – 306, 2009.

[49] A. Finne-Wistrand and A.-C. Albertsson, "The use of polymer design in resorbable colloids," *Annual Review of Materials Research*, vol. 36, no. 1, pp. 369–395, 2006.

[50] Z.-W. Dai, X.-H. Zou, and G.-Q. Chen, "Poly(3-hydroxybutyrate-co-3-hydroxyhexanoate) as an injectable implant system for prevention of post-surgical tissue adhesion," *Biomaterials*, vol. 30, no. 17, pp. 3075 – 3083, 2009.

[51] L. Avérous and E. Pollet, *Environmental Silicate Nano-biocomposites.*

[52] Y.-S. Liang, W. Zhao, and G.-Q. Chen, "Study on the biocompatibility of novel terpolyester poly(3-hydroxybutyrate-co-3-hydroxyvalerate-co-3-hydroxyhexanoate)," *Journal of Biomedical Materials Research Part A*, vol. 87A, no. 2, pp. 441–449, 2008.

[53] C. Bastioli, ed., *Handbook of Biodegradable Polymers.* Smithers Rapra Technology.

[54] R. LeBaron and K. A. Athanasiou, "Extracellular matrix cell adhesion peptides: Functional applications in orthopedic materials," *Tissue Engineering*, vol. 6, no. 2, pp. 85–103, 2000.

[55] C. Wilson, R. Clegg, D. Leavesley, and M. Pearcy, "Mediation of biomaterial–cell interactions by adsorbed proteins: A review," *Tissue engineering*, vol. 11, no. 1-2, 2005.

[56] R. Pytela, M. D. Pierschbacher, and E. Ruoslahti, "Identification and isolation of a 140 kd cell surface glycoprotein with properties expected of a fibronectin receptor," *Cell*, vol. 40, no. 1, pp. 191 – 198, 1985.

[57] M. Yamamoto, Y. Ikada, and Y. Tabata, "Controlled release of growth factors based on biodegradation of gelatin hydrogel," *Journal of Biomaterials Science, Polymer Edition*, vol. 12, no. 1, pp. 77–88, 2001.

[58] J. Taipale and J. Keski-Oja, "Growth factors in the extracellular matrix.," *The FASEB Journal*, vol. 11, no. 1, pp. 51–9, 1997.

[59] S. R. Baglio, *Controllo molecolare del differenziamento osteoblastico per applicazioni nel campo della rigenerazione del tessuto osseo.* PhD thesis, Universitá di Bologna.

[60] U. Edlund, S. Dånmark, and A.-C. Albertsson, "A strategy for the covalent functionalization of resorbable polymers with heparin and osteoinductive growth factor," *Biomacromolecules*, vol. 9, no. 3, pp. 901–905, 2008. PMID: 18247564.

[61] A. Krueger, F. Kataoka, M. Ozawa, T. Fujino, Y. Suzuki, A. Aleksenskii, A. Y. Vula, and E. ÅŒsawa, "Unusually tight aggregation in detonation nanodiamond: Identification and disintegration," *Carbon*, vol. 43, no. 8, pp. 1722 – 1730, 2005.

[62] L. Grausova, L. Bacakova, A. Kromka, S. Potocky, M. Vanecek, M. Nesladek, and V. Lisa, "Nanodiamond as promising material for bone tissue engineering.," *Journal of Nanoscience and Nanotechnology*, vol. 9, no. 6, pp. 3524–3534, 2009.

[63] A. Krueger, "New carbon materials: Biological applications of functionalized nanodiamond materials," *Chemistry – A European Journal*, vol. 14, no. 5, pp. 1382–1390, 2008.

[64] R. Lappalainen, M. Selenius, A. Anttila, Y. T. Konttinen, and S. S. Santavirta, "Reduction of wear in total hip replacement prostheses by amorphous diamond coatings," *Journal of Biomedical Materials Research Part B: Applied Biomaterials*, vol. 66B, no. 1, pp. 410–413, 2003.

[65] D. Steinmueller-Nethl, F. R. Kloss, M. Najam-Ul-Haq, M. Rainer, K. Larsson, C. Linsmeier, G. Köhler, C. Fehrer, G. Lepperdinger, X. Liu, N. Memmel, E. Bertel, C. W. Huck, R. Gassner, and G. Bonn, "Strong binding of bioactive bmp-2 to nanocrystalline diamond by physisorption," *Biomaterials*, vol. 27, no. 26, pp. 4547 – 4556, 2006.

[66] T. Lechleitner, F. Klauser, T. Seppi, J. Lechner, P. Jennings, P. Perco, B. Mayer, D. Steinmueller-Nethl, J. Preiner, P. Hinterdorfer, M. Hermann, E. Bertel, K. Pfaller, and W. Pfaller, "The surface properties of nanocrystalline diamond and nanoparticulate diamond powder and their suitability as cell growth support surfaces," *Biomaterials*, vol. 29, no. 32, pp. 4275 – 4284, 2008.

[67] K. Hristova, E. Pecheva, L. Pramatarova, and G. Altankov, "Improved interaction of osteoblast-like cells with apatite–nanodiamond coatings depends on fibronectin," *Journal of Materials Science: Materials in Medicine*, vol. 22, no. 8, pp. 1891–1900, 2011.

[68] Y. Sun, A. Finne-Wistrand, A.-C. Albertsson, Z. Xing, K. Mustafa, W. J. Hendrikson, D. W. Grijpma, and L. Moroni, "Degradable amorphous scaffolds with enhanced mechanical properties and homogeneous cell distribution produced by a three-dimensional fiber deposition method," *Journal of Biomedical Materials Research Part A*, vol. 100A, no. 10, pp. 2739–2749, 2012.

[69] K. Odelius, P. Plikk, and A.-C. Albertsson, "Elastomeric hydrolyzable porous scaffolds: Copolymers of aliphatic polyesters and a polyether-ester," *Biomacromolecules*, vol. 6, no. 5, pp. 2718–2725, 2005. PMID: 16153111.

[70] A. Krüger, F. Kataoka, M. Ozawa, T. Fujino, Y. Suzuki, A. Aleksenskii, A. Y. Vul', and E. Osawa, "Unusually tight aggregation

in detonation nanodiamond: Identification and disintegration," *Carbon*, vol. 43, no. 8, pp. 1722 – 1730, 2005.

[71] D. Kwok and A. Neumann, "Contact angle measurement and contact angle interpretation," *Advances in Colloid and Interface Science*, vol. 81, no. 3, pp. 167 – 249, 1999.

[72] W. A. ZISMAN, *Relation of the Equilibrium Contact Angle to Liquid and Solid Constitution*, ch. 2, pp. 1–51.

[73] T. Young, "An essay on the cohesion of fluids," *Philosophical Transactions of the Royal Society of London*, vol. 95, pp. pp. 65–87, 1805.

[74] P. Gill, T. Tohidi Moghadam, and B. Ranjbar, "Differential scanning calorimetry techniques: Applications in biology and nanoscience," *Journal of Biomolecular techniques*, vol. 21, no. 4, p. 167–193, 2010.

[75] E. Freire, "Differential scanning calorimetry," in *Protein Stability and Folding* (B. Shirley, ed.), vol. 40 of *Methods in Molecular Biology*™, pp. 191–218, Humana Press, 1995.

[76] E. Fischer, H. Sterzel, and G. Wegner, "Investigation of the structure of solution grown crystals of lactide copolymers by means of chemical reactions," *Kolloid-Zeitschrift und Zeitschrift für Polymere*, vol. 251, no. 11, pp. 980–990, 1973.

[77] V. Crescenzi, G. Manzini, G. Calzolari, and C. Borri, "Thermodynamics of fusion of poly-β-propiolactone and poly-ϵ-caprolactone. comparative analysis of the melting of aliphatic polylactone and polyester chains," *European Polymer Journal*, vol. 8, no. 3, pp. 449 – 463, 1972.

[78] B. Gupta, A. Arora, S. Saxena, and M. S. Alam, "Preparation of chitosan–polyethylene glycol coated cotton membranes for wound dressings: preparation and characterization," *Polymers for Advanced Technologies*, vol. 20, no. 1, pp. 58–65, 2009.

[79] H. M. de Oca and I. Ward, "Structure and mechanical properties of {PGA} crystals and fibres," *Polymer*, vol. 47, no. 20, pp. 7070 – 7077, 2006.

[80] E. Meyer, "Atomic force microscopy," *Progress in Surface Science*, vol. 41, no. 1, pp. 3 – 49, 1992.

[81] C. R. Blanchard, "Atomic force microscopy," *The chemical educator*, vol. 1, pp. 1–8, 1996.

[82] D. B. Hall, P. Underhill, and J. M. Torkelson, "Spin coating of thin and ultrathin polymer films," *Polymer Engineering and Science*, vol. 38, no. 12, pp. 2039–2045, 1998.

[83] D. M. DeLongchamp, B. M. Vogel, Y. Jung, M. C. Gurau, C. A. Richter, O. A. Kirillov, J. Obrzut, D. A. Fischer, S. Sambasivan, L. J. Richter, and E. K. Lin, "Variations in semiconducting polymer microstructure and hole mobility with spin-coating speed," *Chemistry of Materials*, vol. 17, no. 23, pp. 5610–5612, 2005.

[84] L. Carlsson, S. Utsel, L. Wagberg, E. Malmstrom, and A. Carlmark, "Surface-initiated ring-opening polymerization from cellulose model surfaces monitored by a quartz crystal microbalance," *Soft Matter*, vol. 8, pp. 512–517, 2012.

[85] G. Hu, J. A. Heitmann, and O. J. Rojas, "In situ monitoring of cellulase activity by microgravimetry with a quartz crystal microbalance," *The Journal of Physical Chemistry B*, vol. 113, no. 44, pp. 14761–14768, 2009. PMID: 19827780.

[86] A. R. Morrill, D. T. Duong, S. J. Lee, and M. Moskovits, "Imaging 3-aminopropyltriethoxysilane self-assembled monolayers on nanostructured titania and tin (iv) oxide nanowires using colloidal silver nanoparticles," *Chemical Physics Letters*, vol. 473, no. 1â€“3, pp. 116 – 119, 2009.

[87] E. T. Vanderberg, l. L. Bertilsson, B. Liedberg, K. Uvdal, R. Erlandsson, H. Elwing, and I. Lundstrom, "Structure of 3-aminopropyl triethoxy silane on silicon oxide," *Journal of Colloid and Interface Science*, vol. 147, no. 1, pp. 103–118, 1991.

[88] Q. Zhang, V. N. Mochalin, I. Neitzel, K. Hazeli, J. Niu, A. Kontsos, J. G. Zhou, P. I. Lelkes, and Y. Gogotsi, "Mechanical properties and biomineralization of multifunctional nanodiamond-plla composites for bone tissue engineering," *Biomaterials*, vol. 33, no. 20, pp. 5067 – 5075, 2012.

[89] F. R. Kloss, R. Gassner, J. Preiner, A. Ebner, K. Larsson, O. Hächl, T. Tuli, M. Rasse, D. Moser, K. Laimer, E. A. Nickel, G. Laschober, R. Brunauer, G. Klima, P. Hinterdorfer, D. Steinmueller-Nethl, and G. Lepperdinger, "The role of oxygen termination of nanocrystalline diamond on immobilisation of bmp-2 and subsequent bone formation," *Biomaterials*, vol. 29, no. 16, pp. 2433 – 2442, 2008.